Optimal Screening, Monitoring, and Prevention Strategies in Infectious Disease Management

A DISSERTATION
SUBMITTED TO THE FACULTY OF THE GRADUATE SCHOOL
OF THE UNIVERSITY OF MINNESOTA
BY

Anthony Zhenhuan Zhang

IN PARTIAL FULFILLMENT OF THE
REQUIREMENTS
FOR THE DEGREE OF
DOCTOR OF PHILOSOPHY

January 2021

Acknowledgements

This dissertation owes much to people I've had the privilege to work with during my time at University of Minnesota. I would like to thank my advisors, Dr. Diana Negoescu, Dr. Eva Enns, and Dr. Ying Cui. Diana taught me how to ask good research questions, provided me with many collaborative opportunities and helped me understand the role of disease modelling in engineering, and for the society. Eva has been a wonderful mentor, advisor, and collaborator who provided continuous academic support during the last few years. Ying taught me how to think critically, pursue mathematical rigor and integrity, and more. I am very grateful for their support not only in academic side, but also many other aspect of life.

Special thanks go to the rest of my thesis committee members: Dr. Steven Wu, and Dr. William Cooper. I am grateful for their precious time and insightful comments on my research proposal and dissertation.

My friends at the U and internship colleagues at Facebook and Mayo Clinic consists of a great part of my wonderful and exciting life in the past few years. Special thanks go to Jiali Huang, Zeyang Wu, Ruizhi Shi, Yuanchen Su, Xiaochen Zhang, Ming Zhang, Junyu Zhang, Bingnan Lu, Chenglong Ye, Jueyu Wang, Kang Kang, and Jing Gao.

Finally, I would like to thank my family. Their invaluable and continued support helped me get through those tough times during my Ph.D.

Dedication

For my mom, myself, and those who help me up over the years.

Abstract

Mathematical models of infectious disease such as Markov models, dynamic compartmental models have been increasingly utilized in medical decision making. Most studies primarily focus on assessing the effectiveness, cost-effectiveness of policies, interventions by balancing costs and direct health benefits (often in qualify-adjusted life years gained, or disability-adjusted life-years averted). There are challenges with this classical approach. First, it may overlook the future impact of current decision. For example, in treating bacterial infections, antibiotic over-prescription is an increasingly urgent healthcare issue to be addressed. Second, previous works focus less on incorporating individual response and heterogeneity effect into an infectious disease control policy optimization setting.

In Chapter 2, we address the antibiotic over-prescription in febrile illness management, by formulating the problem of minimizing the weighted average of antibiotic underuse and overuse to inform the optimal diagnostic test and antibiotic treatment options for given occurrence probabilities of several bacterial and viral infections. The model accounted for multiple infections simultaneously and incorporated test, treatment, and other direct and indirect costs, as well as the effect of delays in seeking care and test turnaround times. We used the Markov models to numerically estimate disability-adjusted life years (DALYs), pre-penalty costs, and the likelihood of antibiotics overuse per patient for fifteen different strategies in Thailand settings (a typical viral and bacterial endemic setting).

In Chapter 3, we formulate a Markov decision process to address patient adherence heterogeneity by optimizing viral load monitoring strategies for HIV-infected patients.

In Chapter 4, we provide a framework to optimize public health control policies in responding to an infectious disease outbreak like COVID-19 pandemic. We use a multinomial discrete choice model to characterize an individual activity level and integrate it

into a repeated game-theoretical model with a SIR disease transmission dynamics. We derive a few insightful structural properties from these models and conduct numerical studies based on representative data for COVID-19 in Minnesota.

We conclude with a discussion of the work and directions for future research in Chapter 5.

Contents

List of Tables

List of Figures

Chapter 1

Introduction

To assess the effectiveness and cost-effectiveness of health strategies, policies, and interventions, mathematical models of infectious disease have become increasingly preferred over the last few decades. This is partially due to the advancement in computing powers, and particularly because randomized clinical trials are often time-consuming, expensive, and sometimes unethical. The medical community has been using models like Markov models, dynamic compartmental models to evaluate costs and health benefits for candidate interventions. However, most studies have focused on balancing costs and direct health benefits (often represented in quality-adjusted life-years or disability-adjusted life-years). Few studies have explicitly considered either the impact of proposed policies in the long run.

On the other hand, due to the rise of personalized and precision medicine in the last decade, there have been many studies supporting the existence of patient heterogeneity in different contexts. However, much fewer works have focused on incorporating the individual heterogeneity preference/behavior into an optimization problem. Overlooking these factors might result in myopic, greedy (that is to say, only focus on the immediate benefits without considering the future), ending up in the one-size-fits-all type of policies. Last, to design an optimal public health intervention, it is equally important, if not

more, for decision-makers to consider how individuals change their behaviors according to the development of the pandemic and public health interventions enacted.

For my dissertation, I propose and apply a few novel stochastic modeling techniques to optimize patient health outcome in three settings. First, we use Markov models to assess cost-effectiveness of test-and-treat strategies for acute febrile illnesses (an acute infectious diseases setting) by taking possible future harm due to current decision into consideration. Second, we optimize monitoring strategies for HIV patients by considering the patient heterogeneity in adherence behaviors (a chronic infectious disease setting). Last, we optimize the timing and intensity of public health interventions (in responding to an infectious disease outbreak) such as lockdown and social distancing by explicitly considering human responses to these policies (an infectious disease outbreak setting).

Antibiotic resistance has become an increasingly pressing public health issue. Nevertheless, both in the literature (i.e., the cost-effectiveness analysis for treating bacterial disease), and in clinical practices, the negative impact of antibiotic over-prescription is frequently overlooked. It is an even more urgent problem in tropical countries facing a growing number of febrile illness patients due to climate change and the increasing counts of weather-related disasters. There is, therefore, a great need for screening and treatment policies that consider potential long-term side effects of antibiotics treatment.

Meanwhile, in chronic disease management, as many as 40% of patients fail to adhere to treatment recommendations ([92]). Poor adherence leads to a waste of medical resources, higher treatment failure rates on designated therapies and worsened health outcomes. Both the frequentist and Bayesian model on adherence data provided evidence of adherence heterogeneity. One-size-fits-all treatment plans might not be optimal in this setting, and personalized treatment plans adapted to heterogeneous patient adherence patterns might yield better health outcomes. With this motivation in mind, we constructed an optimization model to assess the benefit(i.e., the value of information) of differentiating HIV-infected patients by adherence types.

Last, the COVID-19 pandemic calls for an urgent investigation of strategic public health interventions to minimize their socioeconomic loss while effectively containing infectious disease outbreaks [163]. Strategic planning of public health interventions requires central planners such as regional governments and health departments to optimize the timing, and intensity of these interventions. Central Planners should calibrate these decisions according to the disease dynamics (e.g., number of infections and infection rate) and the socioeconomic impact of interventions (e.g., estimated financial loss). On the one hand, an intervention that comes too late, lasts for a too short period, or lacks the necessary intensity (e.g., requires businesses to operate at 50% capacity instead of 25% capacity) may fail to contain the pandemic and cause an unaffordable disease burden (or cost of infection). On the other hand, an intervention that is initiated too early, lasts for an extended period, or is too stringent could cause excessive economic burden and severe disruption to social activities [171, 115].

Both antibiotic over-prescription and treatment non-adherence and infectious disease outbreaks are increasingly pressing public health problems nowadays. In this dissertation, we present the stochastic modeling frameworks that we developed for acute, chronic infectious disease setting, or an outbreak. We use these examples to illustrate how to make more informed, responsible, and efficient medical decision by incorporating a long-term perspective considering future harms (Chapter 2), a differentiated care perspective (Chapter 3), or a game-theoretic perspective (Chapter 4) . We also quantified the "when-and-where" regions for optimized policies to gain more health benefits in all settings.

1.1 Dissertation Overview

In Chapter 2 ("Optimal Test-and-treat Strategies for Acute Febrile Illnesses"), we formulated the problem of minimizing the weighted average of antibiotic underuse and overuse to inform the optimal clinical management strategy of diagnostic test options

and antibiotic treatment for given occurrence probabilities of several bacterial and viral infections and diagnostic test parameters (sensitivity and specificity). Detailed Markov cohort models of febrile illness progression were used to estimate the weight of antibiotic underuse. We modeled the weight of antibiotic overuse as a monetary penalty per unnecessarily administered course, which we vary in the case study, and sensitivity analysis. The model accounted for multiple infections simultaneously, incorporate test, treatment and other direct and indirect costs, as well as the effect of delays in seeking care and in test result wait times. We then discussed and analyzed the generic problem, and numerically evaluated fifteen different strategies in two example settings in Thailand based on existing literature, one with a higher prevalence of bacterial infections (Northern Thailand, Scenario A) and one with a higher prevalence of viral infections (Bangkok, Scenario B).

In Chapter 3 ("Monitoring Policy Optimization for HIV patients with Heterogeneous Adherence Types"), we develop a stochastic (i.e., a Markov Decision Process) model framework to optimize the monitoring interval for HIV-infected patients on the first-line regimen in resource-limited settings, where we assume there exist only two available antiretroviral therapies (ARTs). We present a Markov decision process modeling approach where we incorporated adherence heterogeneity explicitly in the disease progression model, and provided 1) structural analysis of the model (optimal value function) and the optimal policy; 2) the exact equation to directly compute the optimal policy. Then, we present a case study (an economic analysis quantifying the benefit of differentiating adherence type) using a previously well-calibrated simulation model in [106]. We also provide several possible extensions of the model towards the end.

In Chapter 4 ("No Panic in Pandemic: The Impact of Individual Choice on Public Health Policy and Vaccine Priority"), we use a multinomial logit choice model to characterize an individual activity level and integrate it into a disease transmission model (SIR disease transmission dynamics) in a game-theoretical setting. We derive a few insightful structural properties from these models and conduct numerical studies based

on representative data for COVID-19 in Minnesota. We compare the effectiveness of lockdown and social distancing, and numerically characterize the vaccine priority under different circumstances.

We conclude in Chapter 5 with a discussion of promising directions for future research.

Chapter 2

Optimal Test-and-treat Strategies for Acute Febrile Illnesses

2.1 Introduction

Clinical manifestations such as the sudden onset of acute fever, chills, and headache are the common features among several tropical and emerging diseases, including dengue, Zika, yellow fever, leptospirosis and scrub typhus ([140]). Depending on the specific etiology, if untreated, patients could experience respiratory distress, multi-organ failure, and even death ([78], [113]). Due to climate change and the increasing counts of weather-related disasters ([69], [49], [50]), healthcare providers are facing a growing number of febrile illness patients, especially in low-resource settings ([120]). The global annual burden of diseases under the umbrella of febrile illness is estimated to be on the order of millions of cases ([38], [16], [35]).

There are currently no evidence-based guidelines to inform diagnostic and treatment strategies and the necessary health care investments ([127]). Early diagnosis of bacterial infection is essential since antibiotic therapy is more beneficial when initiated early ([78]). Moreover, early diagnosis could avoid unnecessary antibiotics administration to

patients with non-bacterial infections such as dengue ([126]). Due to limited laboratory services, low quality of test results and prohibitively expensive diagnostic test costs, current World Health Organization (WHO) guidelines recommend for malaria-endemic, resource limited regions the use of rapid malaria screening, and prescribing antibiotics to those with signs of severe illness or specific bacterial infections ([41]). Studies have also shown that empirical antibiotics prescription to suspected leptospirosis patients is cost-effective when not considering antibiotic overuse ([139]).

Nevertheless, antibiotic overuse has been recognized as the key driver of antibiotic resistance development, which is an increasingly pressing public health issue. In the U.S. alone, antibiotic resistance causes more than 2 million infections and 23,000 deaths per year ([29]). Additional mean hospital charges due to the presence of antimicrobial-resistant organism (i.e., methicillin-resistant S. aureus) is around $ 86,400 USD (after Consumer Price Index (CPI) inflation adjustment) according to a study in the U.S. ([53]). The social impact might still be underestimated due to the transmission of antimicrobial-resistant organisms.

Most existing research in the domain of assessing the cost-effectiveness of protocols managing acute febrile illness has focused on either a single cause of infection or a specific strategy. As pointed out by [40], the literature on comprehensive cost-effectiveness assessment of clinical management strategies for non-malarial acute febrile illnesses is scarce. [154] conducted a prospective observational study to investigate the causes of acute undifferentiated fever and concluded that pathogen-specific rapid diagnostic tests could inform the correct use of antibiotics and improve antimicrobial stewardship in their setting. Under the same stream of work, [87] conducted a cost-effectiveness analysis of the management of scrub typhus and dengue in rural Laos setting comparing the approaches of using pathogen-specific diagnostics and biomarker tests. However, potentially crucial assumptions such as illness progression, health-seeking behaviors, and diagnostic test accuracy in relation to the stage of illness were not examined in these studies. On the other hand, studies have shown that empirical antibiotics administration

might be the most cost-effective strategy in resource-limited settings when treating suspected leptospirosis patients [139]. However, this may lead to poor outcomes for non-bacterial infections, which are subsequently treated inappropriately with antibiotics ([41]). Moreover, antibiotic overuse has become a significant health issue worldwide. As a consequence, the extent to which diagnostic and treatment strategies may be cost-effective under given scenarios remains unknown.

The objective of this study was to inform the optimal diagnosis and antibiotic treatment strategies for patients with undifferentiated febrile illnesses. We determined the optimal decision by considering the tradeoff between antibiotics underuse (i.e., higher disability-adjusted life years (DALYs) and health care cost) and antibiotics overuse (i.e., unnecessary courses of antibiotics prescribed). We selected Thailand as an exemplary setting because it is endemic for several of the pathogens of interest, including dengue, leptospirosis, and scrub typhus at varying occurrence probabilities and present availability of published data for model development ([140], [89]).

2.2 Methods

Overview

In order to understand the degree to which different strategies achieve the balance between antibiotics overuse and underuse, we seek to quantify the expected consequences and proportions of patients falling in both categories for each strategy. To capture the consequences of antibiotic underuse, we developed a Markov cohort model that describes febrile disease progression with and without treatment. The long-term consequences of antibiotic overuse, such as the development of bacterial resistance, are much more difficult to estimate. Consequently, we assign a monetary penalty (weight) to every patient unnecessarily prescribed a course of antibiotics in order to capture how different values for this weight might drive optimal decision-making.

Balancing Antibiotic Overuse and Underuse

We first consider a simplified setting where patients presenting with fever can suffer from one of four causes:

1. A specific bacterial infection for which a test exists, and which is treatable with a commonly prescribed antibiotic (i.e., doxycycline) ([139], [41]);
2. A bacterial infection for which no test exists, but which is also treatable with doxycycline;
3. A specific viral infection for which a test exists (and which is not treatable with doxycycline);
4. Other infections for which there is no test and are not treatable with doxycycline.

We consider three strategies:

1. Empirical doxycycline treatment (antibiotic treatment for all patients, without any tests);
2. Testing all patients using the bacterial infection test (with sensitivity $sens_b$ and specificity $spec_b$, and administering antibiotic treatment to patients with positive results;
3. Testing all patients using the viral infection test (with sensitivity $sens_v$ and specificity $spec_v$, and administering antibiotic treatment to patients with negative results.

We denote by p_{bac} the probability of presenting with bacterial infection for which a test exists, $p_{other_{bac}}$ the probability of presenting with bacterial infection for which no test exists, p_{viral} the probability of presenting with a viral infection for which a test exists, and p_{other} the probability of presenting with infections not treatable with doxycycline for which no test exists. We assume that all test sensitivities and specificities fall between 50% and 100% , and that any test's sensitivity is less than or equal to any specificity.

If the penalty (weight) for each patient with a bacterial disease not prescribed antibiotics is w_{under}, and the penalty (weight) for each patient with non-bacterial disease prescribed antibiotics is w_{over}, then we would like to choose a strategy that minimizes

the expected total penalty per patient: w_{under}Prob(no antibiotics, bacterial disease) + w_{over}Prob(antibiotics, no bacterial disease). The first and second term corresponds to antibiotic underuse and overuse penalty, respectively, associated with each strategy. We rewrite this objective as

$$w_{under}Prob(under) + w_{over}Prob(over) \tag{2.1}$$

	Strategy list	P(under)	P(over)
1	"no testing"	0	$p_{viral} + p_{other}$
2	"bacterial test"	$p_{bac}\left(1 - sens_b\right) + p_{other_{bac}} spec_b$	$\left(p_{viral} + p_{other}\right)\left(1 - spec_b\right)$
3	"viral test"	$\left(p_{bac} + p_{other_{bac}}\right)\left(1 - spec_v\right)$	$p_{viral}\left(1 - sens_v\right) + p_{other} spec_v$

Table 2.1: Analytical expressions of antibiotic overuse and underuse percentage for a given strategy

We show the analytical expression of antibiotic underuse and overuse under each strategy in Table 2.1 above. We then evaluate the strategy performance by comparing the weighted average of $P\left(under\right)$ and $P\left(over\right)$. (Equation 2.1). Strategy "bacterial test" has a smaller objective value compared to "no testing" when the following condition is satisfied:

$$\left(\frac{w_{under}}{w_{over}} * \frac{\left(1 - sens_b\right)}{spec_b} + 1\right) p_{bac} + \left(\frac{w_{under}}{w_{over}} + 1\right) p_{other_{bac}} \leq 1 \tag{2.2}$$

Similarly, Strategy "viral test" gives a smaller objective value compared to "no testing" when the following condition is satisfied:

$$\left(\frac{w_{over} * sens_v}{w_{under} * \left(1 - spec_v\right)} + 1\right) p_{viral} + \left(\frac{w_{over}}{w_{under}} + 1\right) p_{other} \geq 1 \tag{2.3}$$

We have also compared the two testing strategies. "bacterial test" provides a smaller objective value compared to "viral test" when the following condition is satisfied (by

comparing the analytical objective values):

$$\begin{aligned} &-\frac{w_{under}}{w_{over}} p_{bac} sens_b + p_{viral} sens_v + \left(\frac{w_{under}}{w_{over}} P_{other_{bac}} - P_{other} - p_{viral} \right) spec_b \\ &+ \left(\frac{w_{under}}{w_{over}} \left(P_{other_{bac}} + p_{bac} \right) - p_{other} \right) spec_v - \left(\frac{w_{under}}{w_{over}} P_{other_{bac}} - P_{other} \right) \leq 0 \end{aligned} \tag{2.4}$$

On the other hand,"viral test" provides a smaller objective value compared to "bacterial test" when the following condition is satisfied:

$$\begin{aligned} &-\frac{w_{under}}{w_{over}} p_{bac} sens_b + p_{viral} sens_v + \left(\frac{w_{under}}{w_{over}} P_{other_{bac}} - P_{other} - p_{viral} \right) spec_b \\ &+ \left(\frac{w_{under}}{w_{over}} \left(P_{other_{bac}} + p_{bac} \right) - p_{other} \right) spec_v - \left(\frac{w_{under}}{w_{over}} P_{other_{bac}} - P_{other} \right) \geq 0 \end{aligned} \tag{2.5}$$

We simplify the first two inequalities above to determine the disease distribution condition (such that the two testing strategies outperform "no testing") for any given weights. We note that the left-hand side (henceforth LHS) of Inequality 2.2 is bound above (reached its maximum) by setting is $sens_b$ and $spec_b$ to the smallest possible values (50% each):

$$\max \left(\frac{w_{under}}{w_{over}} * \frac{(1 - sens_b)}{spec_b} + 1 \right) p_{bac} = \left(\frac{w_{under}}{w_{over}} + 1 \right) p_{bac} \tag{2.6}$$

Then, we have the following simplified condition:

$$p_{bac} + p_{other_{bac}} \leq \frac{w_{over}}{w_{over} + w_{under}} \tag{2.7}$$

Similarly, we simplify the Inequality 2.3 to

$$p_{viral} + p_{other} \geq \frac{w_{under}}{w_{over} + w_{under}} \tag{2.8}$$

In addition, note that $p_{bac} + p_{other_{bac}} + p_{viral} + p_{other} = 1$. Then, we can rewrite Condition 2.8 as: $1 - \frac{w_{under}}{w_{over} + w_{under}} \geq p_{bac} + p_{other_{bac}}$, which is the same as Condition 2.7.

We then derived sufficient conditions (without test sensitivity and specificity requirements) for "bacterial test" to outperform "viral test" , and vice versa. We have the following observations on the LHS (the same for Inequality 2.4, 2.5):

1. $sens_b$ has a non-positive coefficient.
2. $sens_v$ has a non-negative coefficient.
3. if $\frac{w_{under}}{w_{over}}\left(P_{other_{bac}} + p_{bac}\right) \leq p_{other}$ (denoted as $*$ henceforth), the coefficient of $spec_v$ is non-positive (otherwise positive).
4. if $\frac{w_{under}}{w_{over}}\left(p_{other_{bac}}\right) > p_{other} + p_{viral}$ (denoted as X henceforth), the coefficient of $spec_b$ is positive (otherwise non-positive).

We claim that $(*)$ and (X) are mutually exclusive. To see this, first note that all disease occurrence probabilities and the weight ratio are non-negative. Then, given (X), we have:

$$\frac{w_{under}}{w_{over}}\left(p_{other_{bac}} + p_{bac}\right) \geq \frac{w_{under}}{w_{over}}\left(p_{other_{bac}}\right) > p_{other} + p_{viral} \geq p_{other},$$

which leads to $\frac{w_{under}}{w_{over}}\left(p_{other_{bac}} + p_{bac}\right) > p_{other}$. This is a contradiction to $(*)$. Similarly, given $(*)$, we have

$$\frac{w_{under}}{w_{over}}\left(p_{other_{bac}}\right) \leq \frac{w_{under}}{w_{over}}\left(p_{other_{bac}} + p_{bac}\right) \leq p_{other} \leq p_{other} + p_{viral},$$

which leads to $\frac{w_{under}}{w_{over}}\left(p_{other_{bac}}\right) \leq p_{other} + p_{viral}$, a contradiction to (X).

Now, suppose $(*)$ is true. Then, from the LHS of inequality 2.4, we have

$$\begin{aligned}
LHS &= -\frac{w_{under}}{w_{over}} p_{bac} sens_b + p_{viral} sens_v + \left(\frac{w_{under}}{w_{over}} P_{other_{bac}} - P_{other} - p_{viral} \right) spec_b \\
&\quad + \left(\frac{w_{under}}{w_{over}} \left(P_{other_{bac}} + p_{bac} \right) - p_{other} \right) spec_v - \left(\frac{w_{under}}{w_{over}} P_{other_{bac}} - P_{other} \right) \\
&\leq -\frac{w_{under}}{w_{over}} p_{bac} sens_b + \left(\frac{w_{under}}{w_{over}} P_{other_{bac}} - P_{other} \right) spec_b \\
&\quad + \left(\frac{w_{under}}{w_{over}} \left(P_{other_{bac}} + p_{bac} \right) - p_{other} \right) spec_v - \left(\frac{w_{under}}{w_{over}} P_{other_{bac}} - P_{other} \right) \\
&\leq -\frac{w_{under}}{w_{over}} p_{bac} 0.5 + \left(\frac{w_{under}}{w_{over}} P_{other_{bac}} - P_{other} \right) 0.5 \\
&\quad + \left(\frac{w_{under}}{w_{over}} \left(P_{other_{bac}} + p_{bac} \right) - p_{other} \right) 0.5 - \left(\frac{w_{under}}{w_{over}} P_{other_{bac}} - P_{other} \right) \\
&= 0
\end{aligned} \tag{2.9}$$

The first inequality follows because $p_{viral} \left(sens_v - spec_b \right) \leq 0$, the second inequality follows by setting $sens_b = spec_b = spec_v = 50\%$ (i.e., smallest possible values) since they all have non-positive coefficients.

Then, under $(*)$, we have the LHS of 2.4 bounded above by 0. Thus, $(*)$ is a sufficient condition to 2.4.

We also derive the sufficient guarantee of "viral test" outperforming "bacterial test"

. Now suppose (X) is true. From the LHS of inequality 2.5, we have

$$\begin{aligned}
LHS &= -\frac{w_{under}}{w_{over}} p_{bac} sens_b + p_{viral} sens_v + \left(\frac{w_{under}}{w_{over}} P_{other_{bac}} - P_{other} - p_{viral} \right) spec_b \\
&\quad + \left(\frac{w_{under}}{w_{over}} \left(P_{other_{bac}} + p_{bac} \right) - p_{other} \right) spec_v - \left(\frac{w_{under}}{w_{over}} P_{other_{bac}} - P_{other} \right) \\
&\geq p_{viral} sens_v + \left(\frac{w_{under}}{w_{over}} P_{other_{bac}} - P_{other} - p_{viral} \right) spec_b \\
&\quad + \left(\frac{w_{under}}{w_{over}} P_{other_{bac}} - p_{other} \right) spec_v - \left(\frac{w_{under}}{w_{over}} P_{other_{bac}} - P_{other} \right) \\
&\geq p_{viral} 0.5 + \left(\frac{w_{under}}{w_{over}} P_{other_{bac}} - P_{other} - p_{viral} \right) 0.5 \\
&\quad + \left(\frac{w_{under}}{w_{over}} P_{other_{bac}} - p_{other} \right) 0.5 - \left(\frac{w_{under}}{w_{over}} P_{other_{bac}} - P_{other} \right) \\
&= 0
\end{aligned} \tag{2.10}$$

The first inequality follows since $-\frac{w_{under}}{w_{over}} p_{bac} \left(sens_b - spec_v \right) \geq 0$, the second inequality follows by setting $sens_v = spec_b = spec_V = 50\%$ (similar reason as before). Then, we conclude that the LHS of 2.5 is bounded below by 0 given (X). Thus, (X) is a sufficient condition to 2.5.

To briefly summarize, we derived analytical expressions of antibiotics overuse and underuse probabilities for each strategy, estimated the weights, and evaluated all three generic strategies using the objective defined in Equation 2.1 in order to understand the role that overuse penalties, along with disease probabilities of occurrence and test accuracy parameters, play into determining the best strategy among the three options. Notably, we found simple conditions involving only the probabilities of disease occurrence and the ratio $\frac{w_{under}}{w_{over}}$ that guarantee that administering a specific test leads to a lower total penalty than administering the other test or no test at all (and administering antibiotics to all patients).

Viral- versus bacterial-endemic settings: a case study for Thailand

After gaining intuition from analyzing the simplified version of the balancing problem, we turned to a more realistic setting in order to account for multiple bacterial

disease scenarios, incorporate test, treatment and other direct and indirect costs, as well as the effect of delays in seeking care and in test result wait times. We categorized sources of infections into the following five types based on whether they are bacterial or viral, and whether they are treatable with doxycycline:

1. Leptospirosis (bacterial, treatable with doxycycline);
2. Scrub typhus (bacterial, treatable with doxycycline);
3. "Other bacterial", treatable with doxycycline, such as spotted fever group rickettsioses ([139]);
4. Dengue (viral, not treatable with antibiotics); and
5. All other possible causes of infection as a general category of "others" which are not treatable with doxycycline.

Settings	Leptospirosis	Scrub typhus	Other bacterial	Dengue	Others
Scenario A (Northern Thailand)	52.80%	4.60%	4.50%	12.20%	26%
Scenario B (Bangkok, Thailand)	6.80%	1.70%	8.50%	67.10%	15.80%

In Scenario A (Northern Thailand), bacterial disease is predominant; in Scenario B (Bangkok, Thailand), viral disease is predominant. Values obtained from [140].

Table 2.2: Disease Prevalence

We assumed that all cases are malaria negative, which is consistent with current practices of screening with highly accurate rapid tests for malaria first ([61], [68], [4]). We selected two contrasting settings in Thailand with varying infection prevalence (Table 1): Northern Thailand, where leptospirosis, scrub typhus (bacterial infections) are more endemic – Scenario A ([140]), and Bangkok, where dengue (viral) is the most common cause of acute fever – Scenario B ([89]).

The Disease Progression Model

We developed detailed Markov cohort models to capture each febrile disease's progression and used the model outcomes to evaluate alternative clinical management strategies. We modeled a hypothetical cohort of 40-year-old adult patients (age varied in the sensitivity analysis) with acute but undifferentiated fever since symptom onset

(first day of illness). We set the time horizon to 45 days since most patients would be either recovered or deceased by then. We tracked patients' health states daily. On each day, patients may recover, progress to severe disease stage or die. We considered cases when patients present to hospitals on their first, fourth or tenth day of illness, which captures the minimum, average, and maximum of time for patients presenting to hospitals seeking care. We simplified the health states for any infection type to four core states: Mild, Severe, Recovered and Death. The exact daily transition probabilities depended upon the specific infection etiology, as well as the corresponding treatment (i.e., with or without antibiotics). We assumed that all Severe patients were immediately hospitalized and assigned to a diagnostic and treatment strategy if it was the first hospital visit (no prior testing). We also assumed that deaths during the 45-day time horizon were caused only by severe complications of infections. Details on model parameterization and calibration can be found in Appendix A.

Diagnostic and Treatment Management Strategies

In the two Thai settings, we evaluated fifteen strategies with different test and treatment options towards febrile disease management (Figure 2.1). Treatment for leptospirosis and scrub typhus was assumed to be a one-week course of antibiotics (commonly doxycycline). There is no specific treatment for dengue and many other viral infections with supportive care as standard practice. A positive bacterial test results or a negative viral test result would generally lead to the prescription of antibiotics. Diagnostic testing considered pathogen-specific rapid diagnostics tests (RDT) and Polymerase Chain Reaction (PCR) tests for leptospirosis, typhus, and dengue. Although still not widely available in health care settings, we also considered the use of multiplex nucleic acid amplification for all three pathogens in a single test (multiplex PCR) ([151], [59]). We assumed RDT results could be obtained within a day whereas PCR tests take up to two days. For this reason (and to limit the total number of possible candidate strategies), we did not include typhus-led testing strategies (i.e., single typhus RDT/PCR). We assumed all Mild state patients received outpatient care (with or without antibiotics

prescription), where practices such as follow-up of patients, adequate bed rest and fluid intake are common. Patients who progressed to Severe state (i.e., demonstrate various clinical signs in severe febrile illness) were hospitalized. Empirical antibiotic treatment of Severe patients is the current protocol recommended by the WHO in resource-limited settings ([41]). In this study, we considered an expanded empirical treatment strategy that includes treating Mild and Severe patients with antibiotics without any diagnostic testing. Lastly, we also considered a "No Antibiotics" strategy to monitor natural disease progression, where no test and no antibiotics were given to patients, but patients in Severe states were hospitalized. We sketched the patient flow through our model in Figure 2.2.

Figure 2.1: Test and treat strategies evaluated in the cost-effectiveness analysis for acute febrile illness.

		Strategy	*Test interpretation treatment decision*
No tests	1	No Antibiotics	Reference. No antibiotics for neither mild nor severe patients
	2	Empirical to all	Antibiotic to all patients
	3	Empirical to Severe	Antibiotic to patients in Severe states
Single Tests	4	Dengue RDT	Dengue RDT positive: out(in)patient care w/o antibiotics Dengue RDT negative: antibiotic
	5	Dengue PCR	Dengue PCR positive: out(in)patient care w/o antibiotics Dengue PCR negative: antibiotic
	6	Lepto RDT	Lepto RDT positive: antibiotic Lepto RDT negative: out(in)patient care w/o antibiotics
	7	Lepto PCR	Lepto PCR positive: antibiotic Lepto PCR negative: out(in)patient care w/o antibiotics
Sequential Tests	8	S: Lepto RDT, typhus RDT	Lepto RDT positive: antibiotic Lepto RDT negative: perform Typhus RDT Typhus RDT positive: antibiotic Typhus RDT negative: out(in)patient care w/o antibiotics
	9	S: Lepto PCR, typhus RDT	Lepto PCR positive: antibiotic Lepto PCR negative: perform Typhus RDT Typhus RDT positive: antibiotic Typhus RDT negative: out(in)patient care w/o antibiotics
	10	S: Lepto RDT, typhus PCR	Lepto RDT positive: antibiotic Lepto RDT negative: perform Typhus PCR Typhus PCR positive: antibiotic Typhus PCR negative: out(in)patient care w/o antibiotics
Parallel Tests	11	P: Lepto PCR, typhus PCR	Lepto PCR or Typhus PCR positive: antibiotic Lepto PCR and Typhus PCR negative: out(in)patient care w/o antibiotics
	12	P: Lepto RDT, typhus RDT	Lepto RDT or Typhus RDT positive: antibiotic Lepto RDT and Typhus RDT negative: out(in)patient care w/o antibiotics
	13	P: Lepto PCR, typhus RDT	Lepto PCR or Typhus RDT positive: antibiotic Lepto PCR and Typhus RDT negative: out(in)patient care w/o antibiotics
	14	P: Lepto RDT, typhus PCR	Lepto RDT or Typhus PCR positive: antibiotic Lepto RDT and Typhus PCR negative: out(in)patient care w/o antibiotics
Multiplex PCR	15	Multiplex PCR	Lepto or typhus PCR positive: antibiotic Dengue positive: out(in)patient care w/o antibiotics Lepto, typhus, or dengue negative: out(in)patient care w/o antibiotics

Each strategy consists of testing options from no testing to testing using: Rapid tests (RDT), polymerase chain reaction (PCR), and Multiplex PCR for leptospirosis, typhus, and dengue simultaneously, Sequential (S): run tests in sequence; Parallel (P): run tests simultaneously.

Figure 2.2: Patient Flow Diagram.

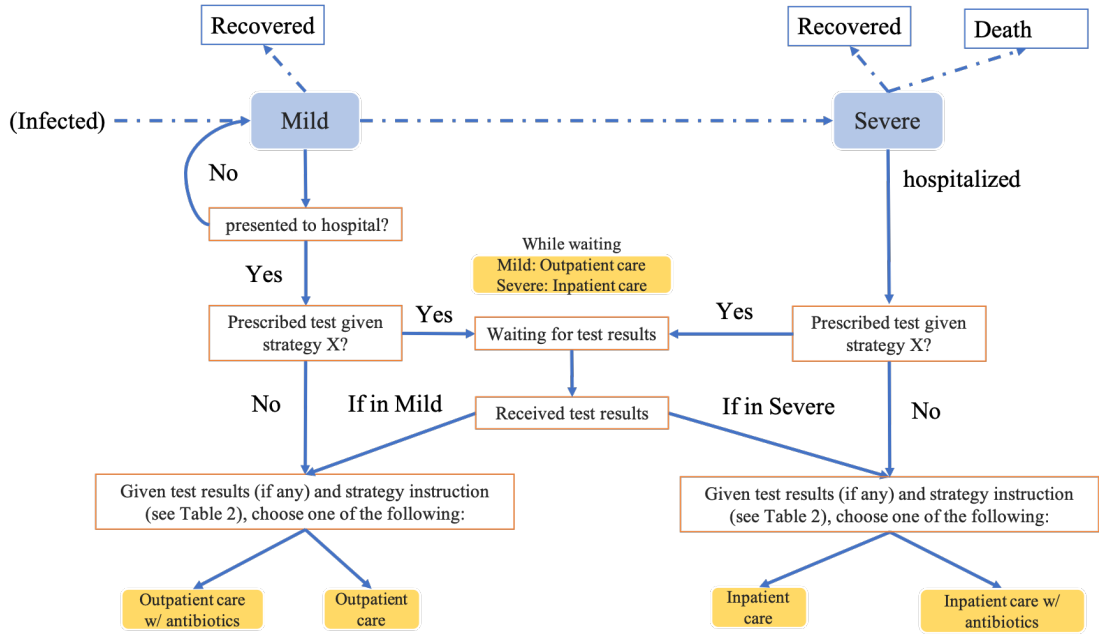

Patients present to the hospital (in either Mild or Severe state) for the first time will be prescribed one of the strategies (say Strategy X) listed in Table 2. Patients who progressed to the Severe state (i.e., they demonstrate various clinical signs in severe febrile illness) are assumed to be hospitalized. We assumed that antibiotics would only be prescribed to patients when all pending test results (if any) were obtained. A positive bacterial test result or a negative viral test result would generally lead to the prescription of antibiotics, whereas a negative bacterial test result or a positive viral test result would not.

Outcomes Measured

Outcome measures included: 1) costs and health outcomes: direct and indirect healthcare costs incurred and health burden (in DALYs, definition and calculation provided in Appendix A), 2) antibiotics underuse and overuse. For a given strategy, we tracked the proportion of presenting patients over- and under-treated with antibiotics (Prob(over) and Prob(under)). To account for antibiotic overuse when evaluating the strategies, we first considered the three-dimensional outcome space consisting of DALYs, costs, and Prob(over) instead of the standard two-dimensional outcome space consisting of only DALYs and costs (details on the methodology for finding a three-dimensional Pareto frontier are in the next section). Secondly, for each strategy (say Strategy X), we assigned a penalty per unnecessarily prescribed course of antibiotics (w_{over}), and

monetize DALYs by assigning a willingness-to-pay (WTP) per DALY averted. DALY averted is the DALY difference between strategy X and "No Antibiotics". We define incremental costs and incremental P(over) similarly. In our main analysis, we set the WTP value to be Thailand's GDP per capita in 2016, $5,907.91 USD ([167]). Then for each strategy, we compute its resulting net monetary benefit (NMB), where

$$NMB = (DALYs\ averted)WTP - (incremental\ costs) - w_{over}(incremental\ P(over)).$$

By considering a range of values for willingness-to-pay per DALY averted, and for penalty per unnecessary course of antibiotics, we quantify the ranges of net monetary benefit of each strategy, and conduct a cost-effectiveness analysis comparing the different strategies.

Linear Program to identify 3D Pareto Frontier

In this section, we develop a method to identify whether a given strategy output is on the three-dimensional Pareto Frontier in terms of DALYs, costs, and antibiotics overuse. Previous work on cost-effectiveness analyses tends to focus on two-dimensional problems by considering only the tradeoff between health benefits (i.e., QALYs or DALYs averted) and costs) ([56]). For our problem, without considering the dimension of "antibiotics overuse" - a primary focus of our study, Strategy 2 (Empirical to All – initiating antibiotics treatments right upon clinical visits) will dominate all other strategies by incurring the least DALYs and costs. However, when considering the trade-offs in three dimensions – costs, DALYs and antibiotics overuse, different strategies may appear on the Pareto frontier.

To identify the three-dimensional Pareto frontier, we employ the idea that a given point (strategy output) is on this frontier if and only if the convex set formulated by perturbations of this point in one improving direction (i.e., smaller DALYs, costs or antibiotic overuse) is disjoint from the convex hull determined by the original set of points (including the point from which the perturbation was obtained).

We define e_j as the unit vector along jth dimension in $\mathbb{R}^3$ (i.e. $e_2 = (0,1,0)$). Let $p_{i,j}$ represent the model output from strategy i along j th dimension ("DALYs" , "costs" , and "antibiotics overuse") and p_i be the three-dimensional output. Denote P as the set of all outputs. We then define the convex hull formulated from P as $Conv\,(P) = \{\sum_{k=1}^{n} \alpha_k p_k | (\forall k : \alpha_k \geq 0) \wedge \sum_{k=1}^{n} \alpha_k = 1, n = |P|\}$ in the "DALYs", "costs" and "antibiotics overuse" space. For each p_i , we first construct three points $(q_i^{(1)}, q_i^{(2)}, q_i^{(3)})$ where $q_i^{(j)} = p_i - \epsilon e_j, j = 1,2,3$: subtract a sufficiently small positive ϵ from "DALYs" , "costs" and "antibiotics overuse" dimensions respectively (i.e., ϵ should be much smaller than the minimum pairwise difference in any dimension: $\epsilon < min|p_{i,j} - p_{i',j}|, \forall i, i' = 1, \ldots, n, j = 1,2,3$). Denote $Q_i = \{q_i^{(j)} | j = 1,2,3\}$ .We then construct the convex set $Conv\,(Q_i) = \left\{\sum_{l=1}^{3} \beta_l q_i^{(l)} | (\forall l : \beta_l \geq 0) \wedge \sum_{l=1}^{3} \beta_l = 1\right\}$. The intuition behind $Conv\,(Q_i)$ is to construct a convex set contains points in the space that dominates p_i in one or more dimensions. By separating hyperplane theorem (see [19]), we know that if two convex sets are disjoint, there exists a hyperplane $G = \left\{x \in \mathbb{R}^3 : z^T x = z_0\right\}$ that separates one set from the other.

We formulate the following feasibility testing linear program to find a separating hyperplane between $Conv\,(Q_i)$ and $Conv\,(P)$. This hyperplane (defined by decision variable (z_0, z) with $z_0 \in R, z \in R^3$), if exists, restricts $Conv\,(P)$ to be at one side (i.e. satisfying the first inequality), and $Conv\,(Q_i)$ at another side (i.e. satisfying the first inequality) of the hyperplane.

$$
\begin{aligned}
\max_{z_0, z} \quad & 0^T z \\
\text{subject to} \quad & z^T p_k - z_0 \leq 0 \;\; \forall\, p_k \in P \\
& z^T q_i^{(l)} - z_o \geq 1; \forall\, q_i^{(l)} \in Q_i
\end{aligned}
$$

Theorem 2.2.1. *Strategy output p_i is on the 3-D Pareto Frontier if and only if there exists (at least) one feasible solution (z_0, z) such that a separating hyperplane could be found, given $Conv\,(P)$ and $Conv\,(Q_i)$.*

Proof. We apply the definition of Pareto optimality from (35), page 177: Given a set of feasible points P, a point $p_i \in \mathbb{R}^3$ is Pareto optimal if and only if $\left(p_i + \mathbb{R}^3_-\right) \cap P = \{p_i\}$. Since smaller values are preferred along each dimension, the convex cone $\left(p_i + \mathbb{R}^3_-\right)$ can be interpreted as the set of values that are better than or equal to p_i . The above condition states that the only value that is better than or equal to p_i should be p_i itself. We will show the condition $\left(p_i + \mathbb{R}^3_-\right) \cap P = \{p_i\}$ is equivalent to $Conv\left(Q_i\right) \cap Conv\left(P\right) = \varnothing$.

The forward direction: We first show $\left(p_i + \mathbb{R}^3_-\right) \cap P = \{p_i\}$ leads to $\left(p_i + \mathbb{R}^3_-\right) / \{p_i\} \cap Conv\left(P\right) = \varnothing$. This can be simply proved by contradiction: suppose $\left(p_i + \mathbb{R}^3_-\right) / \{p_i\} \cap Conv\left(P\right) \neq \varnothing$, there must exist at least one vertex of $Conv\left(P\right)$ inside the set $\left(p_i + \mathbb{R}^3_-\right) / \{p_i\}$, which contracdicts our assumption. Now, given $\left(p_i + \mathbb{R}^3_-\right) / \{p_i\} \cap Conv\left(P\right) = \varnothing$ and by definition of $Conv\left(Q_i\right)$,we know that $Conv\left(Q_i\right)$ is a subset of $\left(p_i + \mathbb{R}^3_-\right) / \{p_i\}$, thus $Conv\left(Q_i\right) \cap Conv\left(P\right) = \varnothing$ is true.

The reverse direction: (by contradiction) Suppose $\left(p_i + \mathbb{R}^3_-\right) / \{p_i\} \cap P \neq \varnothing$. Let p_j be one of the points in the intersection. Since we restricted ϵ should be smaller than the minimum pairwise difference in any dimension (i.e., $\epsilon < min|p_{i,j} - p_{i',j}|, \forall i, i' = 1, \ldots, n, j = 1, 2, 3$)), then the line segment $\lambda p_i + (1 - \lambda) p_j, 0 \leq \lambda \leq 1$ intersect with $Conv\left(Q_i\right)$. Also, $\lambda p_i + (1 - \lambda) p_j \subset Conv\left(P\right)$ (by definition) leads us to $Conv\left(Q_i\right) \cap Conv\left(P\right) \neq \varnothing$. Given $\left(p_i + \mathbb{R}^3_-\right) / \{p_i\} \cap P \neq \varnothing \Rightarrow Conv\left(Q_i\right) \cap Conv\left(P\right) \neq \varnothing$, we have $Conv\left(Q_i\right) \cap Conv\left(P\right) = \varnothing. \Rightarrow \left(p_i + \mathbb{R}^3_-\right) \cap P = \{p_i\}$. This completes the proof. □

Sensitivity Analysis

We conducted univariate and probabilistic sensitivity analyses where we varied the disease occurrence probabilities, the delay in patients presenting for care, as well as other parameter values including the test sensitivities and specificities, test and treatment costs, health utilities and disease progression parameters.

2.3 Results

Balancing antibiotic over- and underuse

When minimizing the total weighted penalty of antibiotic under- and overuse (Equation (1)) in the initial setting where there are only four types of infections and three treatment strategies (empiric doxycycline to all patients, bacterial test and if positive administer doxycycline, viral test and if negative administer doxycycline) we found the following conditions:

- If $(p_{bac} + p_{other_{bac}}) \leq 1/\left(1 + \frac{w_{under}}{w_{over}}\right)$, then both the bacterial and the viral test strategies have a smaller overall penalty than the empiric doxycycline strategy. Here, $p_{bac}+p_{other_{bac}}$ is the probability of presenting with bacterial disease treatable with doxycycline, whether or not a test exists for this infection, and w_{under}/w_{over} is the ratio of the penalties per patient under/over treated with doxycycline. This condition states that, when the prevalence of bacterial disease is low, or when the penalty for overuse of antibiotics is large, using a strategy that tests for either viral or bacterial disease before prescribing antibiotics is preferred to the strategy that distributes antibiotic treatment to all patients.

- If $\frac{w_{under}}{w_{over}} (p_{bac} + p_{other_{bac}}) \leq p_{other}$, then the strategy administering the bacterial test incurs a smaller overall penalty than the strategy administering the viral test. This condition states that, when the probability of presenting with doxycycline-treatable infection is low, or when the penalty for over-treating is high, then the bacterial test strategy outperforms the viral test strategy.

- If $\frac{w_{under}}{w_{over}} (p_{other_{bac}}) > p_{other} + p_{viral}$, then the strategy administering the viral test leads to a smaller overall penalty than the strategy administering the bacterial test. This condition states that when the probability of presenting with infections non-treatable with doxycycline is low, or when the penalty for under-treatment is high, then the viral test strategy outperforms the bacterial test strategy.

Numerical Results: Bacterial- versus Viral-endemic settings in Thailand

We now turn to evaluate health outcomes, costs and antibiotic overuse outcomes in the more realistic bacterial-endemic setting (Scenario A) and viral-endemic setting (Scenario B) in Thailand. The per-patient costs incurred (in USD), health burden (in DALY) and antibiotics overuse (Prob(over)), underuse (Prob(under)) for each strategy are shown in Table 2.3 for patients seeking care on the fourth day of illness (average day of hospital presentation). Results for patients seeking care on the first, and tenth day of illness can be found in Appendix A.

We note that, under a standard analysis that considers only the dimensions of health benefit (DALY averted) and incremental costs, without penalizing antibiotic overuse, empirical antibiotic treatment to all patients (Strategy 2) always dominated all other strategies regardless of when patients present for care or which endemic scenario we consider. Empirical antibiotic treatment incurs the lowest cost: \$100.6/patient in bacterial-endemic Scenario A and \$108.7/patient in viral-endemic Scenario B when patients delay in presenting for care to day four of illness. This strategy also incurs the lowest DALYs: 0.9 DALYs/patient in Scenario A and 0.7 DALYs/ patient in Scenario B. If patients delay in presenting for care to day ten of illness, both costs and DALYs increase (compared to day four), but remain the lowest for Strategy 2: \$149.5/patient (Scenario A), \$122.1/patient (Scenario B); 1.7 DALYs/patient in Scenario A, and 0.9 DALYs/patient in Scenario B. For patients presenting to hospital on the first day of illness, both costs and DALYs decrease (compared to day four), again still being the lowest for Strategy 2: \$47.5/patient (Scenario A), \$94.1/ patient (Scenario B); 0.2 DALYs/patient in Scenario A, and 0.5 DALYs/patient in Scenario B.

However, Strategy 2 resulted in the highest likelihood of antibiotic overuse per patient (Scenario A: 38.1%, 19.3%, 7.5% for patients presenting on day one, day four, and day ten respectively; Scenario B: 82.9%, 42.1%, 16.3% for day one, day four, and day ten respectively). In the bacterial-endemic Scenario A, Strategy 2 became suboptimal

Strategies / Scenarios		Scenario B: Viral-Endemic				Scenario B: Viral-Endemic			
		Costs	DALYs	P(over)	P(under)	Costs	DALYs	P(over)	P(under)
1	No Antibiotics *º	216.166	2.911	0	0.394	138.978	1.258	0	0.109
2	Empirical All *º	100.576	0.964	0.193	0	108.692	0.721	0.421	0
3	Empirical Severe*	137.058	1.44	0.055	0.248	118.573	0.851	0.119	0.068
4	Dengue RDT	137.329	1.546	0.102	0.085	119.048	0.881	0.144	0.023
5	Dengue PCR *º	122.947	1.254	0.102	0	116.484	0.801	0.095	0
6	Lepto RDT *º	160.5	1.94	0.003	0.163	133.291	1.127	0.007	0.072
7	Lepto PCR *	148.763	1.696	0.007	0.086	133.176	1.089	0.015	0.056
8	S: Lepto RDT, typhus RDT º	155.767	1.859	0.006	0.28	131.57	1.097	0.012	0.125
9	S: Lepto PCR, typhus RDT *º	152.117	1.627	0.009	0.143	138.125	1.063	0.019	0.096
10	S: Lepto RDT, typhus PCRº	152.708	1.844	0.008	0.254	129.575	1.092	0.016	0.113
11	P: Lepto PCR, typhus PCR	165.897	1.581	0.014	0.063	154.246	1.04	0.03	0.046
12	P: Lepto RDT, typhus RDT	163.842	1.838	0.007	0.143	140.368	1.089	0.014	0.064
13	P: Lepto PCR, typhus RDT	159.399	1.612	0.01	0.069	146.815	1.055	0.021	0.049
14	P: Lepto RDT, typhus PCR	175.228	1.881	0.01	0.121	148.564	1.085	0.021	0.055
15	Multiplex PCR*º	184.539	1.524	0.007	0.052	176.346	1.042	0.015	0.047

Table 2.3: Strategy outcomes: patients seeking care on the **fourth** day of illness

For each scenario, we identified the strategies that were on the three-dimensional effectiveness frontier, where the three dimensions are DALY, cost and antibiotic overuse. * = strategies on the cost-effectiveness frontier (economically efficient) for Scenario A (bacterial-endemic); º = strategies on the cost-effectiveness frontier (economically efficient) for Scenario B (viral-endemic).

for net monetary benefit (with WTP = Thailand GDP per capita) when the antibiotic overuse penalty was larger than $12,800/course, $18,400/course, $23,900/course for patients presenting on day one, day four, and day ten respectively. In the viral-endemic Scenario B, Strategy 2 became suboptimal when the antibiotic overuse penalty was larger than $1,100/course, $1,500/course, $1,600/course for patients presenting on day one, day four, and day ten respectively. The effectiveness of the current protocol recommended by WHO guidelines (Strategy 3, empirical antibiotic treatment to only severe patients) was sensitive to the disease probability distribution: Strategy 3 was on the three-dimensional effectiveness frontier only in Scenario B for day one, and in Scenario A for day four. Compared to Scenario A, we observed that single test strategies (Dengue PCR, and Lepto RDT) had the highest NMB for a much wider range of WTP and penalty values in Scenario B than in Scenario A. These findings were consistent with our analytical results: testing strategies are more likely to be optimal when the probability of presenting with antibiotic-treatable disease is smaller. Multiplex PCR

test (Strategy 15), with sensitivities >= 90% for each disease component, dominated other strategies for penalty >= \$13,000/course in both settings when the WTP per DALY averted is set to Thailand's GDP per capita. More importantly, when we set the penalty (w_{over}) and the WTP to Thailand's GDP per capita, we found that empirical antibiotic treatment (Strategy 2) was only cost-effective in Scenario A (not in Scenario B), which is consistent with the analytical results (details in Appendix A).

Figure 2.3 shows the optimal policy (with highest NMB) at varying values of WTP on the y-axis and antibiotic overuse penalty on the x-axis, for patients presenting on day one of illness (Figure 2.3a), fourth day of illness (Figure 2.3b) and tenth day of illness (Figure 2.3c). For Bacterial-endemic Scenario A on day four, we did not show the cost-effectiveness region for Strategy 3 since it is only cost-effective for a tiny region around the left corner. Policies with highest NMB for patients presenting on the fourth day of illness are similar to those for patients presenting on the (Figures 2.3a and 2.3b). RDT-led strategies had higher NMB when patients presented on the tenth day of illness (Figure 2.3c).

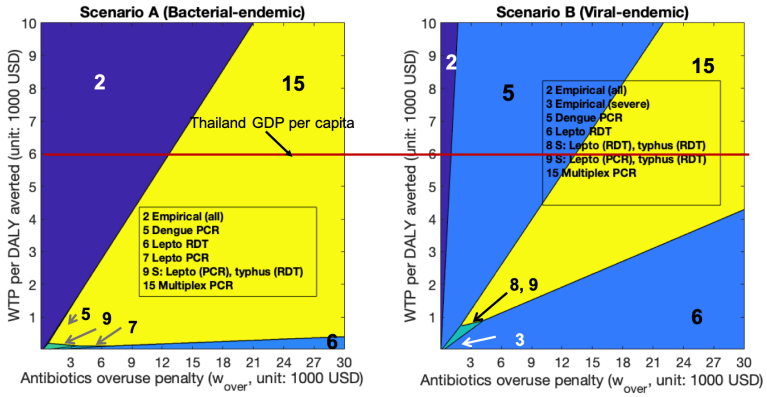

(a) Presenting on first day of illness

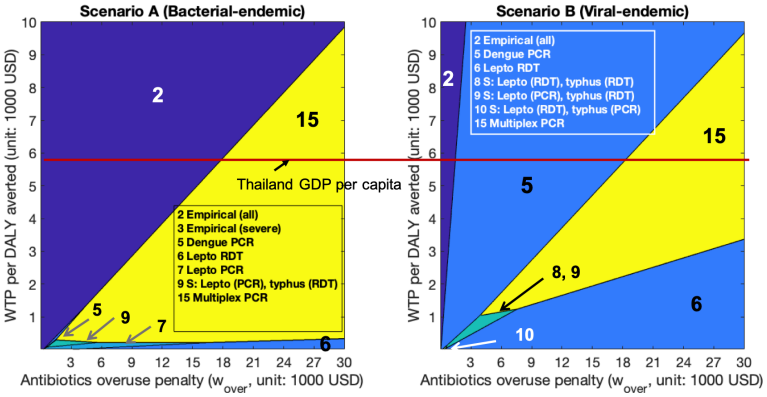

(b) Presenting on fourth day of illness

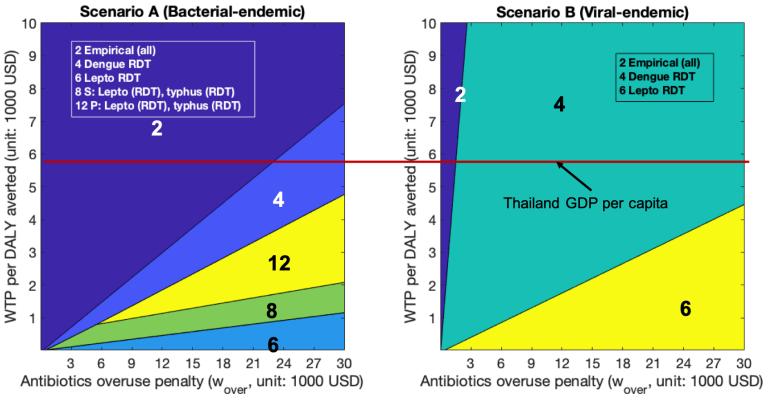

(c) Presenting on tenth day of illness

Figure 2.3: Optimal Policies with highest NMB

Sensitivity Analysis

The general structure of the optimal strategy sequence did not change when considering two additional disease probability distribution scenarios in Thailand, and conclusions remained consistent with the analytical and numerical results: first, test strategies were more likely to be cost-effective with a lower prevalence of bacterial diseases, and higher penalty (w_{over}). Second, RDT-led strategies stood out for patients presented on the tenth day of illness. Third, patients are always encouraged to present early to avoid worsened health outcomes.

We performed one-way sensitivity analysis for all other variables, where we fixed the disease occurrence probabilities to the ones in Scenario A, and assumed patient present on day one. We found that the empirical antibiotic treatment strategy has the highest NMB, or equivalently, gives smaller ICER compared to Multiplex PCR (Figure A.2) with younger patient age, lower leptospirosis-component sensitivity, higher disease-specific mortality rate, and longer test wait time. The remaining parameters like test and health costs, disability weights were not sensitive to variation.

Lastly, we conducted a probabilistic sensitivity analysis using Monte Carlo simulation (details in Appendix A). Our analyses indicate that when the penalty on antibiotics overuse is between \$0 to \$15,000/course, empirical treatment is most likely to be cost-effective, while strategies with single dengue tests (Strategy 5 Dengue PCR and Strategy 4 Dengue RDT) could be alternatives to reduce antibiotics overuse. Another key observation is that PCR-led strategies (Strategy 15 with at most 40% chance, Strategy 11 with at most 30% chance) had a much higher chance of being cost-effective than RDT-led strategies even when patients' delays (0 – 10 days) in seeking care and test wait times (0 – 3 days) were randomly sampled, suggesting that PCR-led strategies are more robust under parameter uncertainty.

2.4 Discussion and Conclusion

Febrile illness presenting similar symptoms has become a pressing public health problem worldwide. Empirical antibiotics administration without testing is the most cost-effective clinical management strategy if antibiotics overuse is not a concern. However, antibiotics misuse/overuse has become a significant health issue all over the world, and has been identified as the critical driver for antibiotics resistance ([131], [9], [150]).

In this paper, we proposed a simple framework to evaluate the cost-effectiveness of different clinical management strategies to balance antibiotics overuse and underuse. Our analysis suggests that empirical antibiotics treatment will always be the best strategy when antibiotic use reduction is not a concern. However, as the priority of reducing antibiotic overuse increases, strategies with tests stand out. Our three-dimensional cost-effectiveness analysis with case studies in Thailand has confirmed that disease prevalence, test sensitivity and specificity are highly influential to the choice of optimal strategy. By varying patients' delay in seeking care, we conclude that patients should be encouraged to present to hospital in the earlier stage of disease (i.e., first a few days of illness) to avoid worsened health outcomes.

In addition to disease prevalence and test parameters, sensitivity analysis shows that the choice of the optimal strategy was also sensitive to cohort age, the amount of resources available (WTP) and the level of importance of antibiotics reduction (overuse penalty) in the respective setting. In all cases, empirical antibiotics administration was the most cost-effective strategy when antibiotics overuse is not a concern. However, strategies involving diagnostic tests (i.e., multiplex PCR tests) produced higher net monetary benefit than the empirical treatment strategy once the decision makers started penalizing antibiotics overuse.

In both bacterial-endemic Scenario A (Northern Thailand) and viral-endemic Scenario B (Bangkok), for patients referred to hospitals on their first day of illness, we found that PCR-led strategies are more likely to be on the cost-effectiveness frontier

rather than RDT-led strategies. This is because that test sensitivities of PCR tests are higher than RDT tests when patients present to hospitals early (see Appendix Table A.1). However, if patients presented to hospitals in the later stage of diseases (i.e., >= fifth day of illness) RDT-led strategies perform better. Nevertheless, when all parameters were varied simultaneously (probabilistic sensitivity analysis), PCR-led strategies are more likely to be cost-effective than RDT-led strategies. This suggests that PCR-led strategies such as prescribing multiplex PCR, or parallel test of leptospirosis and scrub typhus are relatively robust under parameter uncertainty.

Our analysis has several limitations. First, we assumed that the underlying disease probabilities are known to policy makers. In practice, it might be difficult for clinicians to estimate the true underlying prevalence of competing source of infections. Second, we did not model the transmission of diseases, as the focus of this present study was to address the critical questions of what diagnostic test to use and when to administer antibiotics to already infected patients. However, the optimal strategy structure remains the same through various sensitivity analyses performed.

Our study can better inform clinical decisions about when to administer antibiotics and which diagnostic tests to apply for undifferentiated febrile patients. To the best of our knowledge, we are the first to propose a decision-making framework balancing antibiotic overuse and underuse in order to optimize the choice of clinical management strategy. Besides, our disease progression model captures essential features such as multiple competing causes of infections, patients' delays in seeking care and the illness-stage-dependent accuracy (of diagnostic tests). Our analysis highlights the importance of diagnostic tests in helping reducing antibiotics usage in the clinical management of febrile illnesses, although the choice of strategy depends on the disease distribution and diagnostic test parameters (sensitivity, specificity).

Chapter 3

Monitoring Policy Optimization for HIV patients with Heterogeneous Adherence Types

3.1 Introduction

Over the last a few decades, a trend of increasing total expenditure in healthcare has been witnessed worldwide [46], the cost associated with wasteful, inefficient healthcare delivery has risen sharply in the meantime [112]. Estimates of hospitalization costs due to medication nonadherence are as high as $13.35 billion annually, in the U.S. alone [92]. The uncertainty in patient adherence to medication regimens for chronic conditions results in wasted medical resources, a higher chance of treatment failure on designated therapies and worsened health benefit of patients [129].

In the context of human immunodeficiency virus (HIV) management, antiretroviral therapy (ART), which aims at suppressing viral load in patient body, is recommended worldwide. In order to be effective, ART regimens require 70 - 90% adherence from patients [103]. However, current estimates of ART treatment adherence varies from

a mean of 55% to 75% in different studies [169, 80, 30]). For HIV-infected (HIV+) patients on ART treatment, viral load (henceforth VL) monitoring is recommended by the World Health Organization (WHO) guideline [166]. Timely detection of virologic failure (i.e., failure to suppress HIV VL in the patient body) can help improve patient health outcomes and reduce the chance of HIV transmission by switching to a to a second-line ART. However, frequent clinical visits, VL tests are often prohibitive due to its high cost [75], especially in low-resource settings.

The fundamental trade-off in this context is to balance "over-monitoring" and "under-monitoring" of HIV-infected patients. Frequent monitoring might incur a higher healthcare-related cost but ensures patients are in the preferred health states (i.e., virally suppressed), however, it might be too costly for patients in low-resource settings. On the other hand, infrequent check-up might incur fewer VL test costs, but patients might spend longer time in unfavorable health states, and transmit HIV virus to potentially more people.

Previous literature has shown that patient adherence differs from each other in different chronic disease contexts [12, 137]. Thus, one might expect HIV patient to hav heterogeneity effect in adherence behavior. If this is the case, one-size-fits-all monitoring policies might not be optimal. Although adaptive, and personalized care using VL test has been studied in the literature [118, 106], the extent to which monitoring policies that differentiating patient adherence type that might be cost-effective remains unknown.

The preceding discussions give rise to a few important research questions in HIV management: First, how the decision maker could optimize monitoring policies utilizing a patient adherence information up to date? More importantly, would the optimized monitoring policy outperform the status quo?

Our work could be viewed as a one key step further toward answering these questions. We first formulate a stylized HIV disease progression model, and used the model to identify optimal monitoring interval. We derive theoretical results and structural properties of the optimization model. We provide an equation where the exact optimal

policy can be directly computed. We also present extensions of the base model which captures a unique, important feature of HIV disease: opportunistic infections. Second, we present a case study using representative data [106] for Uganda (an African county with GDP per capita at $615 USD in 2016 [167]). We numerically proved that the optimized policies are all on the cost-effectiveness frontier, and in certain circumstances dominates the fixed policies.

Our contributions in this work are threefold. First, we provide policy-relevant structural properties of the stochastic model that allow our framework to be useful in contexts of the particular application of HIV management. Our analyses lead to theoretical guarantees which allow us to interpret the model and derive optimal monitoring interval for any patient demographic distribution. Second, we validate our approach with a representative numerical study using Uganda's HIV patient profile. Our study can help make better monitoring decisions to improve patients outcome, save costs, and reduce transmission in the presence of heterogeneous adherence behavior.

The remainder of this chapter is organized as follows. We present the base model in Section 3.2, Then, we performed structural analysis on the base model, and provide the equation to compute the exact optimal solution in Section 3.3. In Section 3.4, we extend the base model to incorporate opportunistic infections, and discuss the relationship among all models introduced in this work. In Section 3.5, we present a case study with a benchmark in Uganda, where the societal resources are limited. We conclude our study in Section 3.6.

3.1.1 Literature Review

There is a rich literature on adapting Markov Decision Processing modeling frameworks to optimize for better informed medical decisions. For example, [11] used a POMDP to personalized mammography screening decisions for breast cancer patients; [136] proposed a POMDP model to find the optimal timing of drug sensitivity testing

for patients on first-line tuberculosis treatment. In terms HIV applications, [132] applied an MDP model framework to decide the optimal time to initiate HIV treatments. However, none of these studies have addressed the impact of disease transmission in monitoring policy optimization in chronic disease management. There is also a line of work addressing patient heterogeneity in different context into the medical decision-making framework. For example, [107] considered patient heterogeneity in treatment effectiveness in treating chronic diseases like multiple sclerosis. [13] and [137] considered patient heterogeneity in screening and treatment adherence accordingly. Our study shares similarity to the aforementioned studies. Nevertheless, most studies defined defined "non-adherence" as non-compliance (i.e., losses of follow-ups), where we address the partial non-adherence of missing pills, but not completely losses of follow-ups.

3.2 Model framework

We formulate a discrete time, infinite horizon stochastic model on decision epoch $t = 1, 2, \cdots, \infty$, to capture HIV disease progression on (first-line) ART, in which a single decision maker (henceforth DM) (e.g., a physician) is aiming at maximizing the total discounted expected patients' health benefit by making decisions on the optimal time interval (denoted by N) to perform HIV VL test at each decision epoch. We do not consider optimizing monitoring intervals for patients on second-line ART since detection of virologic failure could not help further improve patient health outcome. We assume patient adherence behavior is heterogeneous: the probability of being adherent (denoted by θ) at each month is patient-specific. We prove the exact distribution, existence and significance of considering patient adherence heterogeneity in Section B.2.

We assume the patient adherence type is fully revealed to the DM prior to treatment initiation, and the frequency of clinical visits does not affect patient adherence behavior. We also simplify the health state space to track only the viral load status (i.e., whether the patient is virally suppressed, or in virologic failure). CD4 cell count is another an

important biomarker that indicates HIV patients health states. In Appendix Section B.2, we discuss the reason why we selected viral load as our health state instead of CD4 cell count.

At time t, if the patient has a VL test, and VL failure is detected, he or she would switch to a second-line regimen and quit the decision process by receiving a terminal reward (denote by R). Otherwise, the patient continues the decision process if virologic failure was not detected. In addition, we estimate the number of secondary infections/transmissions at each month based on the patient's health state (patients in virologic failure have a much higher chance of transmitting HIV to others). We summarize the notations used in the model as follow:

- Time: $t \in \mathcal{T} = \{0, 1, 2, ..., \infty\}$, discretized in month.
- Decision times: $k = 0, 1, 2, .., N$. We assume that the k-th screening and monitoring decisions are made at the time t_k. We define $t_0 = 0$.
- Action $N_k \in \mathcal{N} = \{1, 2, ..., \infty\}$: a_k represents the decision on the VL monitoring interval (i.e., time for the clinical visit, $t_{k+1} = t_k + N_{k+1}$)
- Adherence state $A_t \in \mathcal{A}$: Patients could either be adherent (A^+) or non-adherent (A^-) at each month. Adherence state A_t will be revealed to DM if there is a clinical visit at month t. The probability of being adherent is determined by the patient-specific adherence type θ: $P(A^+|\theta) = \theta$. We assume θ is fixed and given.
- Core Health States: $X_t \in \mathcal{S} = \{s_1 : \text{virally suppressed};\ s_2 : \text{virologic failure};\ s_3 : \text{dead}\}$. Upon failure detection (in state s_2 and performed VL test), the patient will be switched to a second-line regimen. Death (s_3) is an absorbing state. Living states $\{s_1, s_2\}$ are observable during clinical check-ups visits by performing a VL test, and not observable in between monitoring intervals.
- $P(X_{t+1}|X_t, A_t)$: health state transition probability. The probability that a patient will be in state $s' \in \mathcal{S}$ at time $t+1$, given that he or she was in state s at time t and

his or her adherence state A_t. Denote the transition probability matrix (TPM) given A_t as $\mathbb{P}(A_t) =$

$$\begin{bmatrix} p_{11,A_t} & p_{12,A_t} & p_{13} \\ 0 & p_{22} & p_{23} \\ 0 & 0 & 1 \end{bmatrix}$$

We have $p_{11,A+} > p_{11,A-}$, and $p_{12,A+} < p_{12,A-}$. That is to say, the monthly probability of virologic failure is higher for a non-adherent patient. We let $\mathbb{P}(\theta)$ represent the expected TPM given adherence type θ, which is computed as $\mathbb{P}(\theta) = \theta\mathbb{P}_t(A+)+(1-\theta)\mathbb{P}_t(A-)$. We denote the space of all possible transition probability matrices as $\mathcal{P}$.

- $e_t \in \{0, 1\} = \mathcal{E}$: At any month t, an HIV-infected patient could induce secondary infections (i.e., $e_t = 1$) or no transmission (i.e., $e_t = 0$). Even though we do not tend to explicitly model HIV transmission in our framework, we estimate the number of secondary infection given patient health status at each month [122, 164][1]. We denote $P(e_t = 1|X_t)$, for $X_t \in \{s_1, s_2\}$ as the probability of having a secondary infection at time t, conditioning on the patient's health state.

- rewards space $\mathcal{R}$, which contains all possible rewards and costs including monthly rewards, VL test cost, and the terminal reward.

  - $r(X_t, e_t)$: reward between time t to $t + 1$, given patient health state X_t, and $e_t \in \mathcal{E}$.
  - $r(X_t)$: expected reward gained between time t to $t + 1$, given patient health state X_t. We have $r(X_t) = \sum_{e\in\{0,1\}} r(X_t, e_t)P(e_t|s)$.
  - VL test cost : $c > 0$
  - R: terminal reward received upon failure detection (estimated cumulative

[1] We recognize that theoretically, e can be large than 1 (i.e., more than one secondary infections per month). However, as we will see in Section 3.5, e is generally less than one in reality.

rewards when a patient switched to a second-line regimen). Without loss of generality, we assume R is non-negative.

- (monthly) discount factor: $0 < \delta < 1$

We use the tuple $(\mathcal{T}, \mathcal{N}, \mathcal{A}, \mathcal{S}, \mathcal{P}, \mathcal{E}, \mathcal{R})$ to summarize the parameters used in the stochastic model. We write infinite state sequence as $\mathbf{X} = \{X_0, X_1, X_2, ...\}$ and action sequence as $\mathbf{N} = \{N_1, N_2, ...\}$,then, the Decision Maker (DM)'s goal is to find an action sequence $\mathbf{N}$ such that the total expected discounted rewards $\mathbb{E}_{\mathbb{P}}\, r(\mathbf{X}, \mathbf{N})$ is maximized:

$$\mathbb{E}_{\mathbb{P}}\, r(\mathbf{X}, \mathbf{N}) = \mathbb{E}_{\mathbb{P}} \sum_{k=0}^{\infty} \left[\left(\sum_{t=t_k}^{t_{k+1}} \delta^t \cdot r_t(X_t) \right) \mathbb{1}_{\{X_{t_k} = s_1\}} + \delta^{t_{k+1}} R \cdot \mathbb{1}_{\{X_{t_{k+1}} = s_2\}} - \delta^{t_{k+1}} \cdot c \cdot \mathbb{1}_{\{X_{t_{k+1}} \neq s_3\}} \right] \tag{3.1}$$

In Equation (3.1), $\mathbb{P}$ is the transition probability matrix (which determines the state sequence $\mathbf{X}$), and $\mathbf{N}$ is the controllable action sequence such that $t_{k+1} = t_k + N_{k+1}$.

3.3 Model Analysis

We first provide an overview of this section. In this section, we first rewrite the objective (Equation 3.1) in a recursive manner, and provide structural analyses including the quasi-concavity of the objective function (Theorem 3.3.1), and structure of the optimal policy (Proposition 1). In particular, the optimal policy can be derived by solving a simple exponent equation (Equation B.8 in Theorem 3.3.1). The analysis requires a few mild assumptions to hold, including the relative order among the event probabilities, and rewards (Assumption 3.3.1, 3.3.2, 3.3.3). In addition, we assume the state transition probabilities have the "increasing failure rate" property (which is equivalent to totally positive of order 2 for finite, discrete state transition matrix, see Definition B.1.1): patients in "better" health states have a higher probability of moving to any particular health state or better (Definition B.1.1, and Lemma B.1.3). To simplify

notation in our proofs, we suppress the parameter θ whenever possible (since in our non-learning model, it is assumed to be known). We defer the some of the auxiliary lemmas, propositions, and definition details, and all proofs in Appendix Section B.1.

We write the total discounted reward starting at time t_k as follows:

$$r(\mathbf{X_{t_k}}, \mathbf{N_k}) = \sum_{t=t_k}^{t_{k+1}-1} \delta^{t-t_k} \cdot r_t(X_t) + \delta^{N_{k+1}} \left[r(\mathbf{X_{t_{k+1}}}, \mathbf{N_{k+1}}) \mathbb{1}_{\{X_{t_{k+1}}=s_1\}} + R\mathbb{1}_{\{X_{t_{k+1}}=s_2\}} - c\mathbb{1}_{\{X_{t_{k+1}}\neq s_3\}} \right], \tag{3.2}$$

where $r(\mathbf{X_{t_k}}, \mathbf{N_k})$ is the reward mapping function given the truncated state sequence starting from X_{t_k} $\mathbf{X_{t_k}} = \{X_{t_k}, X_{t_k+1}, ...\}$ and the truncated action sequence $\mathbf{N_k} = \{N_{k+1}, N_{k+2}, ...\}$. Given any state and action sequence $\mathbf{X_{t_k}}$ and $\mathbf{N_k}$, one can construct a recursive expression of total expected rewards using Equation (3.2). The recursive formula can be applied to any of the health states defined earlier. Nevertheless, by the model assumption, virologic failure will be detected during clinical visits, by performing VL test (and thus switched to a second-line regimen).. That is, in reality, the patient cannot start with state s_2 (virologic failure). Death (s_3) on the other hand, is directly observable at beginning of each time t. Since the time horizon is infinite, we focus on finding stationary policies $\{N_k = N\}_{k\geq 1}$ for some N (such that $t_{k+1} = t_k + N$, for all $k = 0, 1, 2, ...$) that maximizes the objective (Equation 3.1). Also, we can always reset the beginning of time to $t = 0$ in the infinite time horizon case. Given Equation 3.2, we can rewrite the object as follows:

$$\begin{aligned} &\mathbb{E}_{\{\mathbb{P}, X_0=s_1\}} r(\mathbf{X}_{t_k}, N) \\ =&\mathbb{E}_{\{\mathbb{P}, X_0=s_1\}} \left\{ \sum_{t=0}^{N-1} \delta^t r_t(X_t) + \delta^N \left[r(\mathbf{X_N}, N) \mathbb{1}_{\{X_N=s_1\}} + R\mathbb{1}_{\{X_N=s_2\}} - c\mathbb{1}_{\{X_N\neq s_3\}} \right] \right\} \end{aligned} \tag{3.3}$$

We can further express the objective in Equation 3.3 as follow using Lemma B.1.2:

$$\begin{aligned}
\mathbb{E}r(\mathbf{X}, N) &= \mathbb{E}\Bigg\{ \sum_{t=0}^{N-1} \delta^t r_t(X_t) + \delta^N \Big[r(\mathbf{X_N}, N)\mathbb{1}\{X_N = s_1\} + R\mathbb{1}\{X_N = s_2\} - c\mathbb{1}\{X_N \neq s_3\} \Big] \Bigg\} \\
&= \sum_{t=0}^{N-1} \delta^t \Big(r_t(s_1) P_{11}^t(\theta) + r_t(s_2) P_{12}^t(\theta) \Big) + \delta^N \Big[\mathbb{E}r(\mathbf{X}, N) P_{11}^N(\theta) + R P_{12}^N(\theta) - c(1 - P_{13}^N(\theta)) \Big] \\
&= \frac{\sum_{t=0}^{N-1} \delta^t \Big(r_t(s_1) P_{11}^t(\theta) + r_t(s_2) P_{12}^t(\theta) \Big) + \delta^N P_{12}^N(\theta) R - \delta^N c (P_{11}^N(\theta) + P_{12}^N(\theta))}{1 - \delta^N P_{11}^N(\theta)}
\end{aligned} \tag{3.4}$$

The first equality follows by moving the expectation operator into the bracket, and Lemma B.1.2. The second equality follows by moving $\mathbb{E}r(\mathbf{X}, N)$ to the left-hand side.

Before we proceed to the formal analysis of the optimal solution, we first make a few mild assumption and the orders of rewards, event probabilities.

Assumption 3.3.1. *Relative orders among rewards and probabilities.*

- $\forall e \in \mathcal{E},\ r(s_1, e) > r(s_2, e)$ *and* $r(s_3, e) = 0$*;*
- $\forall s \in \{s_1, s_2\},\ r(s, e = 0) > r(s, e = 1)$ *and* $P(e = 1|s_1) < P(e = 1|s_2)$*.*
- $p_{13} < p_{23}$*.*

The first point of Assumption 3.3.1 states that given the same event, patients in a healthier state (i.e., virally suppressed) should always receive higher one-time reward per month. Patients in state s_3 (dead) receive zero health benefit. The second statement means that one-month reward is larger with less severe for any given state s, and the probability of "bad" events happening is smaller for healthier patients. The last point of Assumption 3.3.1 states that the probability of death is smaller for healthier patients. Using Assumption 3.3.1, and the definition of periodic reward $r_t(s)$, we have the following lemma, stating that the expected period reward is higher if the patient is virally suppressed.

Lemma 3.3.1. $r_t(s_1) \geq r_t(s_2)$.

Assumption 3.3.2. $\frac{r(s_1)}{1-\delta} \geq R - c \geq \frac{r(s_2)}{1-\delta}$.

Assumption 3.3.2 states that if possible to stay as virally suppressed, then it is better for a patient to stay in state s_1 up to time infinity (but at with a monthly discount rate δ), rather than perform a VL test and receive the terminal reward. Similarly, the second part of Assumption 3.3.2 states that it is better for a patient to perform the VL test, and receive the terminal reward rather than staying in virologic failure forever. Next, we would like to investigate the structural properties of the objective function (i.e., quasi-concavity, and monotonicity in terms of θ).

Corollary 3.3.1. *Properties of the TPM.*

1. $\mathbb{P}^t(\theta)$ *is TP2, for any* $t \geq 0$.
2. *Let* $p_{11} = \theta p_{11,A+} + (1-\theta)p_{11,A-}$ *and* $p_{12} = \theta p_{12,A+} + (1-\theta)p_{12,A-}$ *(we suppressed* θ *for clarity). Then, we express the explicit form for* $\mathbb{P}^t(\theta)$ *as:*

$$\begin{bmatrix} p_{11}^t & p_{12}p_{11}^{t-1}\frac{1-(\frac{p_{11}}{p_{22}})^t}{1-\frac{p_{11}}{p_{22}}} & 1-p_{11}^t - p_{12}p_{11}^{t-1}\frac{1-(\frac{p_{11}}{p_{22}})^t}{1-\frac{p_{11}}{p_{22}}} \\ 0 & p_{22}^t & 1-p_{22}^t \\ 0 & 0 & 1 \end{bmatrix}$$

Corollary 3.3.1 implies that sick patients has a greater chance of moving to a sicker state (i.e., patients in state s_2 has a higher chance of death than patients in state s_1. In addition, Corollary 3.3.1 also provided an explicit expression for the t-step TPM. For notational convenience, denote $q_{11} = \delta p_{11}$, $q_{12} = \delta p_{12}$, and $q_{22} = \delta p_{22}$, and denote $V(N) = \mathbb{E}r(\mathbf{X}, N)$ as the expected reward gained for monitoring a patient every N time. We then try to refine our objective equation 3.4 to make it more explicit. We express

$V(N)$ (for a patient for given adherence type θ) as

$$\begin{aligned}
&\frac{\sum_{t=0}^{N-1}\delta^t\left(r_t(s_1)P_{11}^t(\theta)+r_t(s_2)P_{12}^t(\theta)\right)+\delta^N P_{12}^N(\theta)R-\delta^N c(P_{11}^N(\theta)+P_{12}^N(\theta))}{1-\delta^N P_{11}^N(\theta)}\\
=&\frac{\sum_{t=0}^{N-1}\delta^t\left(r_t(s_1)p_{11}^t+r_t(s_2)p_{12}p_{22}^{t-1}\frac{1-(\frac{p_{11}}{p_{22}})^t}{1-\frac{p_{11}}{p_{22}}}\right)+\delta^N p_{12}p_{22}^{N-1}\frac{1-(\frac{p_{11}}{p_{22}})^N}{1-\frac{p_{11}}{p_{22}}}R-\delta^N c\left(p_{11}^N+p_{12}p_{22}^{N-1}\frac{1-(\frac{p_{11}}{p_{22}})^N}{1-\frac{p_{11}}{p_{22}}}\right)}{1-\delta^N p_{11}^N}\\
=&\frac{\frac{(1-q_{11}^N)}{1-q_{11}}r(s_1)+\frac{q_{12}\left(\frac{1-q_{22}^N}{1-q_{22}}-\frac{1-q_{11}^N}{1-q_{11}}\right)}{q_{22}-q_{11}}r(s_2)+\frac{\left(q_{12}q_{22}^{N-1}\left(1-\left(\frac{q_{11}}{q_{22}}\right)^N\right)\right)}{1-\frac{q_{11}}{q_{22}}}R-c\left(q_{11}^N+\frac{q_{12}q_{22}^{N-1}\left(1-\left(\frac{q_{11}}{q_{22}}\right)^N\right)}{1-\frac{q_{11}}{q_{22}}}\right)}{1-q_{11}^N}
\end{aligned} \tag{3.5}$$

The first equality follows from Corollary 3.3.1, the second equality follows by doing a change-of-variable representation using q's to replace δ and p's, and summing up the periodic reward terms.

To further analyze the structure of the objective in Equation (3.5), we first relax the feasible region of the decision varaible N. Instead of $N \in \mathbb{R}^+$, we now assume we first construct a relaxation of $V(N)$, such that the decision variable $N \in \mathbb{R}^+$ instead of $\mathbb{Z}^+$. It is a relaxation because we kept the same objective function, but enlarged the feasible region (of the decision variable N). We also require an additional assumption to hold:

Assumption 3.3.3. $p_{12}\left(R-\frac{r(s2)}{1-\delta p_{22}}\right) > (p_{12}+p_{22}-p_{11})c.$

Assumption 3.3.3 states that the "expected" reward gained from failure (i.e., the LHS) should be larger than the "expected" cost spent for detecting failure (i.e., the RHS). We also verified in the Numerical Study (Section 3.5) that our condition is satisfied using Uganda demographic information.

In the following theorem, we proof that $V(N)$ is quasi-concave if $N \in \mathbb{R}+$. This is one of the key theoretical results that guarantees the existence of one unique optimal solution.

Theorem 3.3.1. *Let Assumptions 3.3.1, 3.3.2 and 3.3.3 hold. Then, $V(N)$ is quasi-concave in N if $N \in \mathbb{R}+$.*

The next proposition presents comparatives static analysis of the optimal monitoring interval N^*, solved from Equation 3.4.

Proposition 1. *Let all premises in Section 3.3 hold. Then, the following properties of the optimal monitoring interval N^* hold.*

(a) as patients become more adherent (i.e., θ increases), N^* increases.

(b) as the failure rate increases (i.e., q_{11} increases), N^* decreases.

(c) as the terminal reward increases (i.e., R increases), N^* decreases.

3.4 Extension: incorporating Opportunistic Infections

Opportunistic Infections is one of the HIV-specific events that could happen to patients. Pathogens (bacteria, viruses and fungi) take advantage of the weakened immune systems of HIV patients, and may develop serious complications. Current practice assumed that patient will present to the clinic, and been prescribing for HIV VL test ([106]). This clinic self-referral process may render the disease progression model without OI inaccurate. Moreover, we would like to construct a mathematical model that could measure the performance status quo: Is VL test necessary if the doctor observes OI? Should patient switch to an alternative ART regimen if OI was observed? With these questions in mind, we reformulate the same problem as a semi-Markov decision process (SMDP) in Section 3.4.1. An SMDP formulation is appropriate in this setting because the transition probability matrix is naturally adapted to a discrete-time Markov chain, and our decision variable is the time interval for VL monitoring. The base model (presented in the main report) can be equivalently formulated as a simpler SMDP. To further characterize the optimal policy structure, we reformulated the SMDP into a Partially Observable Markov Decision Process (POMDP) in Section 3.4.2. We discuss the relationship among different models in Section 3.4.3.

3.4.1 SMDP formulation

The action space, time, decision epoch is the same as in the base model. In addition the the health state space defined in Section 3.2, we consider an observation space as follow: at a particular time (month) t, depending on his/her true health state, the patient may experience an OI, and have self-referral to clinics, looking for the corresponding treatments for any specific OIs (but no immediate VL test prescribed). The OI observation might reveal valuable information to the decision maker on the probability of patients true health states. At time t, if the patient has a VL test, and virologic failure is detected, his or her true health state will be updated.

In addition to nations, and model parameters (reward space, action space, state space) defined in Section 3.2, we summarize the new notations for the observation space as follow:

- $o \in \{\overline{OI}, OI\} \equiv \mathcal{O}$: Opportunistic Infection is a special event associated with HIV patients. We let $\overline{OI}$ represent the compliment of OI, (i.e., no OI). We assume when OI happens, patients will show up to the clinic to for the corresponding OI treatment (but no immediate VL test). We denote by $P(o = OI|s)$, for $s \in \{s_1, s_2\}$ as the probability that an opportunistic infection happens at time t, conditioning on the patient's health state. We assume that $P(OI|s_1) < P(OI|s_2)$. For notation consistency, we define $P(OI|s_3) = 1$ and $P(\overline{OI}|s_3) = 0$ although no observation is made in state s_3.

- State Evolution: we define the health state and observation pair (s, o), $\forall (s, o) \in (\mathcal{S} \times \mathcal{O})$ as the augmented "state". We order the states in the following manner:

$$(s_1, \overline{OI}) \succeq (s_1, OI) \succeq (s_2, \overline{OI}) \succeq (s_2, OI) \succeq (s_3, \overline{OI}) \succeq (s_3, OI), \tag{3.6}$$

where we call $(s_1, \overline{OI})$ the "best" health state, and (s_3, OI) the "worst" health state. Here, we abuse the notation for the *death* state (s_3) since dead patients could not

make actions. We did this for national consistency, and for further structural property development.The corresponding state distribution at time t, denoted by π_t, belongs to the following 5-dimensional unit simplex:

$$\{\pi_t \in \mathbb{R}^6 : \mathbf{1}^T \pi_t = 1, 0 \leq \pi_t(i) \leq 1, i \in \mathcal{S}\},$$

where $\pi_t(i)$ is the probability of being in state $i \in (\mathcal{S} \times \mathcal{O})$ at time t. Note that the transition between observations are independent among the transition among health states. We then construct the transition probability matrix $\mathbb{Q}$ (for a given adherence type θ) as:

$$\begin{bmatrix}
p_{11,\theta}P(\overline{OI}|s_1) & p_{11,\theta}P(OI|s_1) & p_{12,\theta}P(\overline{OI}|s_1) & p_{12,\theta}P(OI|s_1) & p_{13}P(\overline{OI}|s_1) & p_{13}P(OI|s_1) \\
p_{11,\theta}P(\overline{OI}|s_1) & p_{11,\theta}P(OI|s_1) & p_{12,\theta}P(\overline{OI}|s_1) & p_{12,\theta}P(OI|s_1) & p_{13}P(\overline{OI}|s_1) & p_{13}P(OI|s_1) \\
0 & 0 & p_{22}P(\overline{OI}|s_2) & p_{22}P(OI|s_2) & p_{23}P(\overline{OI}|s_2) & p_{23}P(OI|s_2) \\
0 & 0 & p_{22}P(\overline{OI}|s_2) & p_{22}P(OI|s_2) & p_{23}P(\overline{OI}|s_2) & p_{23}P(OI|s_2) \\
0 & 0 & 0 & 0 & 0 & 1 \\
0 & 0 & 0 & 0 & 0 & 1
\end{bmatrix} \tag{3.7}$$

Similarly, we can define a t-step transition probability matrix $\mathbb{Q}^t$, and denote $Q^t(j|i)$ as the t-step transition probability from state i to state j. We then update our state distribution as $\pi_{t+1} = (\pi_t)^T \mathbb{Q}$. Similarly, we revise the monthly expected reward $r(s)$ defined in Section 3.2 to incorporate the observation o: we define $r(s, o)$ as the monthly expected reward gained given a patient current health state s, which is calculated as $r_t(s, o) = \sum_{e \in \mathcal{E}} r_t(s, e, o) P_t(e|s)$. Moreover, we can easily show that the enhanced TPM is of TP2, which is stated in the following lemma:

Lemma 3.4.1. *The augmented transition probability matrix $\mathbb{Q}$ is TP2.*

We use the tuple $(\mathcal{N}, \mathcal{O}, \mathcal{A}, \mathcal{S}, \mathcal{P}, \mathcal{E}, \mathcal{R})$ to summarize the parameters used in the stochastic model. Now, let $V(s, o)$ denote the optimal value function for patients in

state (s, o), and let $v_{(s,o)}(N)$ denote the total expected rewards when a patient starts in state (s, o), waits for N periods/months for next VL monitoring, and adopts an optimal policy afterwards. We express $v_{(s,o)}(N)$ as

$$v_{(s,o)}(N) = pr_{(s,o)}(N-1) - \delta^N c + \delta^N \sum_{(s',o')} Q^N\Big((s',o')|(s,o)\Big)V(s',o'), \tag{3.8}$$

where $pr_{(s,o)}(N)$ is the discounted expected lump sum periodic reward (short for pr) up to N periods:

$$pr_{(s,o)}(N) = \begin{cases} 0 & \text{if } N = 0, \\ r(s,o) + \delta \sum_{(s',o')} Q\Big((s',o')|(s,o)\Big) pr_{(s',o')}(N-1) & \text{otherwise} \end{cases} \tag{3.9}$$

Then, the optimal value function obeys the following optimality equation:

$$V(s,o) = \max\{\max_{1\le N\le\infty} v_{(s,o)}(N),\ \ \mathbb{1}_{s\neq s_3}(R-c)\}, \tag{3.10}$$

which says that the optimal action is either to wait for N months, or to switch to a second-line regimen and receive a terminal reward (i.e., quit the decision process). We note that only living patients could select the second option. Patients who are dead will receive zero terminal reward if he/she "*decided*" (in reality, dead patients cannot make any decisions) to terminate the process. Before we proceed to the statement of the optimal reward function and its structural analysis, we provide the following assumptions (on the relative order of rewards), that will be used in the proof of analytical properties of the model.

Assumption 3.4.1. *Relative order among rewards:*

- $\forall e \in \mathcal{E}$ *and* $o \in \mathcal{O}$, $r(s_1, o, e) > r(s_2, o, e) > r(s_3, o, e)$, *and* $r(s_3, o, e) < 0$
- $\forall s \in \{s_1, s_2\}$, $r(s, \overline{OI}, e_\emptyset) > r(s, OI, e_\emptyset) > r(s, \overline{OI}, e_{SI}) > r(s, OI, e_{SI})$

- $r(s_1, OI) \geq r(s_2, \overline{OI})$, *and* $\frac{\sum_o r(s_1,o)P(o|s_1)}{1-\delta} \geq R - c \geq \frac{\sum_o r(s_2,o)P(o|s_2)}{1-\delta}$

The first point in Assumption 3.4.1 states that given the same event and observation, patients in a healthier state (i.e., not in failure) should always receive higher one-time reward per month. Moreover, we assume that dead patients receive negative monthly rewards if they are still on the decision process. Although No more decisions can be made for dead patients, we make this assumption to facilitate our analysis. The second point in Assumption 3.4.1 says that one-month reward is larger with less severe (or no) events or observations for any given health state s. The last assumption was a stronger condition, which tries to order the enhanced state (s, o) such that even when a healthier patient (in s_1) is having an OI, the expected rewards is still better than a failure patient (in s_2) not having OI. As we numerically proved in [106], both the negative impact and severity of an HIV transmission (i.e., SI) is higher than an opportunistic infection (OI). The second part states that, if possible, being virally suppressed forever, is better, rather than perform a VL test and receive the terminal reward. Similarly, we assume that it is better for a patient to perform the VL test, and receive the terminal reward rather than being in virologic failure forever. We assume that $R - c$ is non-negative.

In the next Lemma and Proposition, we prove that periodic reward $pr_{(s,o)}(N)$, optimal value function $V(S, 0)$ are decreasing as the health state (s, o) deteriorates. In the meantime, both $pr_{(s,o)}(N)$ and $V(S, 0)$ are higher for adherent patients.

Lemma 3.4.2. *For any given time period N, we have the following properties of the periodic reward $pr_{(s,o)}(N)$:*

- *$pr_{(s,o)}(N)$ is decreasing in (s, o) (i.e., the periodic reward decreases when started from a "worse" state)*

- *$pr_{(s,o)}(N)$ is increasing in θ (i.e., as patients becomes more adherent, the periodic reward increases).*

Proposition 2. *The optimal value function $V(s, o)$ satisfies the following two properties:*

- $V(s,o)$ *is decreasing in* (s,o).
- $V(s,o)$ *is increasing in* θ *for a given state* (s,o).

From this lemma, we having the following theorem on the structure of the optimal monitoring interval:

Theorem 3.4.1. *There exists an optimal policy in the following form (for a fixed, but unknown threshold state* K*):* $\begin{cases} N^*(s,o) & \text{for } (s,o) \preceq K, \\ 0 & \text{for } (s,o) \succeq K, \end{cases}$ *and* $N^*(s,o)$ *is decreasing in* (s,o)*. Further,* $K \preceq (s_2, \overline{OI})$

Proof of Theorem 3.4.1. The proof is straightforward given Lemma B.1.5 and B.1.6. □

Theorem 3.4.1 implies an order of the optimal monitoring policies for all states: as the health state deteriorates, the optimal monitoring interval becomes smaller; once the patient was identified in failure (regardless of whether OI was observed), they should be switched to a second-line regimen immediately. However, Theorem 3.4.1 does not fully answer the question of whether an OI observation in the healthy state (state s_1) would trigger an immediate VL monitoring. Theorem 3.4.1 states that, if OI was observed, the monitoring interval should be smaller than not observing OI. To characterize the optimal policy more precisely, We reformulate the problem as a POMDP in the next Section.

3.4.2 POMDP reformulation

We reformulate the problem as an infinite-horizon, partially observable Markov decision process. In this section, we assume patient adherence type θ is given. We omit θ whenever possible for notational clarity. We summarize our POMDP as a tuple $(\mathcal{N}, \mathcal{O}, \mathcal{A}, \mathcal{S}, \mathcal{P}, \mathcal{E}, \mathcal{R})$ defined similarly in the SMDP model. The key differences are:

first, instead of determining monitoring interval, the action set in the POMDP formulation is binary at each month: $\mathcal{N} = \{\text{Wait, Peform VL test}\}$. Also, instead of augmenting the health state space with the observation space, we treat them separately. Recall that we defined the observation space in Section 3.4.1 as $o \in \{\overline{OI}, OI\} \equiv \mathcal{O}$ and the probability matrix $\mathbb{P}_O$ has the dimension as the state transition probability matrix$\mathbb{p}$: $|S|\times|S|$.

Then, we express the state distribution to a two-dimensional unit simplex (we omitted time t for clarity):

$$\{\mathfrak{B} \in \mathbb{R}^3 : \mathbf{1}^T\pi = 1, 0 \leq \pi(i) \leq 1, i \in \mathcal{S}\},$$

where $\pi_t(i)$ is the probability of being in state $i \in \mathcal{S}$ at time t. Since death state s_3 is directly observable, we have a truncated state distribution:

$$\Pi = \left\{ \begin{bmatrix} \pi(1) \\ 1-\pi(1) \\ 0 \end{bmatrix}, \begin{bmatrix} 0 \\ 0 \\ 1 \end{bmatrix} \right\} \tag{3.11}$$

If the patient was alive, and performed VL test at current month, the updated belief is: $[1,0,0]^T$ if in state s_1; $[0,1,0]^T$ if in state s_2. At any time t, if the patient died, the updated belief for observing death is $[0,0,1]^T$, if the patient was not prescribed with VL test (and alive) at time t, we compute the updated belief vector as $\mathbb{T}^T\mathbb{P}_A\mathbb{P}_o$, given adherence measurement A, and observation o. Similarly, we could compute the updated belief vector conditioning on the patient's adherence type θ as $\pi_{t+1}|A, o = \mathbb{T}_t^T\mathbb{P}_\theta\mathbb{P}_o$. To get the updated belief π_{t+1}, we normalize the updated belief vector using Bayes rules. If the physician was given a prior π_t, adherence measurement $A \in \{A^+, A^-\}$ and observation $o \in \{\overline{OI}, OI\}$, the updated belief is given by

$$\mathbb{T}'(j)|\ o,\ A = \frac{\sum_{i\in\mathcal{S}} \pi(i)P(s_j|s_i, A)P(o|s_i)}{\sum_{i\in\mathcal{S}}\sum_{j'\in\mathcal{S}} \pi(i)P(s'_j|s_i, A)P(o|s_i)} \tag{3.12}$$

Similarly, given a patient adherence type θ, we express the updated belief as

$$\pi'(j)|\ o,\ \theta = \frac{\sum_{i\in\mathcal{S}} \pi(i)P(s_j|s_i,\theta)P(o|s_i)}{\sum_{i\in\mathcal{S}}\sum_{j'\in\mathcal{S}} \pi(i)P(s'_j|s_i,\theta)P(o|s_i)} \tag{3.13}$$

We have the following Corollary which states that the updated belief of being in virally suppressed in higher if no OI was observed.

Corollary 3.4.1. $\pi'(1)|\ \overline{OI},\ \theta \geq \pi'(1)|\ OI,\ \theta$

We let $V^*(\pi)$ denote the value function that gives the optimal rewards when the patient is in health belief state π_t (and adherence type θ). The decision maker is trying to find the optimal action $N^*(\pi)$ (a function of belief state π) to maximize the discounted total reward, which is represented as a recursive optimality equation as $V^*(\pi) = \max\{V^w(\pi), V^v(\pi))\}$,where $V^w(\pi)$, $V^v(\pi)$ represents the optimal rewards that a patient can attain with the belief state π at time t, and action *Wait* or *Monitor*, respectively:

$$\begin{aligned}
V^w(\pi) &= \sum_s \pi(s)\Big\{r(s) + \delta \sum_{A\in\{A^+,A^-\}}\sum_{s'}\sum_o V^*(\pi'|o,A)P(s'|s,A)P(A|\theta)P(o|s)\Big\} \\
V^v(\pi) &= \sum_s \pi(s)\Big\{r(s) - \delta c + \delta \sum_{A\in\{A^+,A^-\}}\sum_{s'}\sum_o \\
&\qquad \Big((\pi'(1)|o,A)V([1,0,0]^T) + \big(1-(\pi'(1)|o,A)\big)\,R\Big)P(s'|s,A)P(A|\theta)P(o|s)\Big\}
\end{aligned} \tag{3.14}$$

Since the belief distribution is a truncated two-dimensional simplex, we can further simplify our state to only track the probability of being in state s_1. In the following lemma, we show that we can simplify the Equations 3.14 by tracking only state s_1 and applying the total expectation formula over θ ($V_1 \equiv V([1,0,0]^T)$).

Lemma 3.4.3. *Equations 3.14 (optimality equation) can be simplified to*

$$V^w(\pi(1)) = \sum_s \mathbb{m}(s)\Big\{r(s) + \delta \sum_{s'}\sum_o V^*(\pi'(1)|o,\theta)P(s'|s,\theta)P(o|s)\Big\}$$
$$V^v(\pi(1)) = \sum_s \mathbb{m}(s)\Big\{r(s) - \delta c + \delta \sum_{s'}\sum_o \Big((\pi'(1)|o,\theta)V_1 + \big(1-(\pi'(1)|o,\theta)\big)\,R\Big)P(s'|s,\theta)P(o|s)\Big\} \tag{3.15}$$

Next, we show that our optimal policy follows a control-limit rule.

Theorem 3.4.2. *For two belief vector π_1 and π_2 such that $\pi_1(1) \geq \pi_2(1)$ (i.e., $\pi_1 \leq_r \pi_2$), and if the following condition holds:*

$$\sum_s(\pi_1(s)-\pi_2(s))\Big[\sum_{s'}\sum_o V^*(\pi_2'(1)|o,\theta)P(s'|s,\theta)P(o|s)\Big]$$
$$\geq \sum_s(\pi_1(s)-\pi_2(s))\Big[\sum_{s'}\sum_o \Big((\pi_1'(1)|o,\theta)V_1 + \big(1-(\pi_1'(1)|o,\theta)\big)\,R\Big)P(s'|s,\theta)P(o|s)\Big] \tag{3.16}$$

Then,

(a) If $N^*(\pi_1) = Monitor$, then $N^*(\pi_2) = Monitor$,

(b) If $N^*(\pi_2) = Wait$, then $N^*(\pi_1) = Wait$.

From Theorem 3.4.2 we know that the optimal policy is a threshold-type policy. We could further compare the frequency of monitoring using the following corollary:

Corollary 3.4.2. *Let the primitives in Theorem 3.4.2 hold. Then, Monitoring is more frequent for less-adherent patients.*

Corollary 3.4.3. *Let the premises in Theorem 3.4.2 hold. Then, there is only one such threshold π^*.*

3.4.3 Summary of Models

We use the following Venn Diagram to illustrate the relation among the base model (Section 3.2), the Semi-Markov Decision Process (SMDP) model (Section 3.4.1), and the Partially Observable Markov Decision Process (POMDP) model (Section 3.4.2). In the base model, we did not consider the important part of HIV disease, the opportunistic infection. In the SMDP reformulation, we incorporated the event of opportunistic infections into the stochastic model, and relaxed the assumption that patients in virologic failure (i.e., $s = s_2$) will be moved to a second-line regimen upon failure detection (i.e., by performing VL tests). However, as we have seen in Section 3.4.1, under some reasonable assumption, we showed that it is optimal to move failure patients to a second-line regimen. Lastly, We propose an POMDP reformulation of the same problem. wAt the beginning of each month, the patient either undergoes a VL test (*Monitor*) or is suggested to *Wait* for another month. If the patient undergoes a VL test, the DM collects the adherence state from the patient. For all the three models introduced, we assume the frequency of clinical visits does not affect patient's adherence behavior, and the adherence is known prior to treatment initiation. As part of our future (ongoing) work, we propose to study the adherence learning problem as an extension.

Figure 3.1: The relationship among different models introduced in Section 3.2 and 3.4

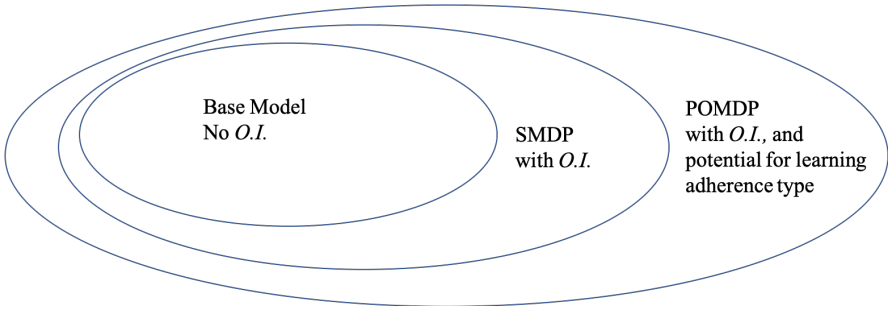

3.5 Numerical Study

We illustrate our framework with a case study in Uganda, a typical resource limited setting where GDP per capita in 2016 is only $615 USD [167]. Moreover, Uganda's HIV prevalence is as high as 2.61% among adults [145]. Also, the cost of VL test increased a lot in the last decade in Africa [20, 75], while certain African countries' GDP per capita growth rate is much lower than the rise in cost [167]. It becomes paramount to optimize monitoring policies, quantify the potential benefit of adherence type differentiation for HIV infected patients in resource limited settings like Uganda.

In Section 3.5.1, we first present the stochastic micro-simulation model which captures HIV patients disease progression, and transmission (through secondary infection). In Section 3.5.2, we present the optimized monitoring policy using the model framework we developed in Section 3.2 and Section 3.4. We then conclude this section by quantifying the total gain in terms of costs saved, and qualify-adjusted life years (QALYs) gained by comparing our optimized policy with a status quo policy (i.e., no adherence typ differentation). We provide a summary of each parameter values in Table B.1.

3.5.1 Simulation Model

We developed a stochastic simulation model to capture HIV disease progression and transmission. We used the model to optimize monitoring intervals at different willingness-to-pay (WTP) thresholds, for any given patient demographics information. The WTP threshold indicates the upper bound of societal resources that are generally considered affordable to gain one qualify-adjusted life-year (QALY).

We simulated patients with Uganda demographic data over a 100-year time horizon. A long time horizon resembles the infinite horizon setting in the Modelling Section. On the other hand, we only optimize the monitoring policies up to 10-years. We did this for two reasons. First, the remaining rewards estimation would be similar over a longer time horizon. Second, we could then better capture the gain of adherence type

differentiation within a reasonable time horizon. In a decade, there might be other more effective treatment available.

Model Parametrization

data source and population Our primary source of model inputs came from a previously well-calibrated disease progression model parametrized using demographics of HIV-infected patients in Uganda [106]. In our setting, we simulated a cohort of 600,000 individuals given Uganda's HIV-infected population profile over a 100-year time horizon. As reported in [106], cohort average age is 36 years old, of which 61% are women, and 25% are considered higher education and beyond.

ART adherence and virologic failure. [106] model monthly patient adherence status using a mixed effect logistic regression, as a function of a few patient demographic info, time between measurements, etc. However, this specific parametric form is not analytically tractable. We thus, modelled adherence heterogeneity effect using a Bayesian hierarchical model. Our results show that adherence heterogeneity can be equivalently modelled using beta distribution, where its mean (i.e., adherence type θ) depends on the patient age, gender, and education level. We defer the details of Bayesian formulation, and proof of existence, statistical significance of the model in Appendix Section B.2,

CD4 cell counts and HIV viral load are the two most important biomarkers of HIV disease progression. Most HIV studies only report health utilities and costs related to patient current CD4 cell counts. Since VL and CD4 cell counts are highly correlated, we assumed CD4 cell count of 200 $cell/mm^3$ for patients in virologic failure ($s = s_2$), CD4 cell count above 550 $cell/mm^3$ for virally suppressed patients $s = s_1$. Although CD4 cell count could be as high as 1200 $cell/mm^3$, most studies report the same cost and health utilities above 550 $cell/mm^3$ threshold [106]. We track our simulated cohort starting at the first month of ART initiation. All patients receive one VL measurement at 6 months on ART.

Similar as in [106], in our simulation model, if virologic failure is detected during clinical visit (for patients on the first-line ART), patients return to the clinic next month for a follow-up VL test. If no spontaneous resuppression occurred, patients will then switch to the second-line ART. As we briefly discussed in Section 3.2, we did not model regimen switching for patients on second-line ART, since detection of virologic failure cold not help improve patient health outcome.

age-specific mortality rates We modelled mortality similarly as in [106]. The monthly probability that a patient dies depends on the patient's gender, age, and virologic failure status.

Opportunistic Infections Patients in any living states can develop opportunistic infections, in which case they will present to their clinic and will be monitored. We use the state-specific OI rates reported in [106]. and shown in Table B.1.

Outcome Measures The simulation model tracks the health utility (Quality-adjusted life years, QALY) and health costs of a patient in a given month depends on the health state of the patient during that month, and whether the patient is on first-line or second-line regimen.

Secondary infections. We estimate the number of secondary HIV infections in the community per month as a function of patients' gender, sexuality, VL and the average number of sex acts per month ([164]). We acknowledge that it is a simpler, and potentially less accurate estimate than the one we used in [106], however, this simplification enables us to estimate number of infections monthly, without tracking the the entire time horizon.

To estimate the loss in QALYs and gain in cost per secondary infection, we assume the newly infected patients will be placed on ART and been treated as an "average" adherence type patient (i.e., $\theta = \mathbb{E}\theta$) as follows: first, we estimate the costs and QALYs

for a healthy individual (assuming a health utility of 0.9) up to $T_{average}$ as

$$QALY_{NoHIV} = 0.9(1 + \delta + ... + \delta^{T_{average}})$$

where $T_{average}$ is the average time spent alive by the HIV-infected patients in the simulation, and δ is the discount factor. Similarly, by denoting $c_{average}$ as the average cost assuming a yearly costs of a non-infected individual is 1/10 of that of an infected person ([106]), we have

$$COST_{NoHIV} = \frac{1}{10} c_{average}(1 + \delta + ... + \delta^{T_{average}})$$

Then, we calculate the average QALYs for a patient in the simulation model (denote as $QALY_{infected}$); and the average costs for a patient with $\theta = 0.5$ in the simulation model (denote as $COST_{infected}$). Wee then estimate the loss in QALYs as

$$QALY_{loss} = QALY_{NoHIV} - QALY_{infected}$$

and costs gained as

$$COST_{gained} = COST_{infected} - COST_{NoHIV}$$

respectively.

Optimizing monitoring intervals We simulate a few benchmark fixed monitoring strategies, where patients are monitoring every 1,3 ,6, 12, 24 months. We use our optimization model developed in Section 3.2 and Section 3.4 to optimize the monitoring interval given patient characteristics, including time since ART initiation, adherence type, age, and gender.

We instantiate reward parameters for each subpopulation (given adherence type, age, gender, etc) by following the classical approach in health economics to combine the

two objective (costs, QALYs gained) into a single net monetary benefit (NMB) objective using a willingness-to-pay(WTP) threshold per QALY gained as follow:

$$NMB = QALY \times WTP - costs,$$

where WTP indicates the amount of societal resource that are considered affordable to gain one QALY, usually taken to be one times or three times a country's GDP per capita as a baseline [158]. In our simulation, we consider three times Uganda's GDP per capita in 2016 as a benchmark, where we set WTP threshold as multipliers (three times, six times, ten times, 30 times, 60 times and 100 times).

To estimate the remaining rewards for patients switched to a second-line regimen, we instantiated the simulation model with patients starting on the second-line regimen. We terminate the simulation when every patient is dead. We then calculated the discounted lump sum rewards.

3.5.2 Optimization Results

We computed the optimal monitoring intervals using the SMDP model formulated in Section 3.4.1. We select a few representative patient demographic and plot the corresponding optimized monitoring intervals. We only show the results for patients who start the decision process with a virally suppressed health state s_1, and no O.I. observed (i.e, $\overline{OI}$). As we have shown in Section 3.4.1, for patients in virologic failure, the optimal decision is to monitoring immediately, and switch regimen to second-line (i.e., $N^* = 0$). In the meantime, Observe from Table B.1 the probability of opportunistic infection is extremely low for virally suppressed patients. One single observation of OI largely increase doctor's belief that the patient is in virologic failure s_2. As a consequence, given our model parameters, numerically we always have $N^*(s_1, OI) = 0$.

Figure 3.2 depicts the optimal monitoring strategy for male patients at 20 years old, 40 years old, and 60 years old respectively. We fixed the WTP to be three times

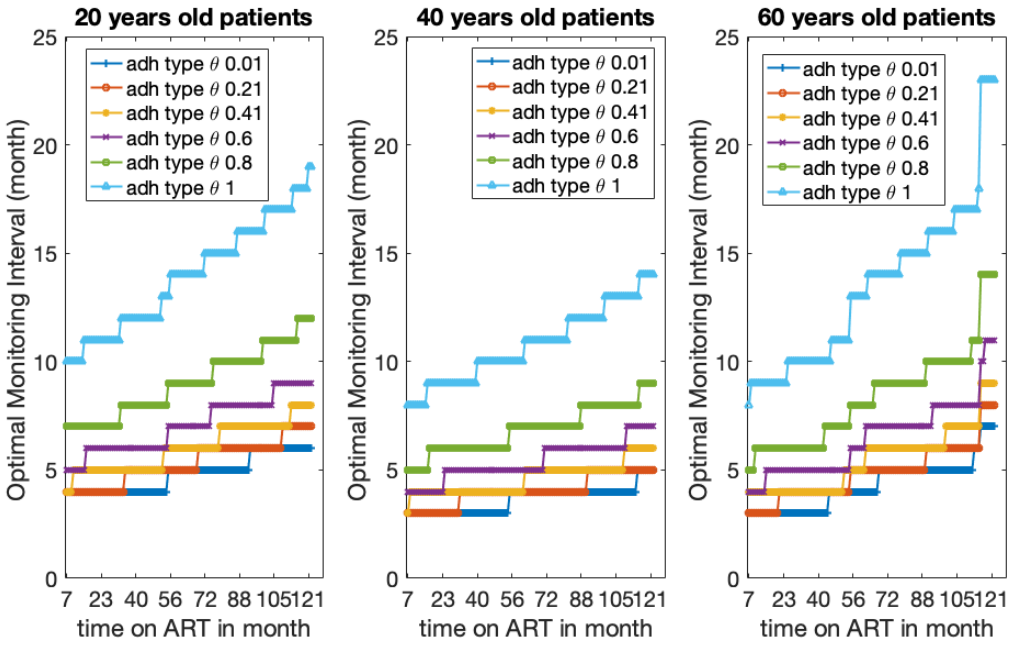

Figure 3.2: Optimal monitoring strategy for male patients at different age. WTP = $1845/QALY

of Uganda's GDP per capita. First, we observe that monitoring intervals are smaller for adherent patients at all ages. This confirms our theoretical finding in Proposition 1. Second, if patients stay longer on the first-line ART, we observe the optimal monitoring intervals increases. This is because the longer the patients stays on first-line regimen, the more stable their viral load could be. When time on ART is 10 years (120 months), optimal monitoring interval again increased for male patients at age 60. This phenomenon is caused by the estimation error of remaining rewards (see Figure B.4a and B.4b). Age-specific mortality rate is on a five-year basis. As a consequence, the remaining reward estimations "jumps" every five years. This led to the sudden increase in the monetary interval on month $t = 121$. This finding is consistent with Proposition 1.

We then turn our attention to Figure 3.3. We focused on 30-year-old female patients when analysis the impact of different WTP, where we vary the WTP per QALY gained

to three times, ten times, and thirty times of Uganda's GDP per capita. Similar as in the previous Figure, we observe that monitoring intervals are smaller for adherent patients at all ages. Second, as WTP increases, monitoring intervals shortens. This is consistent with our theoretical finding in Proposition 1.

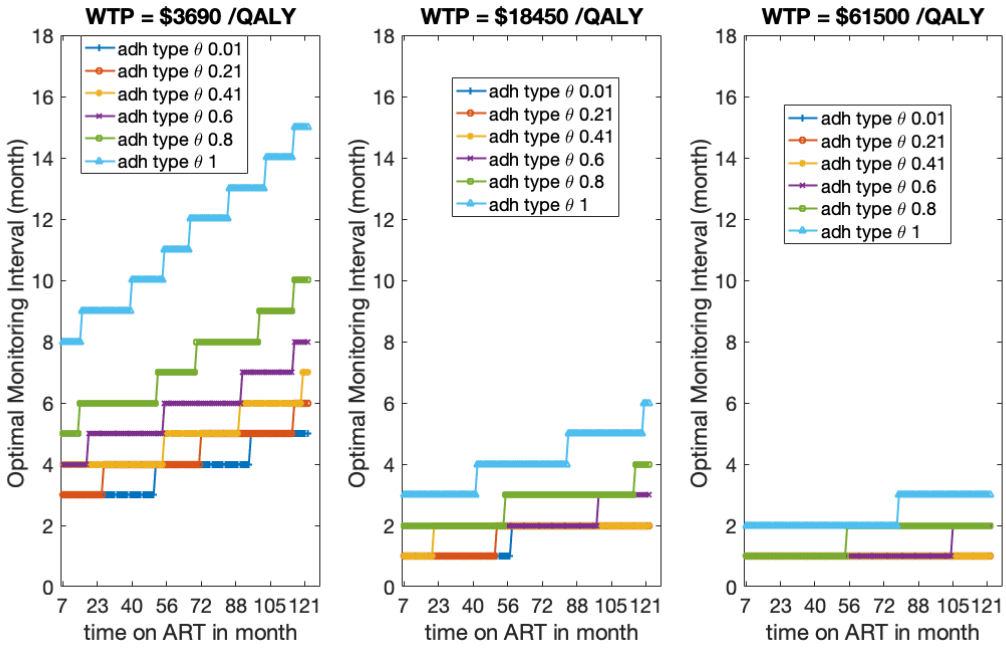

Figure 3.3: Optimal monitoring strategy for 30-year-old female patients at WTP/QALY gained

To quantify the gain of adherence type differentiation (on expectation,), we computed the optimality gap by comparing the weighted optimal value function, V_d^*, to the value function evaluated at a weighted average policy, V_f^* at all WTP levels for a few pre-specified adherence type distribution (i.e., a beta distribution):

$$\frac{V_f^* - V_d^*}{V_f^*} \times 100\%$$

The results are shown in Figure 3.4. Based on our assessment on adherence type distribution in Section B.2, we use gender-specific adherence type: for male patients,

$\alpha = 0.151$ and $\beta = 0.251$; for female patients, $\alpha = 0.129$ and $\beta = 0.207$. The resulting plot look very close to the plot of $\alpha = \beta = 0.2$ in Figure 3.4. For clarity, we did not add them into the Figure. Observing from Figure 3.4, the optimality gap decreases as WTP per QALY gained increases, for all pairs of $\alpha's$ and $\beta's$. This is because, as as WTP increases (i.e., the societal resources becomes less limited), the cost of VL test is less likely to be the barrier of frequent monitoring. As a result, the optimal monitoring interval becomes smaller (for all adherence types) as WTP increases. As a result, the maximum difference in optimal monitoring interval between an always-adherent, $\theta = 1$ patient and an always-nonadherent, $\theta = 0$ patient shrinks as WTP increases. Thus, the benefit (in terms of optimality gaps) of differentiating adherence types at high WTP levels becomes smaller.

Figure 3.4: Optimality Gap with different adherence distribution

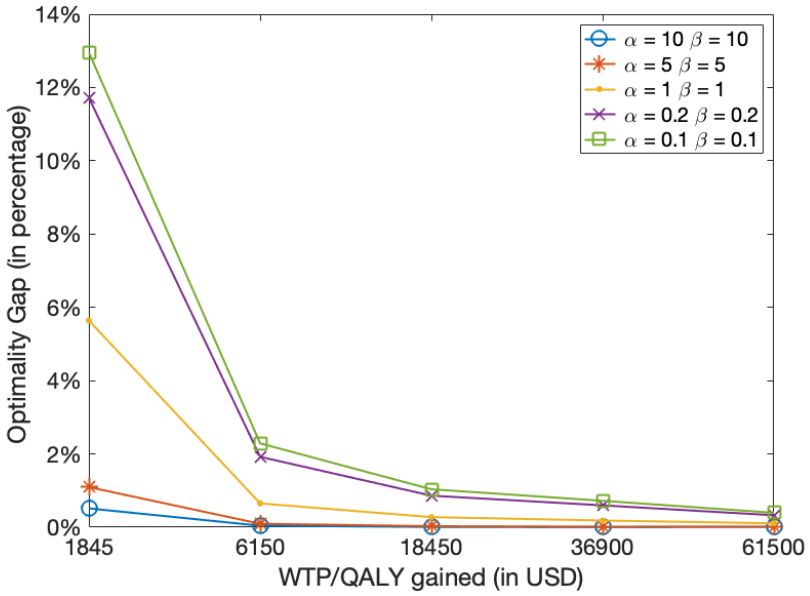

3.5.3 Simulation Results

We apply our optimized policy into stochastic disease progression model. To better understand the impact of adherence type differentiation, we first consider a smaller cohort with homogeneous demographics (i.e., same age, gender, and education level) over a 10-year time horizon. Studies have shown that male adolescent and young adults (15 - 30 years old) contributed nearly 50% nonadherence on ART ([169]), and 48% new cases of sexually transmitted diseases annually ([157]). We quantify the total gain from adherence type differentiation (i..e, QALYs improved, cost saved) in a specific subpopulation of 20-year-old male HIV-infected patients. We then consider patient cohort with a attributes (We then provided the weighted cohort results to match the profile of Uganda's HIV-infected population.

The final cost-effectiveness plots are shown in Figure 3.5 and Figure 3.6, respectively. The data points colored in red are the average QALYs and cost by simulating differentiated policies optimized at different WTP levels. The data points colored in blue are the average QALYs and costs simulating fixed policies (fixed monitoring intervals).

A few themes emerge from Figure 3.5. First, all optimized policies at different WTP thresholds are on the cost-effectiveness frontier, achieving higher QALYs at reasonable costs. Notably, for WTP thresholds equal to six times and ten times Uganda's GDP per capita, the optimized health outcomes are dominating Monitoring every 6 month, and every 3 months respectively. In other words, with adherence type differentiation, optimized policies resulted in higher QALYs and less costs compared to similar fixed policies. Monitor every months achieves the highest expected QALYs gained per patient, but at a much higher costs. Alternatively, the opimized policy using a WTP equals to 60 times Uganda's GDP capita resulted in very similar QALYs (difference of 0.026 QALYs) but saving more than $5,000 USD per patient.

We then analyze the resulting cost-effectiveness plot by consider a representative

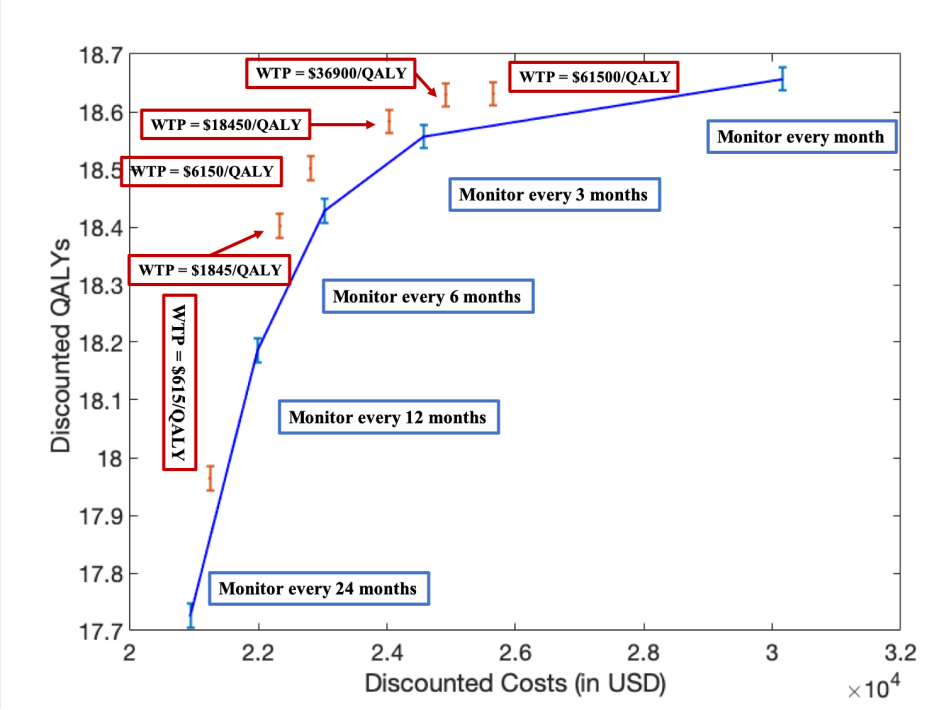

Figure 3.5: Cost Effectiveness Plot for 20-year-old male HIV-infected patients. Abbreviation: QALY, quality-adjusted life-year

cohort of Uganda's HIV-infected population, results shown in Figure 3.6. For the population average plot, we did not show the error bar because the variance becomes extremely small for a cohort of $N = 600,000$ HIV-infected patients. First, we observe from Figure 3.6 that

From this plot, we conclude that there is a significant improvement in the transmission-adjusted patient health outcome to differentiate patients by their adherence types. For the population averaged QALYs and costs, all optimized policies are on the cost-effectiveness frontier. For WTP thresholds equal to one times, and three times Uganda's GDP per capita, the optimized health outcomes are dominating Monitoring every 12 month, and every 6 months respectively. For richer-resource settings such that WTP threshold per QALY gained is about 30 to 100 times of Uganda's GDP per capita, the opimized policy resulted in very similar QALYs (difference in QALYs: 0.06 - 0.01) but

saves about $4,700 - $3,300 USD per patient.

We conclude from Figures 3.5 and 3.6 that adherence type differentiation brings significant improved HIV-infected patient health outcome.

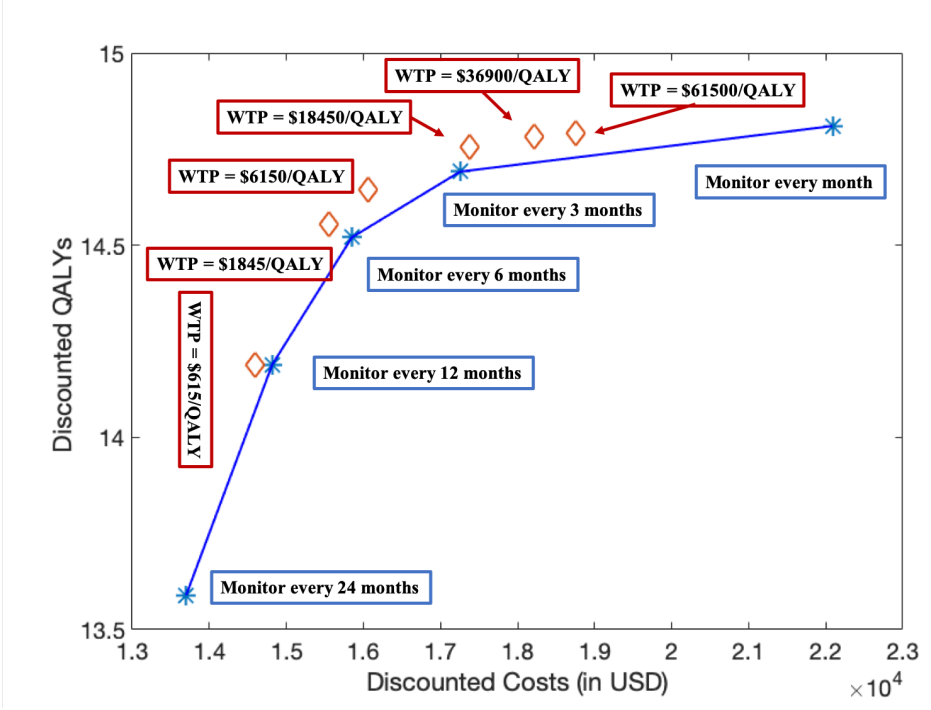

Figure 3.6: population average cost-effectiveness plot. Abbreviation: QALY, quality-adjusted life-year

3.6 Conclusion and Discussion

Designing efficient treatment plans while patient adherence is heterogeneous remains one of the most challenging problems for modern medicine. In this work, we formulated a stylized stochastic disease progression model that captures key features of HIV disease progression, and characterize a few useful and insightful structural properties of the model. In particular, we present an exact equation where the optimal solution can be directly computed. Notably, we also studied an extensions of the base model, by incorporating OI into the model framework.

We present a case study to numerically quantify the total gain from adherence type differentiation, using the demographic profile representing Uganda's HIV-infected patients. We observe a significant improvement in cumulative health outcome. In particular, for settings such as Uganda, optimized monitoring interval considering adherence type heterogeneity outperforms fixed 12-month and 6-month intervals with higher QALYs and less costs. In higher-resource settings, optimized monitoring intervals could lead to significant cost savings with minimal QALYs loss. In setting with WTP threshold of $18,000 - $60,000 USD per QALY gained, we estimate that $ 3,300 to $4.700 could be saved for each patient on ART using the optimized monitoring intervals.

Our model has several limitations. First, our disease progression model and the optimization model do not explicitly capture HIV transmission or changes in adherence behavior arising from prolong time on ART, or varied monitoring intervals. Second, our model assumed patient adherence type is fully revealed to decision makers prior to ART treatment initiation. Our POMDP formulation can be extended to a learning model by collecting patient adherence measurment during clinical visits, or phone calls.

Our study provide better informed decision on when to perform VL test of HIV-infected patients. We quantify the improvement in patient health outcome for adherence type differentiation. Related future work could utilize our model results for adherence learning.

Chapter 4

No Panic in Pandemic: The Impact of Individual Choice on Public Health Policy and Vaccine Priority

4.1 Introduction

The COVID-19 pandemic, caused by the highly infectious SARS-CoV-2 virus, has been the most urgent global healthcare threat since its outbreak in 2019. As of January 29, 2021, it has caused more than 101 million confirmed infections and 2 million deaths in 237 countries and regions worldwide [160]. While effective treatments and vaccines were absent in the early stage of COVID-19, various public health interventions were implemented to contain the pandemic in countries around the globe. In early 2020, U.S. federal and state authorities announced the *social distancing policy*, which required people to maintain a physical distance from others and ordered businesses to adjust their practices to restrict the number of people present in the same space [26, 99]. As the

pandemic developed, U.S. state authorities announced a more stringent *lockdown policy* in March 2020. This policy ordered people to stay at home except for essential activities and mandated public place closures, including schools and nonessential businesses (e.g., restaurants and gyms) [104, 148].

As two of the most widely-implemented COVID-19 mitigation measures, lockdown and social distancing policies have effectively reduced infections and deaths in the COVID-19 pandemic; however, this was not without a cost [70]. These two policies have caused significant disruption to regular economic activities. The U.S. entered a recession in February 2020 after the longest-in-history period of economic expansion (128 consecutive months), attributed to "the pandemic and the public health response" [105]. In April 2020, the unemployment rate increased to 14.7%, reaching both its highest rate in history and reflecting largest monthly increase (10.3%) in history, due to the effects of the "pandemic and efforts to contain it" [18]. Lockdowns and social distancing have also caused significant social impacts. As of April 1, 2020, 1.48 billion students (84.3% of all students) worldwide were affected by school closures [146]. People have also been suffering from mental health issues associated with social isolation and loneliness caused by these policies [91, 116].

The substantial socioeconomic cost highlights the urgent need for a strategic implementation of the lockdown and social distancing policies to contain infectious disease outbreaks and minimize their socioeconomic impact. This requires that government authorities optimize policy timing and stringency according to the disease dynamics (e.g., the number of infections and infection rates) and the socioeconomic impact [163]. On the one hand, an intervention that is initiated too early, lasts for an extended period, or is too stringent could cause excessive socioeconomic burden [90, 171, 153]. On the other hand, an intervention that comes too late, lasts for a short period or is too weak may fail to contain the pandemic and cause an unaffordable disease burden. For example, if the U.S. had begun social distancing measures one week earlier, it could have avoided 56.5% of infections and 54.0% of deaths as of May 3, 2020 [117, 109]. Many U.S. states that

rushed to reopen their businesses against warnings in the summer of 2020 experienced a second wave of the pandemic [155, 37].

"*How individuals respond ... will be as important as government actions, if not more important.*"

— [10] in the *Lancet*

Moreover, government authorities should consider people's responses when planning lockdown and social distancing policies [10]. First, an International Monetary Fund (IMF) report shows that individuals may voluntarily reduce their social interactions because of the fear of being infected [72, 73]. This is also evidenced by the fact that U.S. individuals traveled, dined out, and visited businesses less frequently even when there were no public health interventions [60, 108]. Second, individuals may change their behavior according to public health policies. For example, after the social distancing policy was enacted, U.S. consumers' visits to nonessential businesses (e.g., bars and restaurants) declined [60, 39, 5]. Without considering these responses, public health interventions could be "misguided," or even be "detrimental" [6].

Previous discussions highlight a critical research question in the design of public health interventions to contain an infectious disease outbreak like COVID-19. How should government authorities determine the optimal timing and stringency of lockdown and social distancing policies considering their socioeconomic impacts and individual responses? To answer this question, we use multinomial logit choice models to characterize individual reactions to the risk of infection and public health interventions and integrate it into a repeated Stackelberg game with the Susceptible-Infected-Recovered (SIR) disease transmission dynamics. Structural properties of equilibrium individual responses and optimal interventions reveal interesting results on the optimal timing and effectiveness of public health policies. Moreover, we propose dynamic programming and gradient descent algorithms to optimize these policies to alleviate their socioeconomic loss while effectively mitigating the pandemic. These algorithms enable us to derive additional insights in our numerical experiment based on representative COVID-19 data

from Minnesota.

Furthermore, we investigate another urgent question faced by global policymakers: how to prioritize the administration of vaccines when supply is limited [162, 28]? Given the limited vaccine production capacity, global health authorities have recommended that the elderly should get the vaccines first since they are at higher risk of severe illness and mortality [162, 24, 98]. However, it has been shown that youth and adults are more socially active and thus have a higher risk of spreading the disease [170, 130]. Thus, vaccinating the elderly first may have a limited impact in slowing down transmission in the general population [22, 102]. Therefore, vaccine prioritization is still in question considering both population heterogeneity and individual reactions.

To address this challenge, we modify our analytical framework to incorporate heterogeneity in age-stratified population groups. We show that it is critical to tailor vaccine prioritization plans under different vaccine capacity, mortality rates, and disease transmission rates. Moreover, we suggest that the social distancing policy should be enforced in parallel with vaccine administration to contain the disease transmission and should be more strict when the elderly group is prioritized to receive the vaccine.

Our work contributes to the literature in four major ways. First, our study is among the first to examine public health interventions considering the disease transmission dynamics, socioeconomic impacts, and individual reactions in a pandemic. Second, we derive theoretical properties and provide analytical results on the impact of individual reactions and the timing of public health interventions. Third, we propose dynamic programming and gradient descent algorithms to optimize the implementation of public health interventions that balances the economic loss caused by the policies and the healthcare burden resulting from the disease transmission. Fourth, our numerical results provide unique insights on the effectiveness of public health interventions under economic constraints and favorable vaccine prioritization plans when vaccine production capacity is limited. Our findings address urgent public health challenges that the world is facing in this pandemic.

The remainder of this chapter is organized as follows. Section 4.2 provides an overview of related literature. Section 4.3 describes the modeling framework, and Section 4.4 provides theoretical analysis and presents policy optimization models and algorithms. Section 4.5 presents numerical results on lockdown and social distancing. Section 4.6 presents a heterogeneous model and provides insights on vaccine prioritization. Section 4.7 concludes this paper.

4.2 Literature Review

In this section, we review a few streams of literature that are most relevant to our work among a great influx of COVID-related papers. The first stream of research predicts epidemiological and socioeconomic outcomes of public health interventions in the COVID-19 pandemic. The majority of studies in this stream adopt the dynamic compartmental models introduced by [79] to describe population-level disease progression. Some use Susceptible-Infected-Recovered (SIR) or Susceptible-Exposed-Infected-Recovered (SEIR) models to predict the epidemiological outcomes (e.g., cumulative numbers of infections and deaths) under different public health interventions [168, 121, 84, 124]. Others use simulations to numerically evaluate the trade-off between epidemiological outcomes and the socioeconomic impact of public health interventions [171, 3, 8]. These studies focus primarily on predicting outcomes of pre-defined policies, and do not consider individual responses or policy optimization.

The second stream of literature focuses on optimal intervention design in epidemics. [33] consider the impact of test capacity on disease dynamics in a variant of the susceptible-infected (SI) model. [34] study the impact of hospital admission and the Fangcang shelter system on reducing deaths from COVID-19 and its implication for the lockdown policy. [32] derive optimal antibiotic treatment policy considering drug resistance. [43] and [47] study testing queue management in COVID-19. Unlike [93, 54] and [71] that study vaccine procurement contracts and vaccination scheduling problems, we discuss

the implications of our model on vaccination priority. [31] and [115] model public health policies (e.g., lockdown) as controls on the disease dynamics in SIR or SEIR models and seek for optimal policies. Our work differs from this stream of studies by incorporating individual responses to the pandemic and public health policies.

The third stream of studies considers individual responses in the pandemic. Several studies conduct equilibrium analysis considering individual responses to the risk of infection from COVID-19 [94, 58, 51, 55, 6, 17, 44]. These studies model individual utility or disutility related to staying home, essential/nonessential social activities, and risk of infection and study the equilibrium of individual activity level. They investigate the impact of individual activity level on social welfare, which could guide public health interventions. [77] and [21] model the impact of public health interventions on individual utility and their equilibrium activity level, and conduct simulation-based investigations. Our study differs from these previous studies, as they mostly focus on equilibrium analysis to describe individual behavior. Instead, we model lockdown and social distancing policies as decision variables and investigate individual reactions to these policy decisions. Moreover, we characterize structural properties of optimal interventions and propose dynamic programming and gradient descent algorithms to derive optimal public health policies.

The fourth stream of literature focuses on resource allocation and priority assignment in healthcare. For example, [86] propose several heuristic policies for treatment resource allocation in the Ebola outbreak. [74] study the optimal priority assignment in emergency response. Our work contributes to this stream of work in that we optimize vaccine priority by considering individual response, infectious disease dynamics and limited vaccine capacity. Mostly relevant to our work, [170] conduct equilibrium analysis on individual decisions on whether or not to receive vaccines and study vaccination priority strategy in a static setting without vaccine capacity constraint. Our results for a dynamic setting are consistent with [170]'s results that Elderly first vaccination strategy could result in more infections when vaccine production capacity is large. However,

when vaccination capacity is limited, we show that Elderly first vaccination strategy may result in similar infections but much fewer deaths.

Lastly, we use multinomial logit (MNL) models to capture individual activity level in the equilibrium analysis. MNL models have been widely used to model individual discrete choices, where choices are not bang-bang (e.g., either everyone stays at home or everyone goes out). Distinct from most classic MNL models, our MNL model captures the network effect among individuals due to their social interactions and risk of infection. [152] and [48] present MNL model with network effect but focus on revenue management and assortment pricing problems. To the best of our knowledge, our paper is the first that captures individual behavior using a network MNL model to find optimal public interventions for infectious disease outbreaks.

4.3 Model Framework

We consider a central planner (CP), such as a federal or state government authority, who aims to contain the pandemic by implementing public health policies within a finite time horizon. The CP is interested in minimizing the overall sum of disease burden (healthcare-related costs) and policy implementation cost. In analyzing the hypothetical CP's approach, we focus on two widely-implemented policies: lockdown and social distancing. We propose integrated analytical frameworks to optimize these policies, including the SIR model, game-theoretical models, and discrete choice models. Specifically, we formulate a finite horizon, repeated two-stage Stackelberg game as follows. Every day, the CP announces their policy decision; and then each individual decides the probability that they would like to *go out* or *stay at home* as a reaction to the risk of infection and the public health policy. Instead of using a bang-bang choice, we model the individual decision by a multinomial logit choice model, which is consistent with the true mobility pattern in the pandemic [25].

We first introduce a baseline case without any public health intervention in Section

4.3.1. Then, we introduce the case with lockdown and social distancing policies in Sections 4.3.2 and 4.3.3.

4.3.1 Baseline Case without Public Health Interventions

The baseline case models the epidemic dynamics and individual activity level when no public health intervention is implemented.

Disease model

To capture the disease transmission and progression dynamics, we adopt a discrete SIR model by discretizing the time horizon into days (We use day t and time t interchangeably throughout the paper), which is consistent with epidemiology literature [e.g., 7, 121]. In the SIR model, an individual's health condition is classified into three states: 1) susceptible state S, in which individuals are not infected; 2) infectious state I, in which individuals are infected and can infect others through contacts; and 3) recovered state R, in which patients have recovered from the infection, and are assumed to be immunized from re-infection. We denote $S(t)$, $I(t)$ and $R(t)$ as the proportion of population in each state at the beginning of day t, and normalize the size of the population to 1 (i.e., $S(t) + I(t) + R(t) = 1$ for any t). We call $I(t)$ the *disease prevalence* on day t.

On a given day t, we assume that a susceptible individual becomes infected with a probability $\beta\overline{\alpha}(t)I(t)$ (referred to as the risk of infection), which depends on a known infection rate $\beta \in (0, 1)$ of the disease, the societal average activity level $\overline{\alpha}(t) \in [0, 1]$ and the disease prevalence $I(t)$. Note that for a given disease prevalence $I(t)$, the risk of infection is higher when $\overline{\alpha}(t)$ is larger. Every day, infectious individuals recover at a known rate $r \in (0, 1)$. We do not consider births, deaths, or aging due to the relatively short time horizon used in this study, which is consistent with the literature [121, 168].

Thus, the discretized SIR model can be written as follows:

$$\begin{cases} S(t+1) - S(t) = -\beta\overline{\alpha}(t)I(t)S(t) \\ I(t+1) - I(t) = \beta\overline{\alpha}(t)I(t)S(t) - rI(t) \qquad t = 1, ..., T-1. \\ R(t+1) - R(t) = rI(t) \end{cases} \tag{4.1}$$

Individual/societal activity level

On each day, individuals decide whether they would like to *go out* or *stay at home*. Assume that each individual stays at home with probability $1-\alpha_B(t)$ and goes out with probability $\alpha_B(t)$. Staying at home interrupts people's daily routine and may cause a utility loss. Let $u(\text{stay at home}) = -b_0 < 0$ be the expected utility of staying at home. The utility of staying at home can be written as

$$U(\text{stay at home}) = u(\text{stay at home}) + \epsilon, \tag{4.2}$$

where ϵ captures individual-specific idiosyncrasies. Building on the model introduced in [94], we express the expected utility gained by an individual from going out as follows:

$$u_B(\text{go out}, \ \overline{\alpha}(t)) = b_1 + b_2\overline{\alpha}(t) - b_3\overline{\alpha}(t)\beta I(t).$$

Note that $u_B(\cdot)$ has three factors. First, an individual can gain utility (denoted as $b_1 \geq 0$) from necessary activities to maintain a living (e.g., grocery shopping and doctor visits) or activities without interactions with others (e.g., walk dogs alone). Public health interventions introduced in later sections generally do not impact the accessibility of these activities (hereafter referred to as *essential activities*). Second, additional utility ($b_2 \geq 0$) can be gained through social interactions (e.g., attending social entertainment events). An individual's utility gain through these social interactions (hereafter referred to as *nonessential social interactions*) $b_2\overline{\alpha}(t)$ depends on the societal average activity level $\overline{\alpha}(t)$. That is, this utility increases (decreases) as more people go out (stay at

home). Nonessential social interactions will be subject to the impact of lockdown or social distancing policies. Third, individuals may experience utility loss ($b_3 \geq 0$) due to infection. The term $b_3\overline{\alpha}(t)\beta I(t)$ represents the disease burden associated with the risk of infection if going out, which increases as more people are going out or are infected. We provide utility parameter estimation details in Supplement C.2. Similar to the utility of staying of home, we write the utility of going out as follows:

$$U_B(\text{go out}, \ \overline{\alpha}(t)) = u_B(\text{go out}, \ \overline{\alpha}(t)) + \epsilon.$$

We assume the population is homogeneous in their utility parameters in the base model and will extend it to heterogeneous population in Section 4.6. As a result, all individuals adopt the same strategy (i.e., the same $\alpha_B(t)$) in the base model. Hence, the societal average activity level $\overline{\alpha}(t)$ is equal to $\alpha_B(t)$ (i.e., $\overline{\alpha}(t) = \alpha_B(t)$). We can write the expected utility of going out $u_B(\text{go out}, \alpha_B(t))$ as follows:

$$u_B(\text{go out}, \alpha_B(t)) = b_1 + b_2\alpha_B(t) - b_3\alpha_B(t)\beta I(t). \tag{4.3}$$

As in the standard MNL model, we assume all ϵ's are independent Gumbel random variables. Then, by results of MNL modelling [48, 15], the probability of an individual choosing to go out on day t can be written as:

$$\alpha_B(t) = \frac{\exp(u_B(\text{go out}, \alpha_B(t)))}{\exp(u(\text{stay at home})) + \exp(u_B(\text{go out}, \alpha_B(t)))}. \tag{4.4}$$

The value of $\alpha_B(t)$ affects the utility of going out, which in return affects the probability of going out, i.e., the value of $\alpha_B(t)$. We say $\alpha_B^*(t)$ is an equilibrium point if it satisfies Eq.(4.4). Without loss of generality, we assume $b_0 = 0$. Analytical results for $b_0 > 0$ is equivalent to those for $b_0 = 0$ and $b_1' = b_1 + b_0$. Therefore, we simplify Eq.(4.4) to the following:

$$\alpha_B(t) = \frac{\exp(u_B(\text{go out}, \alpha_B(t)))}{1 + \exp(u_B(\text{go out}, \alpha_B(t)))}. \tag{4.5}$$

Next, we extend the baseline case to consider how an individual changes his/her activity level according to lockdown and social distancing policies.

4.3.2 Lockdown Policy

When the CP implements the lockdown policy, public places like schools and nonessential businesses (e.g., restaurants and gyms) close [104, 148]. As a result, the utility gained from nonessential social interactions is eliminated. However, as discussed in Section 4.1, implementing the lockdown policy could cause socioeconomic loss. Therefore, the CP aims at configuring a lockdown policy which optimally balances total disease burden (e.g., treatment costs if infected), and direct socioeconomic impact/burden of lockdown implementation (e.g., nonessential businesses shutdown).

We denote the CP's lockdown decision on day t as a binary variable $A(t)$, where $A(t) = 1$ when the CP implements the lockdown policy and $A(t) = 0$ otherwise. The CP's lockdown policy in a time horizon T is denoted as $\boldsymbol{A} = (A(t))_{t=1}^{T-1}$. Let d_1 and d_3 be daily socioeconomic burden associated with lockdown implementation, and the expected disease burden associated with each infection, respectively[1]. The CP's total cost under lockdown policy sequence $\boldsymbol{A}$ can be written as:

$$f(\boldsymbol{A}) = d_1 \sum_{t=1}^{T-1} A(t) + d_3[S(1) - S(T)], \tag{4.6}$$

where $[S(1) - S(T)]$ computes the cumulative number of infections. If both the CP and individuals are risk-neutral, then $d_3 = b_3$. We will compare different choices of d_3 is Section 4.5. On day t, given the CP's lockdown decision $A(t)$, individuals decide whether to go out. If the CP selects $A(t) = 0$, people are more likely to go out. As a result, the number of infections could increase, potentially changing the CP's decisions to lockdown in the following days. We model this interplay between the CP and individuals as a

[1]We have ignored the cost of suspending and re-opening businesses in d_1 and could have underestimated the cost of lockdown implementation. However, in Section 4.5, we show that lockdown is not cost-effective even with this underestimated cost.

repeated two-stage Stackelberg game, where the CP announces $A(t)$ on day t followed by individual responses, from $t = 1$ to the end of time horizon.

We denote an individual's probability of going out to be $\alpha_A(t)$, as a response to the lockdown policy. Similar to the baseline model, the societal average activity level $\overline{\alpha}(t)$ is equal to $\alpha_A(t)$ since all individuals adopt the same strategy (i.e., $\overline{\alpha}(t) = \alpha_A(t)$). We express the utility and expected utility for individuals to go out on day t under a lockdown decision $A(t)$ as follows:

$$\begin{aligned} U_{LD}(\text{go out}, \alpha_A(t)) &= u_{LD}(\text{go out}, \alpha_A(t)) + \epsilon, \quad \text{and} \\ u_{LD}(\text{go out}, \alpha_A(t)) &= b_1 + b_2\alpha_A(t)(1 - A(t)) - b_3\alpha_A(t)\beta I(t). \end{aligned} \tag{4.7}$$

When $A(t) = 1$, no utility is gained from nonessential social interactions, i.e., $b_2\alpha_A(t)(1-A(t)) = 0$. Similar to Eq.(4.5), the equilibrium activity level $\alpha_A^*(t)$ under a lockdown decision $A(t)$ satisfies:

$$\alpha_A(t) = \frac{\exp(u_{LD}(\text{go out}, \alpha_A(t)))}{1 + \exp(u_{LD}(\text{go out}, \alpha_A(t)))}. \tag{4.8}$$

4.3.3 Social Distancing Policy

Under a social distancing policy, the CP can limit individual activity level. For example, Minnesota limited indoor gatherings for each household to under ten people at maximum; and required gyms and restaurants to open at 25% and 50% capacity in December 2020 [99]. To reflect these practices, we follow previous literature's modeling approach [153], and model the CP's social distancing policy decision on day t as $\kappa(t)$, where $\kappa(t)$ represents the activity reduction through social distancing. In other words, $1-\kappa(t)$ sets an upper bound for an individual's activity level $\alpha(t)$ such that the feasible region of $\alpha(t)$ becomes $[0, 1 - \kappa(t)]$ on day t. We denote the CP's social distancing policy in a time horizon T as $\boldsymbol{\kappa} = (\kappa(t))_{t=1}^{T-1}$. The CP can choose $\kappa(t) \in [0, \kappa_{\max}]$, where $\kappa_{\max} < 1$ represents the maximum contact reduction through social distancing and is

estimated to be 50% in previous literature [168].

Similar to the lockdown policy, implementing the social distancing decision $\kappa(t)$ incurs a socioeconomic burden denoted as $q(\kappa(t))$. As it is much more costly to implement a more strict social distancing due to a greater socioeconomic loss, we adopt [128]'s convex function form of $q(\kappa(t))$ as

$$q(\kappa(t)) = q_{\max}\left(\frac{\kappa(t)}{\kappa_{\max}}\right)^{1+\phi}, \tag{4.9}$$

where $q_{\max}$ is the cost of implementing the maximum social distancing decision $\kappa(t) = \kappa_{\max}$, and $\phi \geq 0$.

Thus, the CP's total cost under a social distancing policy κ can be written as:

$$g(\boldsymbol{\kappa}) = \sum_{t=1}^{T-1} q(\kappa(t)) + d_3[S(1) - S(T)], \tag{4.10}$$

where the first term is the amortized daily socioeconomic loss due to social distancing policy implementation, and the second term is the total disease burden.

We denote an individual's probability of going out under the social distancing decision $\kappa(t)$ to be $\alpha_\kappa(t)$. The societal average activity level $\overline{\alpha}(t)$ is equal to $\alpha_\kappa(t)$ since the population is homogeneous (i.e., $\overline{\alpha}(t) = \alpha_\kappa(t)$). Thus, the utility for individuals to go out on day t can be written as follows:

$$U_{SD}(\text{go out}, \alpha_\kappa(t)) = b_1 + b_2\alpha_\kappa(t) - b_3\alpha_\kappa(t)\beta I(t). \tag{4.11}$$

As will be shown in Theorem 4.4.2, the individual equilibrium activity level under a social distancing policy, i.e., $\alpha^*_\kappa(t)$, is jointly determined by an individual's baseline equilibrium activity level $\alpha^*_B(t)$ and social distancing policy decision $\kappa(t)$. Specifically, we prove that $\alpha^*_\kappa(t) = \alpha^*_B(t)$ if $\alpha^*_B(t) \leq 1 - \kappa(t)$, and $\alpha^*_\kappa(t) = 1 - \kappa(t)$ otherwise. That

is,

$$\alpha^*_\kappa(t) = \min(1 - \kappa(t), \alpha^*_B(t)). \tag{4.12}$$

4.4 Theoretical Results and Public Health Policy Optimization

In this section, we investigate structural properties of the equilibriums under different policies. We focus on a symmetric equilibrium in which all individuals go out with the same probability. We first show the properties of the baseline case in Section 4.4.1. We then present the equilibrium analysis, formulate mathematical optimization models for the policy optimization, propose solution algorithms, and derive structural properties of the optimal policy decisions for both the lockdown policy (Section 4.4.2) and the social distancing policy (Section 4.4.3), respectively. We include all proofs in Supplement C.3.

4.4.1 Baseline Case

We define the aggregate individual welfare on day t as the weighted sum of expected utility of all individuals. Then, the aggregate individual welfare can be written as:

$$\begin{aligned} u^{\text{aw}}(\alpha(t)) &\equiv (1 - \alpha(t)) \times u(\text{stay at home}) + \alpha(t) \times u(\text{go out}, \alpha(t)) \\ &= \alpha(t)\,[\,b_1 + b_2\,\alpha(t) - b_3\,\alpha(t)\,\beta I(t)\,]\,. \end{aligned} \tag{4.13}$$

We denote $\alpha^*_B(t)$ as the equilibrium of $\alpha_B(t)$ being the solution to Eq.(4.5), and write $\alpha^*_{\text{aw}}(t)$ as the socially optimal activity level that maximizes $u^{\text{aw}}(\alpha(t))$. We compare the individual equilibrium activity level with the socially optimal activity level. We have the following result.

Proposition 4.4.1. *The inequality* $\alpha^*_{\text{aw}}(t) < \alpha^*_B(t)$ *holds for any* $t \in \{1, \cdots, T-1\}$ *if and only if the disease prevalence* $I(t)$ *satisfies* $I(t) > \dfrac{1}{b_3\beta}\left[0.5b_1 + \dfrac{0.5b_1}{\exp(0.5b_1)} + b_2\right]$.

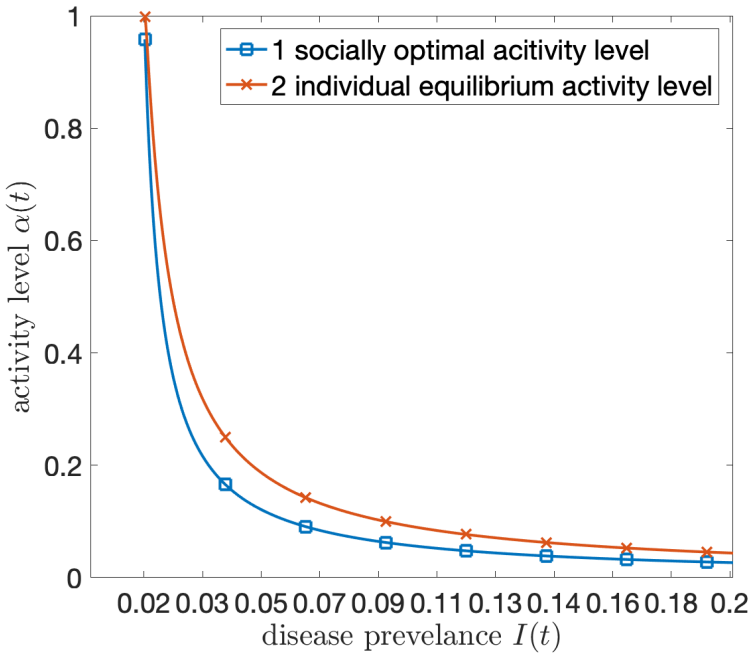

Figure 4.1: Comparison of the socially optimal daily activity level $\alpha^*_{\text{sw}}(t)$, and the self-interested activity level in equilibrium $\alpha^*_A(t)$ by varying the disease prevalence $I(t)$.

The condition in Proposition 4.4.1 translates to $I(t) > 0.013$ numerically. Model parameters are estimated based on the COVID-19 data in Section 4.5 and can be found in Table C.1.

Proposition 4.4.1 indicates that the socially optimal activity level $\alpha^*_{\text{aw}}(t)$ is smaller than the individual equilibrium activity level $\alpha^*_B(t)$ as long as the disease prevalence $I(t)$ is not too small. The numerical example in Figure 4.1 verifies this theoretical discovery, which is based on the COVID-19 data in Section 4.5. In particular, the difference between $\alpha^*_{\text{aw}}(t)$ and $\alpha^*_A(t)$ could be as high as 48% when $I(t)$ is around 1.8%. This is because, when individuals make decisions, they only consider the negative impact of infection on their own, but ignore the negative externality of their decisions to others. That is, their activity could increase others' risk of infection. In contrast,

socially optimal activity level $\alpha^*_{\text{aw}}(t)$ that maximizes the aggregate individual welfare $u^{\text{aw}}(\alpha(t))$ captures this externality. Therefore, the social activity level is smaller than the individual equilibrium activity level. Nevertheless, this deviation decreases as $I(t)$ increases and almost disappears with extremely large $I(t)$ as shown in Figure 4.1. This is because the additional negative externality imposed by an individual on others is limited when the pandemic is severe. This observation is important as it shows that the socially optimal activity level is close to the individual equilibrium activity level when the disease prevalence $I(t)$ is very high. Thus, policy interventions, including both lockdown and social distancing, should focus more on the case where $I(t)$ is moderate.

4.4.2 Lockdown Policy

Equilibrium Analysis in the Lockdown Policy

Under a lockdown policy, the government shuts down nonessential businesses and the utility of nonessential social interaction is eliminated for all individuals when $A(t) = 1$. Theorem 4.4.1 presents the existence and uniqueness of an equilibrium $\alpha^*_A(t)$ specified by Eq.(4.8) on any day t.

Theorem 4.4.1. *Under a lockdown policy sequence* $\boldsymbol{A} \equiv (\, A(t)\,)_{t=1}^{T-1}$*, there exists a symmetric, subgame perfect Nash equilibrium* $\alpha^*_A(t)$ *on each day* t*. Further,* $\alpha^*_A(t)$ *is uniquely determined by* $I(t)$ *and* $A(t)$*.*

Next, we present comparative static analyses of the equilibrium activity level $\alpha^*_A(t)$. We use $\alpha^*_{A=i}(t)$ to denote the equilibrium activity level when the CP's lockdown decision is $A(t) = i$ on day t, where $i \in \{0, 1\}$.

Proposition 4.4.2. *For any* $t \in \{1, \cdots, T-1\}$*, the following two properties hold.*
(a) $\alpha^*_A(t)$ *is increasing in* b_1 *and* b_2*, and is decreasing in* b_3 *and* $I(t)$ *for a given lockdown decision* $A(t) \in \{0, 1\}$*.*
(b) $\alpha^*_{A=1}(t) \leq \alpha^*_{A=0}(t)$*, i.e.,* $\alpha^*_A(t)$ *is smaller when lockdown is enacted.*

As expected, Proposition 4.4.2 shows that individual activity levels are directly related to b_1, b_2, b_3 and $I(t)$. In addition, individuals are more likely to stay at home when the lockdown policy is enacted.

Lockdown Policy Optimization

We formulate the CP's lockdown policy optimization as the *Lockdown Model*. To reflect that frequent policy changes might result in great cost of suspending and re-opening businesses, we assume that the CP is only allowed for a maximum number L of lockdown initiation (from open to closed status).

We define the decision variable $z(t)$ as the number of lockdown initiation till day t. $S(1)$, $I(1)$, and $R(1)$ are known parameters about the disease prevalence at the beginning of the planning horizon. We show that the disease trajectory $\{(S(t), I(t), R(t))\}_{t=1}^{T}$ is a function of the time sequence of the societal activity level $\boldsymbol{\alpha} \equiv (\alpha(t))_{t=1}^{T-1}$ in Lemma C.3.1 in Supplement C.3.4. Therefore, according to Lemma C.3.1 and Theorem 4.4.1, it can be easily verified that $\alpha_A(t)$ and the disease state trajectory $\{(S(t), I(t), R(t))\}_{t=1}^{T}$ is uniquely determined by $A(t)$. The objective in Eq.(4.14) is to minimize the overall cost of a lockdown policy as defined in Eq.(4.6). Disease dynamics and individual choice are modeled in Eq.(4.1), Eq.(4.7), Eq.(4.8), and Eq.(4.17). Constraint (4.15) computes $z(t)$ and Constraint (4.16) limits the total number of lockdown initiation in the planning horizon. Constraints (4.18) and (4.19) present the initial conditions of $A(t)$ and $z(t)$.

Lockdown Model

$$\min_{\boldsymbol{A},\boldsymbol{z}} \quad f(\boldsymbol{A}) = \sum_{t=1}^{T-1} d_1 A(t) + d_3[S(1) - S(T)] \tag{4.14}$$

s.t. Eq.(4.1), Eq.(4.7) and Eq.(4.8)

$$z(t+1) - z(t) = \max(A(t) - A(t-1), 0) \qquad t = 1, \cdots, T-1 \tag{4.15}$$

$$z(T) \leq L \tag{4.16}$$

$$\overline{\alpha}(t) = \alpha_A^*(t) \qquad t = 1, \cdots, T-1 \tag{4.17}$$

$$A(0) = 0; A(t) \in \{0, 1\} \qquad t = 1, \cdots, T-1 \tag{4.18}$$

$$z(1) = 0; z(t) \in \mathbb{Z} \qquad t = 1, \cdots, T. \tag{4.19}$$

The *Lockdown Model* is a mixed integer programming model and is nonconvex because Eq.(4.1) and Eq.(4.8) are nonlinear and nonconvex. To find the optimal solution, we transform the *Lockdown Model* into a deterministic dynamic programming (DP) problem and solve it via backward induction. Note that $d_3[S(1) - S(T)]$ in the objective (4.14) can be written as $d_3 \sum_{t=1}^{T} [S(t-1) - S(t)] + d_3[S(1) - S(0)]$ where we define $S(0) = 0$. Thus, the second term $d_3[S(1) - S(0)]$ is a constant and can be omitted in the optimization problem.

We define the state on day t as $O(t) \equiv (S(t), I(t), S(t-1), z(t), A(t-1))$. Notice that, $O(t)$ contains all information on day $t-1$, including number of susceptible $S(t-1)$, and lockdown decision $A(t-1)$. $O(t)$ also specifies the population disease status in the SIR model since $R(t) = 1 - S(t) - I(t)$. Due to Constraint (4.16), if $z(t) = L$ and $A(t-1) = 0$, the admissible action set on day t is $\widehat{A}_t = \{A(t) = 0\}$; otherwise, $\widehat{A}_t = \{A(t) \in \{0, 1\}\}$. Given the action $A(t) \in \widehat{A}_t$, the state transition is determined by constraints in the *Lockdown Model*, and the deterministic transition matrix is $\mathcal{T}(O', A, O) = \mathcal{T}(O(t+1) = O' | O(t) = O, A(t) = A)) \in \{0, 1\}$. The immediate reward is $G(O(t+1), A(t), O(t)) = d_1 A(t) + d_3[S(t) - S(t-1)]$. Define $V_T(O(T)) = 0$ for any terminal state $O(T)$. Thus,

the Bellman Equation for the value function can be written as follows.

$$V_t(O(t)) = \min_{A(t)\in\widehat{A}_t} \Big(G(O(t+1), A(t), O(t)) + E[V_{t+1}(O(t+1))|O(t), A(t)] \Big).$$

Since $S(t), I(t) \in [0,1]$ are continuous, for computational tractability, we discretize them into N sub-states $\left\{ \frac{i}{N-1}, i \in \{0, 1, \cdots, N-1\} \right\}$. With a finite horizon and finite state and action spaces, we can solve the lockdown policy optimization problem using backward induction.

Structural Properties of Optimal Lockdown Decisions

In this section, we characterize an important structural property of optimal lockdown decisions. Intuitively, one may want to institute a lockdown at the peak of an outbreak. However, as we show in Proposition 4.4.3, this decision may be suboptimal and lockdown policies are less effective when the disease prevalence $I(t)$ is below a low prevalence threshold $\underline{I}$ or above a high prevalence threshold $\overline{I}$, where

$$\underline{I} \equiv \frac{b_1 - \log(\frac{\gamma}{1-\gamma})}{b_3\beta\gamma} \quad \text{and} \quad \overline{I} \equiv \frac{b_1 + b_2\delta - \log(\frac{\delta}{1-\delta})}{b_3\beta\delta}.$$

Here γ and δ are functions of parameters b_2, b_3 and β. The specific functional forms will be given in Supplement C.3.5, where we also prove that $\underline{I} < \overline{I}$.

Next, we omit the day index t and abuse notation for brevity. We denote $\alpha^*_{A=i}(I)$ as the equilibrium activity level given the lockdown decision $A = i$ ($i \in \{0,1\}$), and disease prevalence I in a day. We present Proposition 4.4.3 based on the above defined $\underline{I}$ and $\overline{I}$.

Proposition 4.4.3. *The following two properties hold:*
(a) If $\underline{I} \in [0,1]$, then for any $I_1 < I_2 \le \underline{I}$, the lockdown is more effective at I_2 than at I_1, i.e.,

$$\alpha^*_{A=0}(I_1) - \alpha^*_{A=1}(I_1) \;<\; \alpha^*_{A=0}(I_2) - \alpha^*_{A=1}(I_2)\,.$$

(b) If $\overline{I} \in [0,1]$, then for any $I_2 > I_1 \geq \overline{I}$, the lockdown is more effective at I_1 than at I_2, i.e.,

$$\alpha^*_{A=0}(I_1) - \alpha^*_{A=1}(I_1) \ > \ \alpha^*_{A=0}(I_2) - \alpha^*_{A=1}(I_2)\,.$$

Proposition 4.4.3 sheds light on the timing of lockdown policies by characterizing when a lockdown policy could effectively reduce individual activity level. As illustrated in Figure 4.2, it is more effective to enact lockdowns when the disease prevalence $I(t)$ is moderate, rather than when $I(t)$ is either too high or too low. On the one hand, implementing lockdown in the early or late stage of a pandemic is not effective in disincentivizing the population to go out, because of the low risk of infection (disease prevalence). On the other hand, at a high disease prevalence, individuals may choose to stay at home due to a high risk of infection, rendering a lockdown policy unnecessary. Recall from Figure 4.1 that when disease prevalence is moderate, the difference between socially optimal activity level and the individual equilibrium one is the largest. Consequently, lockdown is most effective when disease prevalence is moderate, wherein individual ignorance of their negative externalities imposed on others manifests.

4.4.3 Social Distancing Policy

While the lockdown policy reduces individual activity level by indirectly eliminating the utility gained from nonessential social interactions, the social distancing policy directly imposes an upper bound $1 - \kappa(t)$ on the individual activity level. We examine the equilibrium under social distancing policies in this section, and discover structural properties of optimal social distancing decisions.

Equilibrium Analysis in the Social Distancing Policy

In the following lemma, we show that when the social distancing policy is stringent and requires an activity level lower than individual baseline equilibrium activity level (i.e., $1 - \kappa(t) < \alpha^*_B(t)$) on a given day t, one possible symmetric equilibrium activity

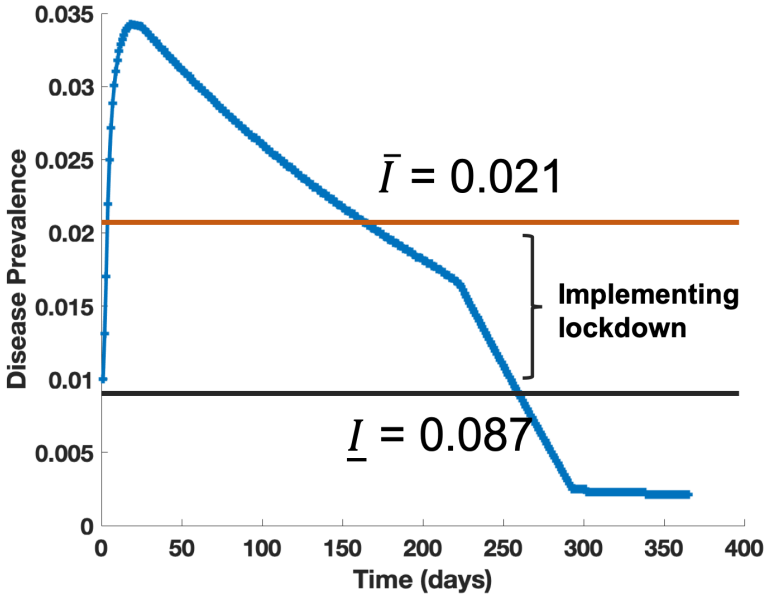

Figure 4.2: Effective interval of disease prevalence to implement lockdown policy based on COVID-19 data presented in Table C.1

The blue curve represents disease prevalence if no lockdown is implemented over the entire time horizon. Calculation of $\underline{I}$ and $\bar{I}$ is presented in Section 4.5.2.

level $\alpha^*(t)$ is exactly $1 - \kappa(t)$.

Lemma 4.4.1. *Suppose that the social distancing policy $\kappa(t)$ on day t satisfies $1 - \kappa(t) < \alpha_B^*(t)$, and $\alpha_{-i}(t) = 1 - \kappa(t)$. Then, individual i's best response activity level is $\alpha_i^*(t) = 1 - \kappa(t)$.*

Based on Lemma 4.4.1, we have the following theorem about the equilibrium activity level $\alpha_\kappa^*(t)$ under a social distancing policy.

Theorem 4.4.2. *Under a social distancing policy $\kappa(t)$ on day t, there exists a unique symmetric equilibrium activity level* $\alpha_\kappa^*(t) = \begin{cases} \alpha_B^*(t) & \text{if } \alpha_B^*(t) \le 1 - \kappa(t); \\ 1 - \kappa(t) & \text{otherwise.} \end{cases}$

Theorem 4.4.2 characterizes the symmetric equilibrium of an individual activity level under two different circumstances. When the baseline equilibrium activity level $\alpha_B^*(t)$ is

outside the region of $[0, 1-\kappa(t)]$, individual equilibrium activity level is $\alpha^*_\kappa(t) = 1-\kappa(t)$. Otherwise, the equilibrium individual activity level is the same as the baseline setting $\alpha^*_\kappa(t) = \alpha^*_B(t)$. In either case, the societal activity level is $\overline{\alpha}(t) = \alpha^*_\kappa(t)$.

Social Distancing Policy Optimization

One can easily show that both $\alpha_\kappa(t)$ and the disease state trajectory $\{(S(t), I(t), R(t))\}_{t=1}^T$ are uniquely determined by $\kappa(t)$ using Lemma C.3.1 and Eq.(4.5). Thus, the trajectory of societal activity level $\overline{\alpha}(t)$ and the disease states are both functions of $\kappa(t)$. Therefore, we formulate the CP's social distancing policy optimization as the *Social Distancing Model*. The objective (4.20) is to minimize the overall cost as defined in Eq.(4.10). The disease dynamics, the policy cost, and individual responses are captured by all constraints.

Social Distancing Model

$$\min_{\boldsymbol{\kappa}} \quad g(\boldsymbol{\kappa}) = \sum_{t=1}^{T-1} q(\kappa(t)) + d_3[S(1) - S(T)] \tag{4.20}$$

$$\text{s.t.} \quad \text{Eq.(4.1)}, \ \text{Eq.(4.5)}, \ \text{Eq.(4.9)}, \ \text{and Eq.(4.12)}$$

$$\overline{\alpha}(t) = \alpha^*_\kappa(t) \qquad t = 1, \cdots, T-1 \tag{4.21}$$

$$\kappa(t) \in [0, \kappa_{\max}] \qquad t = 1, \ldots, T-1.$$

The *Social Distancing Model* is highly nonconvex because Eq.(4.1) is nonconvex. Unlike the *Lockdown Model*, the decision variable $\boldsymbol{\kappa}$ is continuous. Thus, the dynamic programming solution technique used in Section 4.4.2 cannot be directly applied. We propose a gradient descent algorithm in Alg. 1 to solve the *Social Distancing Model*. Specifically, we derive the gradient of the objective function regarding $\kappa(t)$ recursively through $t \in \{T-1, T-2, \ldots, 1\}$ using backpropagation (or the chain rule). Eq.(4.12) is treated as an activation function, where derivatives of $S(t+1)$, $I(t+1)$ and $R(t+1)$ are

0 if $\alpha(t) = \alpha_B^*(t)$. Due to the nonconvexity of the *Social Distancing Model*, a gradient descent algorithm may not generate a sequence that converges to the globally optimal solutions. Therefore, we repeat the gradient descent process with different randomly-generated initial feasible solutions and select the best solution among multiple restarts.

Algorithm 1: Gradient descent algorithm for the *Social Distancing Model*

Data: Initial disease status $(S(1), I(1), R(1))$; parameters b_1, b_2, b_3, d_3 β, r, ϕ, $q_{\max}$, $\kappa_{\max}$; convergence criteria $\epsilon > 0$; iteration limit N; step size λ; number of restarts M

Result: Optimized social distancing policy $\boldsymbol{\kappa}^*$

for $m \leftarrow 1$ **to** M **do**
- Randomly select initial feasible $\boldsymbol{\kappa}_1$; iterator $i \leftarrow 1$;
- **while** $i < N$ *and* $||\boldsymbol{\kappa}_i - \boldsymbol{\kappa}_{i-1}|| > \epsilon$ **do**
  - **for** $t_1 \leftarrow T-1$ **to** 1 **do**
    - **for** $t_2 \leftarrow t_1$ **to** 1 **do**
      - **if** $\alpha(t_1) \geq 1 - \kappa_i^*(t_2)$ **then**
        - Compute $(\frac{\partial S(t_1+1)}{\partial \kappa_i(t_2)}, \frac{\partial I(t_1+1)}{\partial \kappa_i(t_2)}, \frac{\partial R(t_1+1)}{\partial \kappa_i(t_2)})$ based on $(\frac{\partial S(t_1+1)}{\partial \kappa_i(j)}, \frac{\partial I(t_1+1)}{\partial \kappa_i(j)}, \frac{\partial R(t_1+1)}{\partial \kappa_i(j)})$ where $j \in \{t_2+1, \ldots, t_1\}$;
        - `/* derivatives derived from Eq.(4.1) */`
      - **else**
        - $\frac{\partial S(t_1+1)}{\partial \kappa_i(t_2)} = \frac{\partial I(t_1+1)}{\partial \kappa_i(t_2)} = \frac{\partial R(t_1+1)}{\partial \kappa_i(t_2)} = 0$;
      - **end**
    - **end**
    - Compute $\frac{\partial g(\boldsymbol{\kappa}_i)}{\partial \kappa_i(t_1)} = \sum_{j=t_1}^{T-1} \frac{\partial q(\kappa_i(j))}{\partial \kappa_i(t_1)} - d_3 \frac{\partial S(T)}{\partial \kappa_i(t_1)}$;
  - **end**
  - $\boldsymbol{\kappa}_{i+1} = \boldsymbol{\kappa}_i - \lambda \nabla_{\boldsymbol{\kappa}_i} g(\boldsymbol{\kappa}_i)$ where $\nabla_{\boldsymbol{\kappa}_i} g(\boldsymbol{\kappa}_i) = (\frac{\partial g(\boldsymbol{\kappa}_i)}{\partial \kappa_i(1)}, \frac{\partial g(\boldsymbol{\kappa}_i)}{\partial \kappa_i(2)}, .., \frac{\partial g(\boldsymbol{\kappa}_i)}{\partial \kappa_i(T-1)})^T$;
  - $i = i + 1$;
- **end**
- $\boldsymbol{\kappa}^* = \arg\min(g(\boldsymbol{\kappa}^*), g(\boldsymbol{\kappa_i}))$; `/* Update` $\boldsymbol{\kappa}^*$ `as the best solution */`

end

Structural Properties of Optimal Social Distancing Decisions

To proceed, we omit the day index t and abuse notation for brevity. We denote $\alpha_B^*(I)$ as the equilibrium activity level without any public health intervention (baseline case) at disease prevalence I. In addition, we denote $\alpha^*(\kappa, I)$ as the equilibrium activity level given the social distancing decision κ and disease prevalence I in a day, and we denote the corresponding policy cost as $q(\kappa)$.

Proposition 4.4.4. *Given disease prevalence I on a day, the optimal distancing policy κ^* should satisfy one of the following conditions: 1) $\kappa^* > 1 - \alpha_B^*(I)$ and $\kappa^* \leq \kappa_{\max}$. 2) $\kappa^* = 0$.*

Proposition 4.4.4 reveals that CP shall either implement a stringent social distancing policy that affects individual behavior or no social distancing policy at all, which is aligned with previous findings without considering individual reactions [90].

Proposition 4.4.5. *Suppose disease prevalence $I_1 < I_2$,*
(a) For the same social distancing policy κ, $\alpha_B^*(I_1) - \alpha^*(\kappa, I_1) \geq \alpha_B^*(I_2) - \alpha^*(\kappa, I_2)$.
(b) If social distancing policies κ_1 and κ_2 satisfy $\alpha_B^*(I_1) - \alpha^*(\kappa_1, I_1) = \alpha_B^*(I_2) - \alpha^*(\kappa_2, I_2)$, we have $q(\kappa_1) \leq q(\kappa_2)$.

Proposition 4.4.5 characterizes the effectiveness and cost of the social distancing policy at different disease prevalence. First, a given social distancing policy is more effective in changing individual behavior at lower disease prevalence. Second, it is more costly to achieve the same reduction in societal activity level at a higher disease prevalence. This proposition confirms the following intuition: at a high disease prevalence, people have already reduced their activity level due to the risk of infection so that it is more costly for the CP to further restrain their activities.

Due to the maximum possible social distancing stringency $\kappa_{\max}$, when the disease prevalence is higher than a prevalence threshold $\overline{I}_\kappa$, social distancing policy cannot effectively change individual activity level. Thus, it is more cost-effective to implement

the social distancing policy when the disease prevalence is lower than $\overline{I}_\kappa$, where $\overline{I}_\kappa$ is a function of parameters b_1, b_2, b_3, β and $\kappa_{\max}$, defined as:

$$\overline{I}_\kappa = \frac{b_1 + b_2(1-\kappa_{\max}) - \log(\kappa_{\max}^{-1} - 1)}{b_3\beta(1-\kappa_{\max})}.$$

Next, we formally present this result.

Corollary 4.4.1. *If $\overline{I}_\kappa \in [0,1]$, the social distancing policy does not reduce individual activity level on a given day when the disease prevalence is $I \geq \overline{I}_\kappa$.*

Corollary 4.4.1 and Proposition 4.4.5 shed light on the timing when the social distancing policy is cost-effective. The social distancing policy is most effective in influencing individual behaviors if the disease prevalence is smaller than the threshold $\overline{I}_\kappa$. When the disease prevalence is high, an individual's activity level is low regardless of the implementation of social distancing policy. Thus, our results highlight the importance of enforcing the social distance policy even when the disease prevalence is not at its peak level (below $\overline{I}_\kappa$). It is more effective in reducing individuals' activity levels and is less costly than when the disease prevalence is peak. We derive the specific values and validate the existence of $\overline{I}_\kappa$ in our numerical experiments in Section 4.5.2.

4.5 Numerical Experiment

We conduct numerical experiments and derive insights using Minnesota COVID-19 data [98, 100] in this section. In Section 4.5.1, we explain the model parameterization procedure. In Section 4.5.2, we evaluate the effectiveness of the lockdown policy and the social distancing policy.

4.5.1 Model Parameterization

We obtain disease dynamic parameters, including infection rate β and recovery rate r, from public epidemiological data in Minnesota [98] and a validated Minnesota

COVID-19 micro-simulation model [100]. We quantify the overall health impacts of COVID-19 using the disability-adjusted life-year and Net Monetary Benefit framework [159, 57]. Specifically, we estimate the expected disease burden associated with COVID-19 infection (b_3 and d_3) as follows:

$$\begin{aligned}\text{Disease Burden} = (\text{treatment cost} + \text{cost per non-fatal case}) \times \text{symptomatic rate} \\ \times \text{clinical confirmation rate} + \text{cost per fatal case} \times \text{mortality rate}.\end{aligned} \tag{4.22}$$

Treatment cost is obtained from [14]. Cost per non-fatal cases consists of: 1) the years of life lost (YLL) due to disability for being sick [159]; and 2) the productivity loss due to workdays lost. Cost per fatal case is the monetized YLL due to death.

In the base case, we consider $d_3 = b_3$. However, if the CP considers the cost related to sequelae of COVID-19 as part of the CP's perceived disease burden of infection, then d_3 could be higher than b_3. Moreover, d_3 might be higher if the healthcare system is overloaded (e.g., exceeding ICU capacity). Therefore, we consider an additional scenario where d_3 is 20 times higher than b_3 (roughly \$500,000 higher), which mimics an extreme case where the CP's perceived cost of infection is much higher than an individual's disease burden.

Daily costs of lockdown (d_1) and maximum-level social distancing ($q_{\max}$) are estimated based on GDP loss due to public health policy implementation [171, 147, 168]. Personal utility parameters b_1 and b_2 are estimated based on Minnesota annual average income [42] and the GDP loss data. The full list of parameters is presented in Table C.1 in the Appendix. A detailed parameterization is explained in Supplement C.2.

4.5.2 Policy Evaluation

In our experiment, we assume initial disease states $S(1) = 0.99$, $I(1) = 0.01$ and $R(1) = 0$ [52] over a 365-day time horizon ($T = 365$). We deploy the *Lockdown*

Model and the dynamic programming solution algorithm (with discretization parameter $N = 7000$) in Section 4.4.2 to derive the optimal lockdown policy. Then, we use the *Social Distancing Model* and the gradient descent algorithm (with $M = 5000$ restarts) in Section 4.4.3 to derive the optimal social distancing policy. We evaluate outcome measures including disease burden, policy cost, and overall cost under different scenarios in Sections 4.5.2 and 4.5.2, and compare their effectiveness and study a concurrent implementation of both policies in Section 4.5.2. In this section, per-person disease burden refers to individual's perceived per-person disease burden.

Lockdown Results

Cost changes	**Policy specification**	**Individual's perceived per-person disease burden**	**CP's perceived per-person disease burden**	**Per-person policy cost**
$d_3 = b_3$	unlimited lockdown	\$18747	\$18747	\$0
$d_3 = 20 \times b_3$	unlimited lockdown	\$18152	\$363046	\$4289.2
$d_3 = 20 \times b_3$	one lockdown	\$18391	\$18391	\$3119.4
$d_3 = b_3$	social distancing	\$17490	\$17490	\$555.8
$d_3 = 20 \times b_3$	social distancing	\$14146	\$282919	\$11631

Table 4.1: **Cost decomposition for different scenarios**

As shown in Table 4.1, when an individual's perceived disease burden b_3 is equal to the CP's perceived cost of infection d_3, the total per-person disease burden (i.e., $d_3[S(1) - S(T)]$) is \$18747. Also, it is optimal to enforce no lockdown over the entire time horizon, which leads to a \$0 policy cost (Figure 4.3). Note that lockdown reduces individual activity level, thus indirectly impacting the disease spread. It could be perceived as a costly measure when the CP has a low cost of infection (e.g., $d_3 = b_3$). However, if d_3 is much higher ($d_3 = 20 \times b_3$), the CP will implement lockdown in the middle to late phase of the outbreak. The resulting per-person disease burden is \$18152,

and the lockdown policy cost is $4289.2 (Table 4.1).

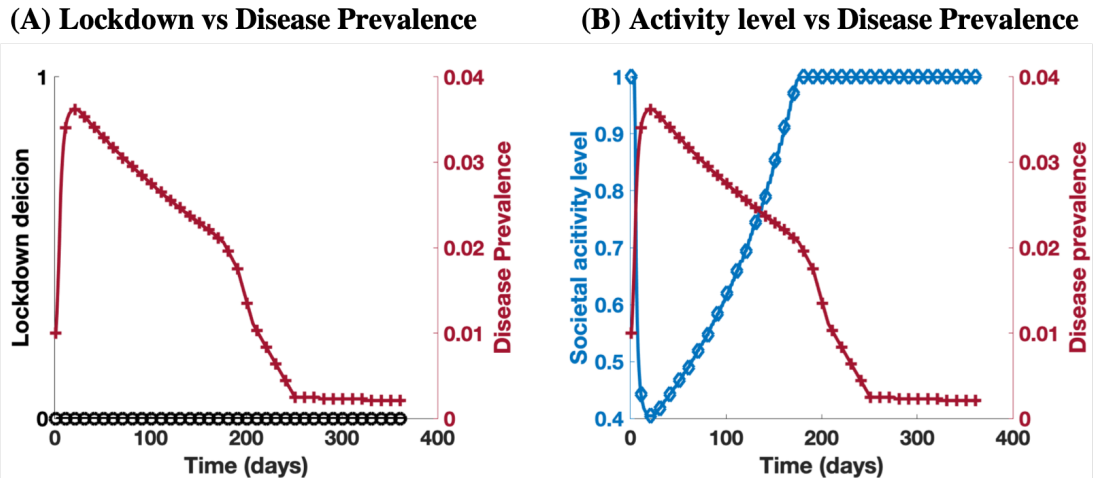

Figure 4.3: Base-case ($d_3 = b_3$) lockdown policy model outcome.

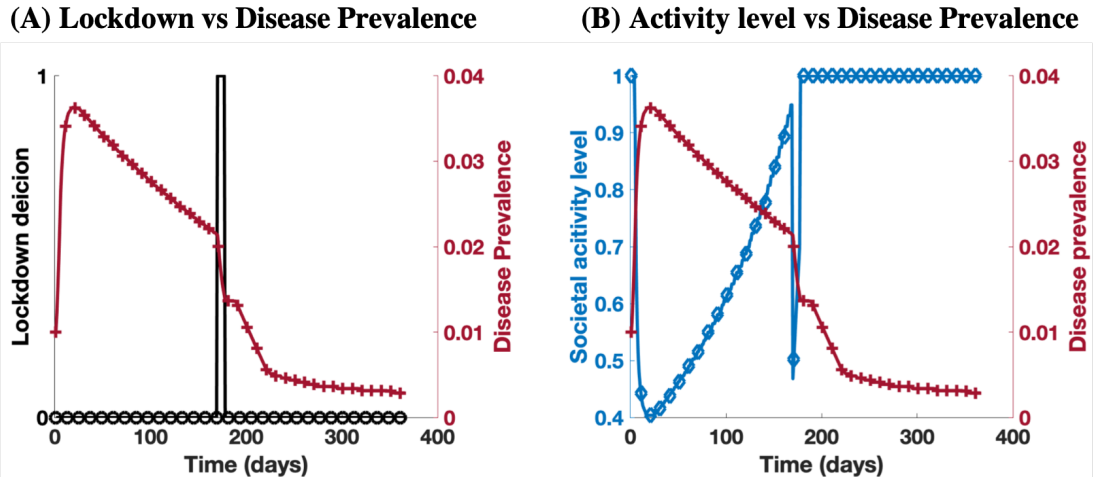

Figure 4.4: Alternative scenario ($d_3 = 20 \times b_3$), and at most one lockdown initiation allowed.

As we discuss in Section 4.4.2, it might be impractical for the CP to enforce frequent lockdowns. Therefore, we consider the case where the CP could only initiate lockdown once. In the base case with $d_3 = b_3$, the outcome is the same as that for infinite lockdowns, as it is optimal to enforce no lockdown. For the case with $d_3 = 20 \times b_3$, we

have a per-person disease burden of \$18391 and lockdown policy cost of \$3119.4 (Table 4.1).

Figures 4.3 and 4.4 illustrate the changes of disease prevalence and activity level over time under optimal lockdown decision sequences. There are a few interesting observations. First, in both figures, the minimum activity level $\alpha_A(t)$ coincides with the highest disease prevalence $I(t)$ over the time horizon. As $I(t)$ decreases, $\alpha_A(t)$ increases. This observation is consistent with the results in Proposition 4.4.2. Second, when $d_3 = 20 \times b_3$, we see in Figure 4.4 that $\alpha_A(t)$ becomes very close to 1 after day $t = 240$. This can be explained by the much larger utility of going out, than that of staying home, at an extremely low disease prevalence (i.e., $b_3\beta I(t) \ll b_1 + b_2$).

Next, we investigate the optimal lockdown period in both scenarios. Using the same set of parameters, we estimate $\underline{I} = 0.87\%$ and $\overline{I} = 2.10\%$ in Proposition 4.4.3. From Figure 4.4 (the one lockdown, $d_3 = 20 \times b_3$ scenario), we observe the lockdown is generally initiated when the disease prevalence is within the interval $[\underline{I},\ \overline{I}]$. This observation confirms our findings in Proposition 4.4.3 that it is more effective to enact lockdowns at a moderate $I(t)$ than at extremely high or low disease prevalence. It is also consistent with the findings from Proposition 4.4.1 and Figure 4.1 that the difference between the socially optimal activity level $\alpha^*_{\text{aw}}(t)$ and equilibrium activity level $\alpha_A(t)$ is larger at a moderate disease prevalence. Consequently, it is more beneficial to enact lockdowns at a moderate disease prevalence. As shown in Table 4.1, implementing lockdown once increases the per-person disease burden by \$239 but reduces the per-person policy cost by \$1169 compared to the unlimited lockdown scenario. This is consistent with our discussion on Figure 4.3: lockdown policy could be costly while not effectively reducing the disease burden.

Social Distancing Results

As shown in Table 4.1, the per-person disease burden is \$17490, and the social distancing policy cost is \$555.8 when $d_3 = b_3$. Figure 4.5 illustrates the changes of

activity level and disease prevalence over time under optimal social distancing decisions. Based on these parameters, we estimate $\overline{I}_\kappa = 2.51\%$ in Corollary 4.4.1. The observation from Figure 4.5 is consistent with our analytical findings in Corollary 4.4.1 that social distancing shall be implemented when the disease prevalence is less than $\overline{I}_\kappa$. It is also consistent with our findings in Proposition 4.4.5. At a large $I(t)$, individuals may voluntarily reduce their activity level. Further reducing the activity level by enforcing strict social distancing would incur a much higher cost. Therefore, we observe that no social distancing is implemented when individuals are vigilant at high disease prevalence.

In the middle to late phase of the outbreak, as $I(t)$ declines, social distancing becomes beneficial. By our model assumption, individuals are myopic and ignore the negative externality imposed on others. As a result, at a moderate disease prevalence (e.g., $0.5\% - 2\%$ people are in the state I), individuals observe a smaller risk of infection compared to the peak and thus prefer to *go out*. However, as evidenced by Proposition 4.4.1, the situation might worsen with increased social activities from a societal perspective. Therefore, the CP could increase societal health benefits by enforcing social distancing in the middle to late stage of the outbreak.

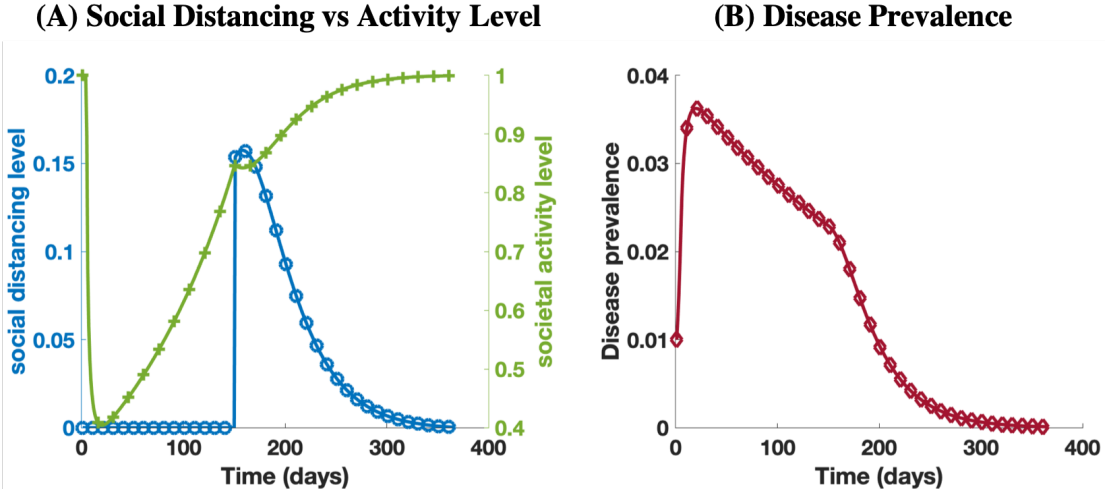

Figure 4.5: Base-case ($d_3 = b_3$) social distancing policy model outcome.

Policy Comparison and Concurrent Implementation

In this section, we compare the effectiveness of these two policies and evaluate the result of implementing both policies simultaneously. Based on the results in Table 4.1, social distancing policy incurs a smaller total cost (i.e., CP's perceived per-person disease burden + per-person policy cost) than the lockdown policy in the base case, where $d_3 = b_3$. When $d_3 = 20 \times b_3$, social distancing policy becomes more effective in reducing the total infection and thus the per-person disease burden, further increasing its advantage over the lockdown policy. Therefore, social distancing policy outperforms lockdown policy in reducing the overall societal burden. This finding is consistent with the literature without considering individual responses [67, 121, 171].

We also consider a concurrent implementation of both policies. When the optimal social distancing policy has already been implemented, our experiment results suggest that no lockdown should be implemented in either scenario $d_3 = b_3$ or $d_3 = 20 \times b_3$. That is, the social distancing policy dominates the lockdown policy.

4.6 Vaccine Strategies under Social Distancing

Besides lockdown and social distancing policies, vaccination is another effective way to contain the pandemic. However, due to the limit of production capacity, the CP has to decide the vaccine priority strategies while maintaining public health interventions. Much empirical evidence indicates that the elderly has been disproportionately affected by the pandemic because they are at higher risk for severe illness [24, 98]. As COVID-19 vaccines become available, CDC and many state authorities recommend that the elderly should be vaccinated first over the general public [24, 97]. However, because the elderly might engage in less social interaction, their activities would have much smaller negative impact on others compared to youth and adults [170]. Thus, it is not straightforward that vaccinating the elderly first is the optimal priority to contain disease transmission. In this section, we discuss vaccine priorities among individuals with different choices

of activity level and negative externality imposed to others due to the heterogeneity in the severity of infection using a similar framework that incorporates individuals' choice but with some modifications. Specifically, we investigate the vaccine priority under social distancing[2] and examine how it changes with the vaccine capacity, the disease transmission rate, and the mortality rate.

4.6.1 SEIR Model with Heterogeneous Individuals and Vaccination Strategy

As age is one of the critical demographic factors in COVID-19, we stratify the population into three age groups: Youth (0 - 19 years old), Adult (20 - 59 years old), and Elderly (60 years old and above). We denote the subscript $i \in \{1, 2, 3\}$ for Youth, Adult, and Elderly age groups. This age stratification is consistent with practices in the medical literature [171, 84], allowing model parameterization and validation with available data.

While the SIR model provides tractable analysis in previous sections and is one of the most relevant mathematical models to describe the spread of an infectious disease [2], we extend the SIR model to the SEIR model to capture the long latent phase of COVID-19 infection and to incorporate the process of vaccination implementation [168]. That is, in addition to the health state $S_i(t)$, $I_i(t)$, and $R_i(t)$ for age group i, we use state $E_i(t)$, $N_i(t)$, and $V_i(t)$ to represent the number of exposed individuals, the total number of living individuals, and the number of vaccinated individuals in age group i on day t. Let β be the per-contact transmission rate (instead of infection rate in the homogeneous model), and a^{-1} be the average incubation period. Given the mortality rate μ_i for age group i, the mortality in each period can be represented by $N_i(t+1) - N_i(t) = -\mu_i I_i(t)$. If an individual in group i is vaccinated, s/he will be excluded from the susceptible state $S_i(t)$, and counted among recovered individuals.[3] We use $\widehat{S}_i(t)$ and $\widehat{R}_i(t)$ to represent

[2] We have shown that the lockdown policy is dominated by the social distancing policy in Section 4.5.2.

[3] We assumed that COVID-19 vaccine has 100% effectiveness (i.e., individuals are fully protected from

the effective number of susceptible and recovered individuals considering vaccination in age group i. The following two equations describe the vaccination process of age group i on day t:

$$\begin{aligned} \widehat{S}_i(t) &= \max(S_i(t) - V_i(t), 0) \\ \widehat{R}_i(t) &= \min(S_i(t), V_i(t)) + R_i(t). \end{aligned} \tag{4.23}$$

In Eq.(4.23), the max and min operators guarantee that the number of daily vaccinated individuals $V_i(t)$ is no more than the number of the susceptible individuals $S_i(t)$ in the same age group. Let $\alpha_i(t)$ represent the activity level of age group i on day t. Denote $\vec{\alpha}(t)$ as the collection $(\alpha_1(t), \alpha_2(t), \alpha_3(t))$ and $\sigma_i(\vec{\alpha}(t))$ as the probability of infection for age group i with the societal activity level vector $\vec{\alpha}(t)$. It follows that

$$\sigma_i(\vec{\alpha}(t)) = \beta \sum_j C_{ij} \alpha_j(t) \frac{I_j(t)}{N_j(t)}.$$

We update the age-structured SEIR model in the presence of vaccination as follows:

$$\begin{aligned} S_i(t+1) - \widehat{S}_i(t) &= -\sigma_i(\vec{\alpha}(t))\alpha_i(t)\widehat{S}_i(t) \\ E_i(t+1) - E_i(t) &= +\sigma_i(\vec{\alpha}(t))\alpha_i(t)\widehat{S}_i(t) - aE_i(t) \\ I_i(t+1) - I_i(t) &= +aE_i(t) - rI_i(t) - \mu_i I_i(t) \\ R_i(t+1) - \widehat{R}_i(t) &= +rI_i(t) \\ N_i(t+1) - N_i(t) &= -\mu_i I_i(t). \end{aligned} \tag{4.24}$$

The three age groups are different in their disease burden (or equivalently, expected severity of infection) $b_{3,i}$, and their normal daily contact (denoted by C_{ij}), which counts the number of interactions for individuals in a given age category i with age group j before the pandemic.

COVID-19 if vaccinated). The actual effectiveness of the COVID-19 vaccine is more than 95% [119]. One can easily adjust the total "effective" vaccine dosage to reflect the lower effectiveness of a vaccine.

The utility of *going out* for age group i can be written as:

$$U_i(\text{go out}, \vec{\alpha}(t)) = b_1 + b_2 \frac{\sum_j C_{ij}\alpha_j(t)}{\sum_j C_{ij}} - b_{3,i}\sigma_i(\vec{\alpha}(t)).$$

Using an MNL model, we have:

$$\alpha_i(t) = \frac{\exp(U_i(\text{go out}, \vec{\alpha}(t)))}{1 + \exp(U_i(\text{go out}, \vec{\alpha}(t)))}. \tag{4.25}$$

One can prove that Eq.(4.25) admits exactly one solution using Tarski Fixed Point Theorem. Still, the CP's goal is to minimize the sum of per-person disease burden and per-person policy cost (we focus on social distancing). Thus, the CP's objective in Eq.(4.20) under social distancing policy and vaccination can be written as follows:

$$\min_{\{\kappa(t)_{t=1}^{T-1}\}} \sum_{t=1}^{T-1} q(\kappa(t)) + \sum_i d_{3,i} \left(\frac{S_{1,i} - S_{T,i}}{N_{1,i}} \right).$$

4.6.2 Model Parameterization and Validation

We use COVID-19 data from Minnesota as of Dec. 13, 2020, as the starting disease status in our simulation, which closely matches the vaccination plan timeline in Minnesota [97]. We assume that the total infectious cases at $t = 1$ in our simulation are equal to the difference between the cumulative number of confirmed infections and the cumulative number of recoveries as of Dec. 13, 2020. Parameters values are summarized in Table C.1, and parameterization is detailed in Supplement C.2.

To validate our model, we use the Minnesota COVID-19 data as of Nov. 30, 2020, as the initial disease state to predict the number of infections on Dec. 30, 2020. Within this one-month period, social distancing was implemented in Minnesota. We choose one month as our prediction horizon since prediction for a longer period may be subject to bias due to Minnesota's frequently-changing policies [99]. As of Nov. 30, 318763

confirmed infections were reported in Minnesota. In our model, we assume that confirmed cases on Nov. 30 were distributed proportionally to the age distribution. We test different scenarios where the social distancing policy reduces contact rate by 30% - 50%, and our model estimates a total of 75781 - 141130 new infections in one month. These estimates are aligned with 94344 new infections reported between Nov. 30 and Dec. 30, 2020, in Minnesota.

4.6.3 Results and Sensitivity Analysis

Results

With limited supply of vaccines, we consider the following six vaccination implementation strategies in the three age groups (in terms of the priority order of receiving vaccines): 1) youth-adult-elderly (i.e., vaccinate youth first, then adults and the elderly last); 2) youth-elderly-adult; 3) adult-youth-elderly; 4) adult-elderly-youth; 5) elderly-youth-adult; and 6) elderly-youth-adult[4]. In our analysis, we consider a daily vaccine capacity of 50000 dosages[5]. We apply the gradient descent algorithm (Alg. 1) to the heterogeneous SEIR model with vaccine implementation to obtain social distancing decisions.

In Table 4.2, we present key outcome measures of the six vaccination implementation strategies, including healthcare/social distancing cost, cumulative deaths and infections, and the average activity level since the vaccination plan is initiated. First, we observe that prioritizing the Adult group in Strategy 3 and 4 for vaccination results in the lowest per-person disease burden and social distancing cost. This is the most cost-effective way to restrict transmission and requires the least strict social distancing policy.

[4]We have considered mixed vaccination plans (i.e., all age groups start vaccination since vaccines become available, but have different daily quotas), but the pure strategies outperform them.

[5]In the first stage, about 250000 vaccine doses would be distributed to Minnesota for people working in health care settings and long-term care facilities [97]. When this paper is written, around 10000 - 30000 dosages of vaccine is administrated per day. The daily capacity may increase in the later stage of the pandemic. For simplicity, we assume that the vaccine can be administrated in one shot, but our analysis can be easily extended to two-shot vaccines.

Second, prioritizing the Elderly group in Strategy 5 and 6 leads to the lowest number of deaths. This is because the Elderly group has an excessively large mortality rate ($\mu_3 = 2.40\%$) compared to the Youth ($\mu_1 = 0.003\%$) and the Adult ($\mu_2 = 0.3\%$) (see Table C.1). However, prioritizing the Elderly group does not necessarily lead to fewer infections and must be accompanied by the strictest social distancing policies. This is because the Elderly group imposes the least negative externality compared to the other two groups. Thus, prioritizing the Elderly may result in higher healthcare and social distancing costs than other strategies. Third, if vaccines are available to the Youth group, prioritizing the Youth group can result in the least cumulative infection (Strategy 1: 4.51%; Strategy 2: 5.00%) because of their high activity level. Finally, under all six vaccination implementation strategies, social distancing policy should be implemented with about 15% - 25% contact reduction. Thus, it is important and more effective to implement both vaccination and social distancing to reduce COVID-19 transmission.

Sensitivity Analysis

The preceding discussions suggest that, besides the mortality risk of specific age groups, vaccination priority plans should also consider the negative effect imposed on others by the age group with high activity level (due to their low mortality risk and a lower disease burden if infected). In this section, we discuss how vaccine capacity, mortality risk, and per-contact transmission rate could affect the three most important outcome measures: the cumulative deaths, cumulative infections, and the total cost. Since all COVID-19 vaccines developed so far primarily target adults that are 19 years and older [97], we focus on Strategy 3: Adult-Elderly-Youth (referred to as "Strategy Adult" hereafter) and Strategy 6: Elderly-Adult-Youth (referred to as "Strategy Elderly" hereafter).

First, we increase the daily vaccine capacity from 50000 doses to 300000 doses per day, with all other parameters remaining unchanged. Similar to the results for 50000-dose capacity in Table 4.2, Figure 4.6 illustrates that Strategy Elderly results in a

lower number of deaths but a higher total cost. Not surprisingly, both the number of deaths and infections decreases with the vaccine capacity. However, as the vaccine capacity increases, the rate at which infection decreases under Strategy Adult is faster than that under Strategy Elderly. This is because the Adult group is more active than the Elderly group, and vaccinating the Adult group could accelerate the reduction of infections due to their stronger negative externality compared to the Elderly group. This is consistent with the findings of [170] where there is no constraint on vaccine production capacity. However, when vaccine capacity is very limited (5000 or 10000 daily capacity), it takes much longer to end the pandemic. Consequently, the majority of the population, including the Elderly group, are infected under either strategy. As a result, the number of infections under the two strategies are very close. Therefore, in contrast to [170]'s findings, Strategy Elderly recommended by CDC becomes more favorable because it results in similar number of infections but much fewer deaths when vaccine production capacity is limited.

Second, we reduce the mortality ratio of the Elderly to the Adult group from roughly 6:1 in the base case to 2:1 with the hope that medical treatments for severe complications of COVID-19 will become more effective. Similar to the results in Table 4.2, Figure 4.7C shows that Strategy Adult dominates Strategy Elderly economically. As expected, both the number of deaths and infections decreases with the mortality ratio. As the mortality ratio becomes smaller (closer mortality rate), the negative externality due to high activity level becomes more salient. Therefore, vaccinating the group with a higher activity level (i.e., the Adult group) could result in both fewer infections and fewer deaths, as shown in Figures 4.7A and 4.7B.

Lastly, we examine the impact of increasing contract transmission rate β up to 80% higher than the base case β because some coronavirus variants might be more infectious [27]. Figure 4.8 shows that, Strategy Elderly poses a lower number of deaths compared to Strategy Adult because of the Elderly group's high mortality rate, but a higher number of infections because of the stronger negative externality imposed by the

Adult group. However, Strategy Elderly becomes an economically dominant strategy with a lower cost compared to Strategy Adult as β increases.

In sum, we find that the trade-off between higher mortality rate and negative externality imposed by the active age/risk group is the key to determining the best vaccination priority strategy. The change of vaccine capacity, mortality rate, and contract transmission rate would result in different vaccination priorities. With the current vaccine capacity (less than 50000 doses per day), the recommended vaccination priority ("elderly first") by CDC [24] leads to fewer deaths and a similar number of infections compared to alternative priority plans. Although "elderly first" incurs a higher overall cost in the current situation, it may become more cost-effective than the "adult first" plan as the coronavirus becomes more infectious.

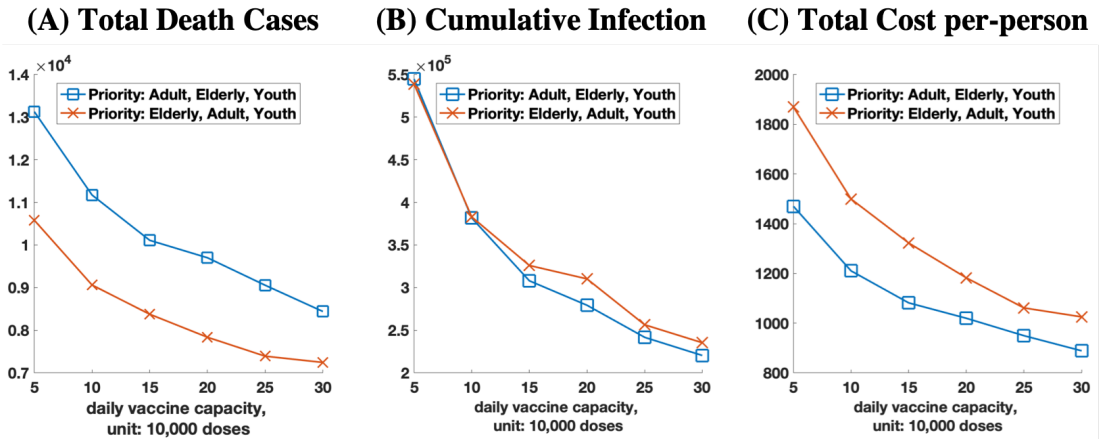

Figure 4.6: Compare vaccination priority strategies under different vaccine capacity per day. All other model parameters are kept unchanged.

4.7 Conclusions

We provide both theoretical and numerical analysis to address the urgent problem of public health intervention design and vaccine prioritization to better contain a pandemic such as COVID-19.

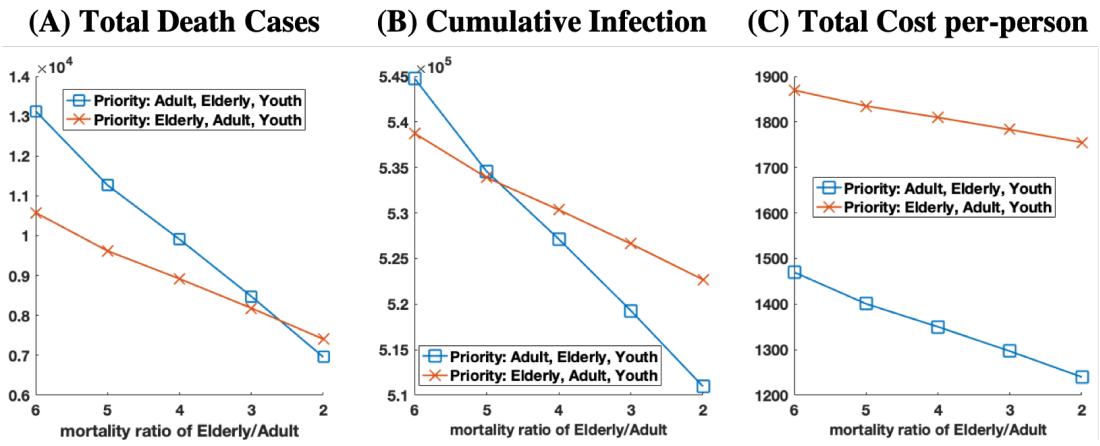

Figure 4.7: Compare vaccination priority strategies under different Elderly/Adult mortality ratio. All other model parameters are kept unchanged.

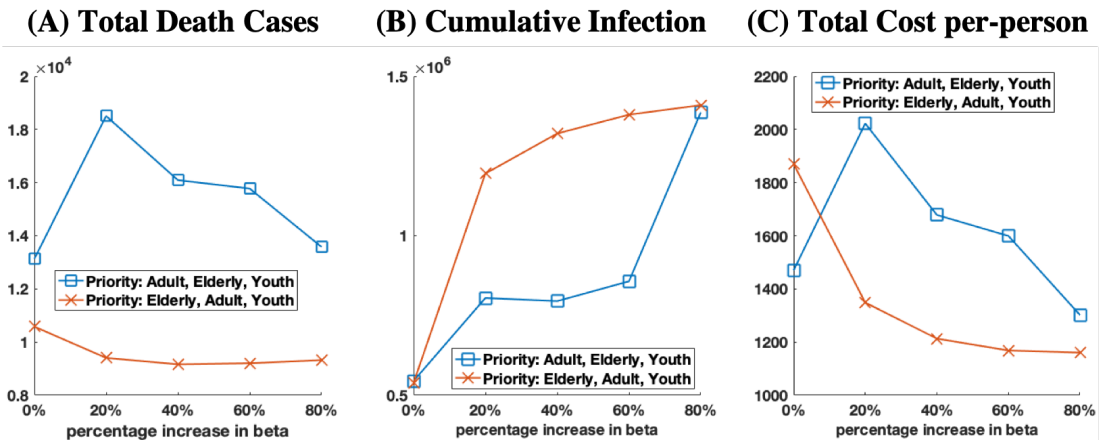

Figure 4.8: Compare vaccination priority strategies under different per-contact transmission rate β. All other model parameters are kept unchanged.

First, we study the strategic planning of lockdown and social distancing policies, two of the most widely-implemented public health interventions, to alleviate the resulting disease burden and socioeconomic loss. We use a multinomial logit choice model to characterize individual reactions to public health interventions and the risk of infection and integrate it into a repeated Stackelberg game model framework.

We derive insightful results from structural properties of equilibrium individual responses and optimal interventions. We show that the individual equilibrium activity level is higher than the socially optimal activity level due to an individual's ignorance of the negative externality imposed on others, with the largest difference at a middle-range disease prevalence. As a result, we find that the lockdown policy is more effective when the disease prevalence is moderate. Similarly, social distancing policy should be more emphasized after the disease prevalence peak. Numerically, we show that the social distancing policy is more cost-effective than the lockdown policy, and simultaneous implementation of both policies does not help contain the disease spread: in fact, it may incur excessive costs.

Second, based on our analytical framework, we investigate the optimal vaccine priority when vaccine production capacity is limited. Due to the heterogeneity of the risk of being in critical condition, younger age groups are more socially active and impose higher negative externality than the elderly. We find that, as a result, vaccine priority highly depends on factors including the government authorities' objective, vaccine capacity, mortality risk and per-contact transmission rate. In particular, our results confirm CDC's recommendation [24] that the "elderly first" strategy prevents excessive deaths and achieves similar cumulative numbers of infections to alternative priority plans due to vaccine capacity constraint. Although the "elderly first" strategy incurs a higher overall cost in the current situation, it may become more cost-effective as the coronavirus becomes more infectious. Finally, we recommend that social distancing be strictly enforced in parallel with vaccine distribution to contain the disease transmission, especially under the "elderly first" vaccination strategy.

To the best of our knowledge, our work is the first to integrate dynamic compartmental models, multinomial logit choice models, game theory, and mathematical optimization into an integrated model framework to study public health interventions for a pandemic. We have made assumptions that are high-level abstraction from reality and are ubiquitous in the literature [48, 94]. Nevertheless, our study has several limitations.

First, our disease progression model only stratifies the population based on age, similar to previous literature [84, 171]. However, other factors like co-morbidity may also influence the severity and mortality of COVID-19 infections. Our model can be easily extended to account for other population demographics as data becomes available. Second, we assume that the disease prevalence is known to both the central planner and the population. Although the exact number of infections might not be known, both agents could infer and estimate the actual prevalence from publicly available information including the number of confirmed infections and test positive rates [123]. Third, we assume the same utility function for all individuals regardless of their health states (i.e., susceptible, infectious or recovered) for analytical tractability. Studies have shown that more than 78% of COVID-19 infections have no symptoms [45] and "80% of infections are mild or asymptomatic"[160]. As a consequence, the majority of the individuals are unaware of their true health states and thus do not differ in their decision-making process for daily activity level. Future work could consider state-specific utility functions using the heterogeneous model developed in the paper. Lastly, we assume that individuals myopically maximize their daily utility when deciding whether to go out or stay at home, but some individuals could be forward looking and maximize their long-term utility in reality. We note that many individual behaviors during COVID-19 are possibly results of myopic decisions, such as holding social events against public health advice [36]. Also, the development of the COVID-19 pandemic has deviated from many scientific predictions [135], which complicates individual long-term decision-making. Therefore, future work should consider these complications when considering forward-looking behaviors.

Target Description	Per-person disease burden	Cumulative deaths	Cumulative infections (percentage)	Average activity level
Strategy 1, vaccine Priority in order of youth-adult-elderly per-person social distancing policy cost: $4029.3				
0-19 years old	$ 53.45	10.52	3.07%	79.56%
20-59 years old	$ 2679.9	4819.8	5.75%	79.56%
60+ years old	$ 1339.7	8487.5	3.38%	79.56%
(weighted) sum	$ 1694.5	13318	4.51%*	79.56%
Strategy 2, vaccine Priority in order of youth-elderly-adult per-person social distancing policy cost: $4951.8				
0-19 years old	$ 53.34	10.50	3.07%	74.45%
20-59 years old	$ 3341.5	6009.7	7.16%	74.45%
60+ years old	$ 957.00	6062.8	2.41%	74.45%
(weighted) sum	$ 1941.2	12083	5.00%*	74.45%
Strategy 3, vaccine Priority in order of adult-elderly-youth per-person social distancing policy cost: $3240.1 *				
0-19 years old	$ 446.32	87.86	25.65%	80.35%
20-59 years old	$ 1968.7	3540.7	4.22%	80.35%
60+ years old	$ 1499.6	9500.4	3.78%	80.35%
(weighted) sum	$ 1470.1*	13129	9.58%	80.35%*
Strategy 4, vaccine Priority in order of adult-youth-elderly per-person social distancing policy cost: $3441.2 *				
0-19 years old	$ 207.18	40.78	11.91%	80.12%
20-59 years old	$ 1912.8	3440.3	4.10 %	80.12%
60+ years old	$ 1661.5	10526	4.19%	80.12%
(weighted) sum	$ 1418.8*	14007	6.11%	80.12%*
Strategy 5, vaccine Priority in order of elderly-youth-adult per-person social distancing policy cost: $5374.2				
0-19 years old	$ 84.70	16.67	4.87%	72.99%
20-59 years old	$ 3487.4	6272.2	7.48%	72.99%
60+ years old	$ 771.21	4885.8	1.95%	72.99%
(weighted) sum	$ 1979.7	11175*	5.51%	72.99%
Strategy 6, vaccine Priority in order of elderly-adult-youth per-person social distancing policy cost: $4215.5				
0-19 years old	$ 382.67	75.33	21.99%	76.90%
20-59 years old	$ 3121.6	5614.2	6.69%	76.90%
60+ years old	$ 772.18	4891.9	1.95%	76.90%
(weighted) sum	$ 1869.6	10581*	9.47%	76.90%

Table 4.2: Result decomposition for different vaccination priorities. (Daily Vaccine = 50000 doses. Initial disease status is the epidemiological status as of Dec 13, 2020. $*$ represents the top two choices in the corresponding outcome measure category)

Chapter 5

Conclusion and Future Work

This dissertation presents applications of stochastic progress modeling for optimizing patient health outcomes in three settings: 1) an acute infectious disease, 2) a chronic infectious disease setting, and 3) an infectious disease outbreak setting. In Chapter 2, we assess the cost-effectiveness of different test-and-treat strategies for AFI patients both analytically and numerically. We formulate the problem to balance the weighted average of antibiotic underuse (short term, and immediate harms) and overuse (long term side effect of developing antibiotic resistance). We find that empirical treatment with antibiotics provided the best outcomes if antibiotics overuse is not the primary concern; otherwise, strategies involving diagnostic tests become cost-effective. PCR-led strategies (e.g., multiplex PCR test or parallel bacterial PCR tests) are robust under parameter uncertainty. Earlier hospital presentation can avoid worsened health outcomes.

In Chapter 3, we introduce a Semi-Markov Decision Process framework for making monitoring decisions for patients with chronic, and potentially infectious diseases with heterogeneous adherence behaviors. We provide policy-relevant structural properties of the stochastic model that allow our framework to be useful in contexts outside the particular application of HIV management. Our results show that all optimized policies

are on the cost-effectiveness frontier, and in certain circumstances, dominating the fixed policies. We conclude that adherence type differentiation could significantly improve patient health outcomes (from a societal perspective) by improving quality-adjusted life-years gained, while saving costs.

In Chapter 4, we use a multinomial discrete choice model to characterize an individual activity level and integrate it into a repeated game-theoretical model with SIR disease transmission dynamics to optimize public health interventions. We find that social distancing is more effective than lockdown. More importantly, an individual activity level is higher than the aggregated optimal activity level, due to an individual's ignorance of the negative externality imposed on others, with the largest difference at a middle-range disease prevalence. Therefore, we find that strict social distancing and lockdown policies should be more emphasized after the disease prevalence peak and is necessary even when vaccines become available. Lastly, due to the heterogeneity of the risk of being in critical condition, the youth and adult group would impose a higher negative externality to the elderly. Thus, vaccine priority can be given to the youth or adult age group rather than the elderly to reduce the overall disease burden and even death rates under certain circumstances.

5.1 Future Research Directions

Our work could be extended in several ways. In Chapter 2, we only study a 45-day time horizon, which is less than all the acute diseases we consider. We can expand our first stage models to account for the surveillance information obtained from implementing different diagnostic tests. We embed the core disease progression models within a longer time horizon modeling framework that incorporates seasonality. Unlike the first stage model that takes the underlying disease prevalence as an input, in this expanded model, diagnostic tests provide additional information on the disease prevalence. We

adopt a Bayesian framework for belief updates: at each time step, we update the belief probability of the disease prevalence given the result(s) of the diagnostic test(s) prescribed in the recently-implemented strategy. This belief update procedure leads to better prevalence estimates and better decisions for future patients. We formulate a stochastic control problem to optimize patient health outcome by choosing the best clinical decision for any given belief of the disease prevalence. To demonstrate the cost-effectiveness of the optimized surveillance policy, we compare Stage 2 model outputs (i.e., DALYs, costs, and antibiotic overuse) to the model outputs of the non-surveillance strategies described in Chapter 2.

In Chapter 3, our model assumed adherence type is known prior to treatment initiation, which generally does not hold in reality. Meanwhile, our model does not consider the impact of frequent monitoring on patient adherence behavior. Researchers found through various studies that adherence intervention programs (i.e., home visits, phone calls, daily tracking, etc.) that could improve patient adherence behavior ([1], [65], [66]). Future work could involve adherence learning, and adherence promoting into the decision-making framework.

In Chapter 4, we focused primarily on motivating the model and developing solution techniques, and made assumptions that are high-level abstraction from reality. Future work could incorporate more detailed stratification on the disease dynamics by incorporating hospitalization, inter-state travels, other possible risk group stratification.

Appendix A

Chapter 2 Supplement Material

A.1 Additional Information

DALY Definition and Calculation

DALY, disability-adjusted life years, is a measure of overall disease burden. We first calculate the Years of Life Lost (YLL) due to premature mortality in the population, and the Years Lost due to Disability (YLD) for people living with the disease. And then the total DALY is calculated by taking the sum of YLL and YLD: DALY = YLL + YLD. For more details on the YLL and YLD, please refer to WHO official definition of DALY ([96]).

In our Result Section, we show the per-patient (expected) DALY where we divide the total DALYs in the population by the population size.

To determine the weights of antibiotic overuse/underuse

For each antibiotic-curable (bacterial) disease, we first computed the difference in and clinical outcomes of the disease progression model with, or without antibiotic treatment to parameterize the weights (reference: Strategy 1, no antibiotics). We then followed the classical approach in healthcare economics to combine the two objectives (incremental costs, DALYs averted) into a single net monetary benefit (NMB) objective

(which is the weight) on cost scale by associating a willingness-to-pay (WTP) threshold per DALY averted: weights = NMB = WTP$*$ DALY averted – incremental costs. In Thailand setting, we estimated w_{under} for leptospirosis: 25777 USD, scrub typhus: 25780 USD, and other bacterial: 25765 USD. To better the problem, we assumed a unified weight (denoted by w_{under}) for all antibiotic-curable diseases: the median, 25777 USD for our case study.

For non-bacterial diseases, the health burden of over-prescribing antibiotics was not captured within the 45-day study horizon. We represented the weight using a monetary penalty (denoted by w_{over} , and the base value was set to the WTP of w_{under}) on every course of antibiotic (over)prescribed to non-bacterial patients. There ha been investigating the cost of resistance by consuming antibiotics. For example, [134] reported the estimated economic cost of resistance per standard unit (per course) of penicillin (an alternative antibiotic to treat bacterial febrile diseases) was $ 0.8 ($ 11.5) in Thailand. Nevertheless, the model might underestimate the cost of resistance to a considerable degree. As discussed in their paper, the model does not take transmission and future medical cost into account. Second, the model only counts a subset of resistant infections, and one death only results in 10 life years lost. More importantly, their definition of estimated cost of resistance deviates from our definition of antibiotic overuse penalty: we only penalize the overused, unnecessary antibiotics prescription, not including those bacterially infected patients whom should indeed receive antibiotic therapy. A higher penalty translates to a higher priority in antibiotics reduction by preventing possible future harm due to antibiotics resistance, not the myopic costs immediately incurred for patients.

We also computed the test sensitivity requirements for testing strategies to dominate "no testing" in scenario A and B (by grouping scrub typhus under the "other bacterial" category). We set w_{over} = WTP = 5,907.91 USD (Thailand GDP per capita in 2016), and $w_{under} = 25777USD$. For Scenario A(bacterial-endemic), we recommend empirical antibiotics treatment without any test, even if the bacterial test or the viral test has

100% sensitivity. On the other hand, both "bacterial test" with any sensitivity, and "viral test" with reasonable sensitivity $\geq 8.76\%$,and most tests have sensitivities $\geq 50\%$) would be better than empirical antibiotics treatment in Scenario B (viral-endemic).

Data, Sources and Model Calibration

1. Transition Probabilities

   Transition probabilities among health states were time-homogeneous. Transition probabilities for each disease were calibrated to match the reported mean duration of fever in the mild stage, and mean duration of hospitalization in the severe state, and mortality rates in the medical literature respectively. We assumed that antibiotic treatment reduced mean fever duration (mean days of hospitalization) by half for mild (severe) leptospirosis and scrub typhus patients ([139], [156]). Transition probabilities for "other" infections not treatable with antibiotics were assumed to be similar to dengue, and were varied in sensitivity analysis. We provide a sample Markov trace plot for leptospirosis disease progression in Figure A.4. Exact values and references for each parameter are provided in Table A.1.

2. Costs, DALYs, test sensitivities and specificities

   We obtained test costs, health costs and DALY-related parameters for all five possible causes of infection from the published literature and WHO life table for Thailand. Disability weights (DW) for "other bacterial" and "other" infections were assumed to be of the same magnitude as dengue, leptospirosis and scrub typhus (i.e., DW in Mild state: 0.2; DW in Severe state: 0.5) ([144], [83]). Sensitivities and specificities of leptospirosis, scrub typhus and dengue diagnostic tests were reported in various studies ([140] [61], [68], [64], [4], [125]). Detailed references can be found in Appendix Table A1. Due to the lack of studies reporting sensitivity and specificity of multiplex PCR tests in Thailand, we set the sensitivity and specificity of multiplex PCR diagnostic test (except for the scrub typhus component ([141])) to be similar (but slightly lower) than values reported for other

places in the medical literature ([151], [59]).

Sensitivity Analysis

1. Varying Disease Prevalence

   We performed sensitivity analysis on the level endemicity of different diseases at different locations in Thailand (1) (i.e., Set 1 and Set 2 in Table A.4). We then induced the optimal strategy sequence for Set 1 and Set 2 when patient present to hospital at their first, fourth and tenth day of illness (Figure A.1). We refer to the disease prevalence employed in the main content (Scenario A and Scenario B) as the base-case.

   We had the followings observations from Figure A.1. First, the main observations are consistent with the base-case analysis: Empirical antibiotics treatment to all patients (Strategy 2) was most cost-effective with small antibiotics overuse penalty. Depending on the specific disease prevalence and WTP level, the threshold (of its cost-effectiveness) may vary. Second, as dengue (or equivalently, viral-diseases) prevalence increases, strategy with single test (i.e., Dengue PCR or Dengue RDT, or Lepto RDT) had the highest NMB for a wider range of WTP and penalty values. Third, For WTP equals to Thailand GDP per capita, the optimal strategy sequence was mostly consistent with the base-case: Empirical Antibiotics to all patients was cost-effective with zero, and low penalty region, but Strategy 15 (Multiplex PCR test) or Strategy 12 (P: Lepto RDT, typhus RDT) became cost-effective for penalty >= $ 13,000/course, >= 20,000/course, and >=30,000/course for patients presenting on day one, day four, day ten respectively with disease prevalence Set 1; and for penalty >=6,000/course, >= 8,500/course, >= $ 15,000/course for patients presenting on day one, day four, day ten respectively with disease prevalence Set 2. Last, when patients present late (i.e. at their tenth day of illness), strategies with rapid diagnostic tests such as Strategy 4 (dengue RDT), Strategy

12 (P: Lepto RDT, typhus RDT), Strategy 13 (P: Lepto PCR, typhus RDT) became cost-effective. This is also consistent with our base-case analysis since RDT is more accurate in the later stage of diseases.

2. One-way Sensitivity Analysis

   We performed one-way sensitivity analysis for all other variables over estimated data ranges (Table A). We kept the disease prevalence the same as in the bacterial-endemic Scenario A (i.e., 52.8% chance of leptospirosis infection, Table A.1) and assumed patients present to hospital on their first day of illness. We display optimal strategies at penalty = $ 0, $ 10,000 and $50,000 USD in Table F. In all cases, empirical treatment was most cost-effective with respect to pure DALY and costs incurred (i.e., penalty = $ 0 k).

   The results were sensitive to a few variables, including cohort age, the wait time of tests (time lag), as well as sensitivity and specificity of diagnostic tests. For a cohort of younger patients, it is more beneficial to apply the "empirical treatment" strategies in order to avoid high DALYs caused by deaths. For a cohort of older patients (i.e., 60 years old), Strategy 15 (Multiplex PCR) would be more likely to cost-effective with a moderate penalty in antibiotics overuse. In bacterial-endemic Scenario A, our analyses show that strategies consisting of high sensitivity and specificity leptospirosis diagnostic had higher chance of being cost-effective.

   Our results were not sensitive to disease progression probabilities, disability weights (DWs) and treatments costs or productivity loss costs in either mild or severe state. This is probably because even though values of DWs, costs, transition probabilities were varied, they were still on different magnitudes for different health states. Among all variables ranges considered, Strategy 2 (Empirical All), 15 (Multiplex PCR test) were generally considered cost-effective. The result of sensitivity analyses imply that Multiplex PCR test could be considered as an alternative when antibiotics misuse/overuse is truly a concern to society/ the Decision Maker.

We also observe from Figure 2.3a that empirical antibiotic treatment (Strategy 2) and Multiplex PCR (Strategy 15) were cost-effective for a wide range of w_{over} and WTP. We then restricted our attention by comparing the relative cost-effectiveness of these two strategies (Figure A.2). We found that the empirical antibiotic treatment strategy is always on the effectiveness frontier, and gives smaller ICER compared to Multiplex PCR with younger patient age, lower leptospirosis-component sensitivity, higher disease-specific mortality rate, and longer test wait time. The remaining parameters like test and health costs, disability weights were not sensitive to variation. All these conclusions are consistent with the results of the aforementioned univariate sensitivity analysis.

3. Probabilistic Sensitivity Analysis

We conducted a probabilistic sensitivity analysis using Monte Carlo simulation, examining the cost-effectiveness of each strategy for each set of sampled parameters. The willingness-to-pay threshold is set to be Thailand GDP per capita in 2016: 5907.91 USD. We randomly generated 10,000 problem instances (i.e., 10,000 scenarios with different parameter sets). For each instance, all parameters that are on a continuous scale were randomly sampled from a triangle distribution with mode given by the base case value, and lowest and highest values corresponding to the ranges in Table A.1. The disease prevalence was randomly generated given the ranges of values reported in [140]. Parameters that are on discrete scales (i.e., wait time of diagnostic tests) were sampled from either triangle distribution (rounded to the nearest integer) or uniform distributions. The Monte Carlo simulation results are shown in Figure A.3. Our analyses indicate that when the penalty on antibiotics overuse is low ($ 0/course to $ 15,000 /course), empirical treatment is most likely to be cost-effective, while strategies with single dengue tests (Strategy 5 Dengue PCR and Strategy 4 Dengue RDT) could be an alternative substitution to reduce antibiotics overuse. However, as the penalty increases,

strategies involving bacterial tests dominates. With a moderate and high penalty (i.e., $ 25,000/course to $ 150,000 /course) Strategy 15 (Multiplex PCR) is most cost-effective. Other than Strategy 15, Strategy 11 (P: Lepto PCR, typhus PCR) are more cost-effective than other strategies within a moderate or high penalty on antibiotics overuse. Similarly in previous analyses, once antibiotic reduction is prioritized (i.e. penalty >= $ 150,000 course), strategies with single leptospirosis PCR test (Strategy 7) would eventually become cost-effective. We observe in PSA analyses, PCR-led strategies dominate RDT-led strategies even though patients' health seeking behavior (delay) were heterogeneous (min: 0 day, mean: 4 days, max: 10 days). Observing the descriptive statistics from Appendix Table A.1, we conclude (qualitatively) that PCR is more accurate (higher sensitivity and specificity) during the early course of illness, whereas RDT is more accurate in the later stage of diseases. However, patients gain much more benefit if antibiotics treatment was initiated early (i.e. diagnostic tests were prescribed during the early course of illness) before they progressed to worsened health states. As a consequence, even though we varied the delay of seeking health in PSA analyses, more health benefits were accrued from early detection and early antibiotics treatment. This is consistent with the findings from other papers [78]. Lastly, we observe the current protocol recommended by WHO can be cost-effective with at most 25% chance at penalty = $ 15,000/course.

A.2 Tables and Figures

Variable	base value	Minimum	Maximum	Source
Population Variable				
probability of leptospirosis infection	52.80%			[140]
Continued on next page				

Table A.1 – continued from previous page

Variable	base value	Minimum	Maximum	Source
probability of typhus infection	4.60%			[140]
probability of other bacterial infection	4.50%			[140]
probability of dengue infection	12.20%			[140]
probability of other infection	26%			[140]
Cohort Age	40	20	60	assumed
Daily Transition Probabilities: Lepto-related				
From mild (with antibiotics)				
to mild	0.51			[139]
to severe	0	0	0	[139]
to recover	0.49	0.243	1	[139]
From severe (with antibiotics)				
to severe	0.833			[156], [138]
to recover	0.146	0.156	0.137	[156], [138]
to death	0.021	0.011	0.029	
From mild (without antibiotics)				
to mild	0.815			[139]
to severe	0.074	0.067	0.083	[139]
to recover	0.111	0.1	0.125	[139]
From severe (without antibiotics)				
to severe	0.929			[144]
to recover	0.048	0.059	0.039	[144]
to death	0.023	0.012	0.033	[144]
Test Parameters: Lepto				
Rapid Test-costs, $	5.7	3	7	[139]
Sensitivity (<= 4 day of illness)	62%	41%	79%	[61]

Continued on next page

Table A.1 – continued from previous page

Variable	base value	Minimum	Maximum	Source
Specificity (<= 4 day of illness)	98%	93%	99%	[61]
Sensitivity (>= 5 day of illness)	81%	69%	90%	[61]
Specificity (>= 5 day of illness)	93%	88%	96%	[61]
time lag (days)	1	0	2	assumed
PCR Test costs, $	14	10	20	assumed
Sensitivity (<= 4 day of illness)	85.00%	73%	97.50%	[125]
Specificity (<= 4 day of illness)	95.00%	90%	100%	[125]
Sensitivity (>= 5 day of illness)	41.50%	26.70%	57.80%	[125]
Specificity (>= 5 day of illness)	95.00%	90%	100%	[125]
time lag (days)	2	0	3	assumed
Health Costs: Lepto				
doxycycline prescription (one-shot)	2	1	3	[139]
Daily costs in Mild	5.25	5	10	[139]
Daily costs in Severe	48.71	30	70	[139]
DALY: Lepto				
DW: Mild	0.21	0.15	0.3	[144]
DW: Severe	0.56	0.4	0.6	[144]
YLL	34.9			[144], [114]
Daily Transition Probabilities: other bacterial				
From mild (with antibiotics)				
to mild	0.625			[139]
to severe	0	0	0	[139]
to recover	0.375	0.063	1	[139]
From severe (with antibiotics)				
to severe	0.833			[156], [138]

Continued on next page

Table A.1 – continued from previous page

Variable	base value	Minimum	Maximum	Source
to recover	0.146	0.156	0.137	
to death	0.021	0.011	0.029	[156], [138]
From mild (without antibiotics)				
to mild	0.811			[139]
to severe	0.075	0.051	0.148	[139]
to recover	0.113	0.076	0.222	[139]
From severe				
to severe	0.929			[142]
to recover	0.048	0.059	0.039	[142]
to death	0.023	0.012	0.033	[142]
Health Costs: other bacterial				
doxycycline prescription (one-shot)	2	1	3	[139]
Daily costs in Mild	5.25	5	10	[139]
Daily costs in Severe	48.71	30	70	[139]
DALY: other bacterial				
DW: Mild	0.2	0.15	0.3	[144]
DW: Severe	0.5	0.4	0.6	[144]
YLL	34.9			[144] [114]
Daily Transition Probabilities: typhus				
From mild (with antibiotics)				
to mild	0.383			[139]
to severe	0	0	0	[139]
to recover	0.617	0.338	1	[139]
From severe (with antibiotics)				
to severe	0.833			[156] [138]
to recover	0.146	0.156	0.137	
to death	0.021	0.011	0.029	[156] [138]
From mild (without antibiotics)				
to mild	0.811			[139]
to severe	0.075	0.076	0.222	[139]

Continued on next page

Table A.1 – continued from previous page

Variable	base value	Minimum	Maximum	Source
to recover	0.113	0.051	0.148	[139]
From severe (without antibiotics)				
to severe	0.929			[142]
to recover	0.048	0.059	0.039	[142]
to death	0.023	0.012	0.033	[142]
Tests Parameters: typhus				
Rapid Test-costs, $	5.7	3	7	[139]
Sensitivity (<= 4 day of illness)	67%	41%	79%	[68]
Specificity (<= 4 day of illness)	98%	93%	99%	[68]
Sensitivity (>= 5 day of illness)	80%	69%	90%	same as lepto
Specificity (>= 5 day of illness)	95%	88%	96%	same as lepto
time lag (days)	1	0	2	
PCR Test costs, $	14	10	20	assumed
Sensitivity (<= 4 day of illness)	85.00%	73%	97.50%	same as lepto
Specificity (<= 4 day of illness)	95.00%	90%	100%	same as lepto
Sensitivity (>= 5 day of illness)	41.50%	26.70%	57.80%	asame as lepto
Specificity (>= 5 day of illness)	95.00%	90%	100%	same as lepto
time lag (days)	2	0	3	
Health Costs: typhus				
doxycycline prescription(one-shot)	2	1	3	[139]
Daily costs in Mild	5.25	5	10	[139]
Daily costs in Severe	48.71	30	70	[139]
DALY: typhus				
DW: Mild	0.21	0.15	0.3	[144]
DW: Severe	0.56	0	0.6	[144]

Continued on next page

Table A.1 – continued from previous page

Variable	base value	Minimum	Maximum	Source
YLL	34.9			[144]
Daily Transition Probabilities: dengue				
From Mild (with standard care)				
to mild	0.815			[88] [23]
to severe	0.027	0.061	0.214	[88] [23]
to recover	0.159	0.01	0.036	[88] [23]
From Severe				
to severe	0.898			[143] [82]
to recover	0.089	0.095	0.073	[143] [82]
to death	0.013	0.007	0.013	[143] [82]
Test Parameters: dengue				
Rapid Test-costs, $	5.7	3	7	same as lepto
Sensitivity (<= 4 day of illness)	68%	60%	75%	[64] [63]
Specificity (<= 4 day of illness)	76%	71%	80%	[64] [63]
Sensitivity (>= 5 day of illness)	90%	80%	99%	[64] [63]
Specificity (>= 5 day of illness)	98%	95%	100%	[64] [63]
Wait time (days)	1	0	2	assumed
PCR Test-costs, $	14	10	20	assumed
Sensitivity (<= 4 day of illness)	85%	51%	100%	[4]
Specificity (<= 4 day of illness)	100%	100%	100%	[4]
Sensitivity (>= 5 day of illness)	50%	30%	70%	[4]
Specificity (>= 5 day of illness)	100%	100%	100%	[4]
time lag (days)	2			assumed
Health Costs: dengue				
Daily costs in Mild, $	5.25	5	10	[133]

Continued on next page

Table A.1 – continued from previous page

Variable	base value	Minimum	Maximum	Source
Daily costs in Severe, $	59.68	40	60	[133]
DALY: dengue				
DW: Mild	0.2	0.15	0.3	[83]
DW: Severe	0.56	0.4	0.6	[83]
YLL	34.9			same as lepto
Real-time Multiplex PCR Parameters				
Price, $	50	30	80	assumed
lepto Sensitivity (<= 4 day of illness)	90%	0.7	1	assumed
lepto Specificity (<= 4 day)	95%	90%	1	assumed
typhus sensitivity (<= 4 day)	87%	74.2	94.4	[141]
typhus specificity (<= 4 day)	100%	97.3	100	[141]
dengue sensitivity (<= 4 day)	90%	0.7	1	assumed
dengue specificity (<= 4 day)	95%	90%	1	assumed
lepto Sensitivity (>= 5 day of illness)	60%	0.4	0.8	assumed
lepto Specificity (>= 5 day)	90%	85%	0.98	assumed
typhus sensitivity (>= 5 day)	55%	0.4	0.8	assumed
typhus specificity (>= 5 day)	97%	85%	0.98	assumed
dengue sensitivity (>= 5 day)	60%	0.4	0.8	assumed
dengue specificity (>= 5 day)	90%	85%	0.98	assumed

Table A.1: Value for model variables

Strategies / Scenarios		Scenario B: Viral-Endemic				Scenario B: Viral-Endemic			
		Cost	**DALY**	**P(over)**	**P(under)**	**Cost**	**DALY**	**P(over)**	**P(under)**
1	No Antibiotics *º	216.166	2.911	0	0.619	138.978	1.258	0	0.171
2	Empirical All *º	47.549	0.239	0.381	0	94.107	0.52	0.829	0
3	Empirical Severe º	130.63	1.323	0.055	0.248	116.784	0.819	0.119	0.068
4	Dengue RDT	104.111	1.034	0.198	0.132	112.024	0.739	0.282	0.036
5	Dengue PCR *º	85.512	0.628	0.197	0	110.094	0.628	0.184	0
6	Lepto RDT *º	137.518	1.576	0.006	0.253	132.471	1.078	0.014	0.112
7	Lepto PCR *	122.619	1.239	0.014	0.131	134.053	1.025	0.029	0.085
8	S: Lepto RDT, typhus RDT º	129.498	1.462	0.011	0.43	129.077	1.036	0.024	0.192
9	S: Lepto PCR, typhus RDT *º	119.643	1.142	0.017	0.216	134.098	0.988	0.037	0.146
10	S: Lepto RDT, typhus PCR	127.176	1.44	0.014	0.387	128.716	1.027	0.031	0.173
11	P: Lepto PCR, typhus PCR	131.534	1.079	0.026	0.097	148.671	0.958	0.057	0.071
12	P: Lepto RDT, typhus RDT	135.543	1.437	0.013	0.222	135.924	1.025	0.028	0.1
13	P: Lepto PCR, typhus RDT	125.833	1.122	0.019	0.106	141.617	0.979	0.041	0.075
14	P: Lepto RDT, typhus PCR	148.592	1.492	0.019	0.186	144.128	1.02	0.041	0.084
15	Multiplex PCR*º	148.696	1.001	0.014	0.08	170.8	0.961	0.029	0.072

Table A.2: Strategy outcomes: patients seeking care on the **first** day of illness

Strategies / Scenarios		Scenario B: Viral-Endemic				Scenario B: Viral-Endemic			
		Cost	**DALY**	**P(over)**	**P(under)**	**Cost**	**DALY**	**P(over)**	**P(under)**
1	No Antibiotics *º	216.166	2.911	0	0.22	138.978	1.258	0	0.06
2	Empirical All *º	149.508	1.72	0.075	0	122.128	0.93	0.163	0
3	Empirical Severe	160.095	1.857	0.055	0.248	124.963	0.967	0.119	0.068
4	Dengue RDT*º	155.717	1.838	0.045	0.004	122.864	0.962	0.038	0.001
5	Dengue PCR	160.426	1.906	0.047	0	124.658	0.981	0.072	0
6	Lepto RDT *º	172.964	2.142	0.005	0.06	133.316	1.147	0.01	0.035
7	Lepto PCR *	196.73	2.548	0.003	0.117	137.11	1.203	0.006	0.041
8	S: Lepto RDT, typhus RDT *	172.399	2.084	0.007	0.099	134.2	1.124	0.015	0.06
9	S: Lepto PCR, typhus RDT	201.927	2.483	0.005	0.203	145.614	1.181	0.01	0.07
10	S: Lepto RDT, typhus PCR	172.814	2.118	0.006	0.096	133.345	1.138	0.014	0.057
11	P: Lepto PCR, typhus PCR	220.263	2.49	0.005	0.107	162.76	1.183	0.012	0.037
12	P: Lepto RDT, typhus RDT*	179.633	2.07	0.008	0.046	142.403	1.117	0.016	0.029
13	P: Lepto PCR, typhus RDT	210.424	2.463	0.005	0.102	153.892	1.173	0.012	0.035
14	P: Lepto RDT, typhus PCR	193.554	2.165	0.006	0.047	151.943	1.138	0.014	0.029
15	Multiplex PCR	233.338	2.332	0.007	0.078	183.249	1.156	0.015	0.032

For each scenario, we identified the strategies that were on the three-dimensional effectiveness frontier, where the three dimensions are DALY, cost and antibiotic overuse. * = strategies on the cost-effectiveness frontier (economically efficient) for Scenario A (bacterial-endemic); º = strategies on the cost-effectiveness frontier (economically efficient) for Scenario B (viral-endemic).

Table A.3: Strategy outcomes: patients seeking care on the **tenth** day of illness

Prevalence	Leptospirosis	Typhus	Other bacterial	Dengue	Other
SET 1	0.358	0.209	0.047	0.071	0.315
SET 2	0.076	0.204	0.022	0.222	0.476

Table A.4: Sensitivity analysis of disease prevalence

Values obtained from [140]

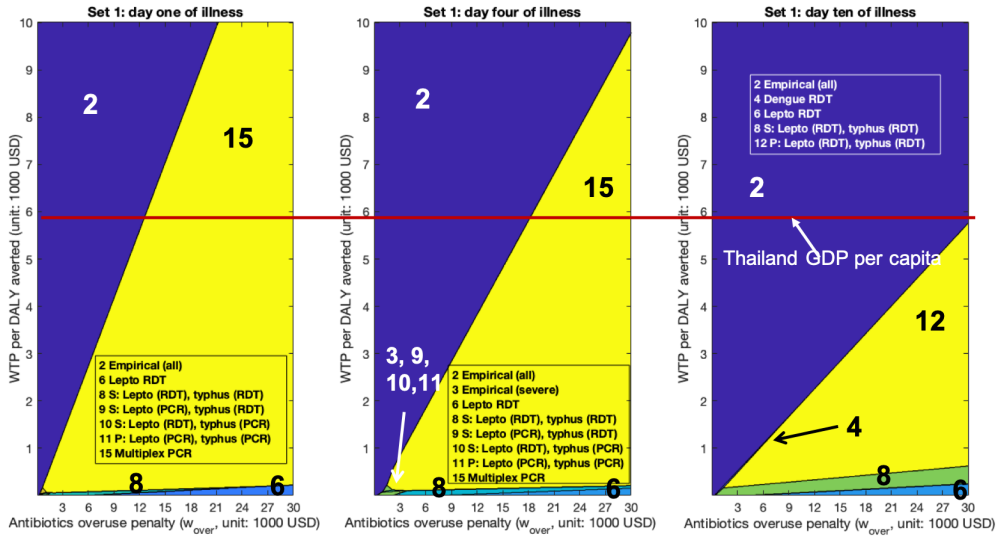

(a) Policies with highest net monetary benefit with by varying willingness-to-pay (WTP) on the y-axis and penalty (w_{over}) on the x-axis, where we fixed disease prevalence vector as Set 1 in Table A.4

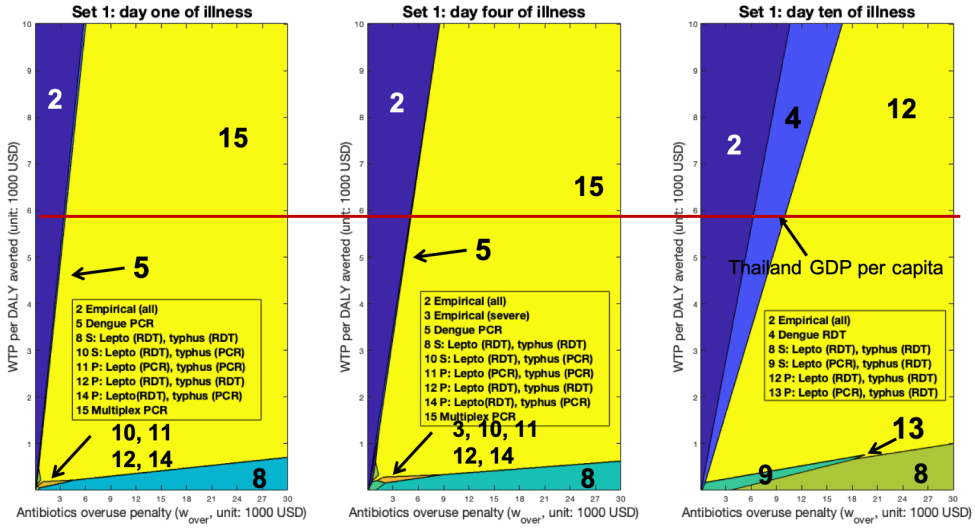

(b) Policies with highest net monetary benefit with by varying willingness-to-pay (WTP) on the y-axis and penalty (w_{over}) on the x-axis, where we fixed disease prevalence vector as Set 2 in Table A.4

Figure A.1: Policies with highest NMB at alternative disease prevalence distributions

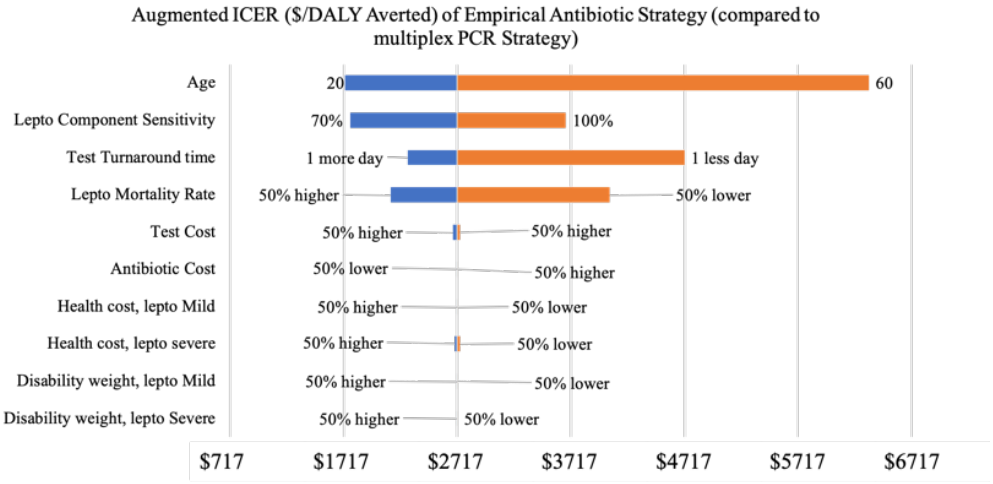

Figure A.2: Tornado diagram with variation in selected model parameters.

One-way sensitivity analysis, each row (bar) display the range of Augmented ICER of empirical antibiotic strategy compared with Multiplex PCR strategy (patients present to a hospital on day one). We only displayed leptospirosis-specific disease parameters, but all other disease categories share the same structure in the range of ICER change. Augmented ICER = augmented incremental cost-effectiveness ratio, calculated by the ratio of DALY difference and augmented cost difference. Augmented cost = cost + penalty * w_{over}; DALY = disability-adjusted life year; PCR = Polymerase Chain Reaction tests.

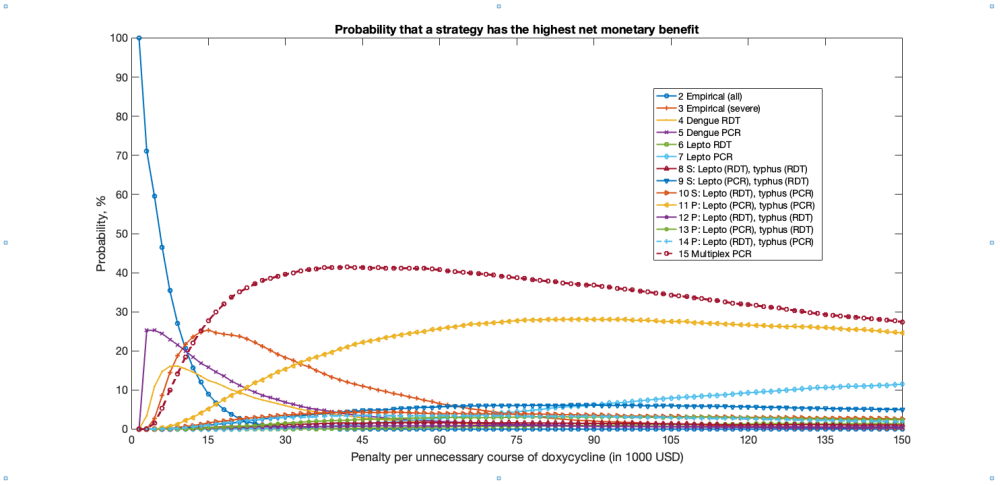

the acceptability curves of the probabilistic sensitivity analysis. We fixed WTP = Thailand GDP per capita. The most cost-effective strategy for a given penalty, is the strategy with the highest NMB value.

Figure A.3: Results of probabilistic sensitivity analysis.

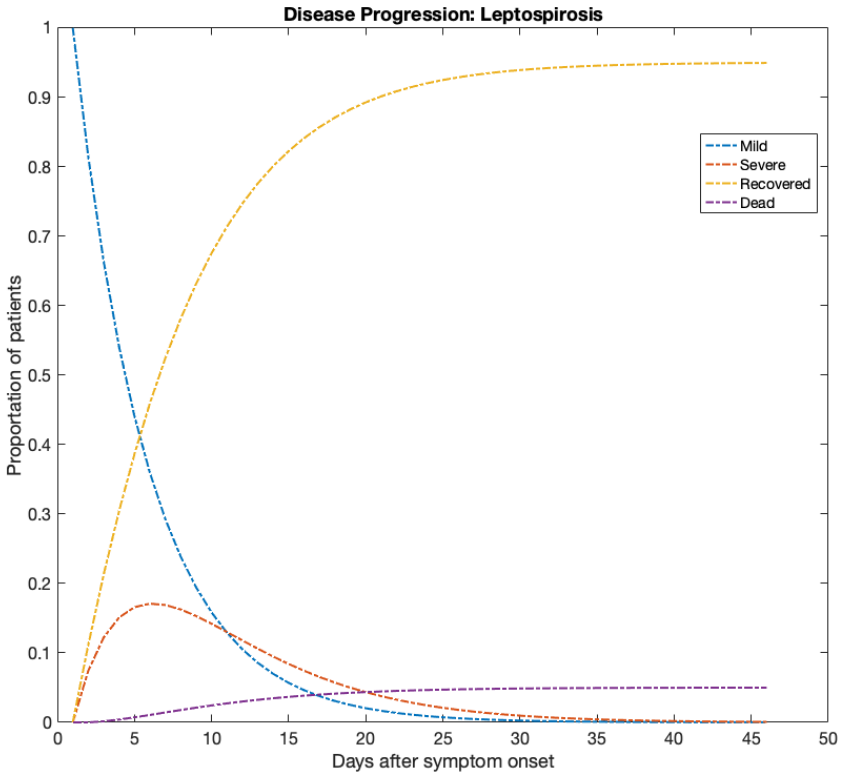

Patients enter the model in Mild state, during the 45-day horizon, they could progress to Severe state, become recovered, or dead.

Figure A.4: Sample Markov trace of disease progression for leptospirosis

Appendix B

Chapter 2 Supplement Material

B.1 Theorems and Proofs

Lemma B.1.1. *Given an adherence state sequence* $\mathbf{A}$*,* $r(\mathbf{X_{t_k}}, N)$ *are equal in distribution for* $k = 0, 1, 2, ...$ *almost surely, where* $\mathbf{A} = \{A_0, ..., A_t\}$*.*

Proof of Lemma B.1.1. Given an adherence state sequence $\mathbf{A}$, we can specify the exact transition matrix $\mathbb{P}(A)$ at each time t. Then, the claim by applying total expectation formula to Equation (3.2).

□

Let $\mathbb{P}^t(\mathbf{A})$ denote the t-step transition probability function, given an adherence measurement sequence $\mathbf{A}$. In addition, one can easily show by induction that $\mathbb{E}_{\mathbf{A}}[\mathbb{P}^t(\mathbf{A})] = \mathbb{P}^t(\theta)$, where $\mathbb{P}(\theta)$ is defined previously as $\mathbb{P}(\theta) = \theta\mathbb{P}(A+) + (1-\theta)\mathbb{P}(A-)$. Denote $P^t_{ij}(\theta)$ as the t-step transition probability from state i to state j, given adherence type θ. We further refine Lemma B.1.1 with respect to $\mathbb{P}(\theta)$ as follow:

Lemma B.1.2. *Given* θ*,* $r(\mathbf{X_{t_k}}, N)$ *are equal in distribution for* $k = 0, 1, 2, ..$ *with respect to* $\mathbb{P}(\theta)$ *almost surely.*

We omit the proof for Lemma B.1.2 since it is almost identical to the proof of Lemma

B.1.1.

We have the following lemma for $r(\mathbf{X}_{\mathbf{t_k}}, N)$: Given Lemma B.1.2, w

We first provide a few definitions, lemmas and theorems (on the structure of TPM $\mathbb{P}(A)$) that will be used in the proof.

Definition B.1.1. *Totally Positive of Order 2. A Matrix $\mathbb{P}$ is of TP2 if all its second order minors are non-negative, or equivalently, $P(j_1|i_1)P(j_2|i_2) \geq P(j_2|i_1)P(j_1|i_2)$, for $i_2 \geq i_1, j_2 \geq j_1$.*

Theorem B.1.1. *First order dominance property, cited from [81]: For any two probability vectors $\mathbb{b}$ and $\mathbb{b}'$, we have $\mathbb{b}' \geq_s \mathbb{b}$, if and only if for any increasing function $f(\cdot)$, $\mathbb{E}_{\mathbb{b}'}[f(x)] \geq \mathbb{E}_{\mathbb{b}}[f(x)]$.*

Lemma B.1.3. *Let $\mathbb{P}_1$, and $\mathbb{P}_2$ be two TP2 TPM. Then,*

- *the Hadamard product of $\mathbb{P}_1$ and $\mathbb{P}_2$ (i.e., $\mathbb{P}_1 \otimes \mathbb{P}_2 = [P_1(i|j)P_2(i|j)]_{i,j\in\mathcal{S}}$) is TP2.*
- *the (usual) product of $\mathbb{P}_1$ and $\mathbb{P}_2$ is TP2.*

Proof of Lemma B.1.3. By definition of TP2, we have $P_1(j|i)P_1(y|x) \geq P_1(y|i)P_1(j|x)$, for $x \geq i, y \geq j$, and $P_2(j|i)P_2(y|x) \geq P_2(y|i)P_2(j|x)$, for $x \geq i, y \geq j$. Then,

$$P_1(j|i)P_1(y|x)P_2(j|i)P_2(y|x) \geq P_1(y|i)P_1(j|x)P_2(y|i)P_2(j|x)$$

Thus, $\mathbb{P}_1 \otimes \mathbb{P}_2$ is TP2.

For the proof of the second part, see [111] and [85]. □

Proof of Corollary 3.3.1. Proof for the first statement. When $t = 0$, $\mathbb{P}^t(\theta)$ becomes an identity matrix, and of TP2. When $t = 1$, it is trivial to check that $\mathbb{P}(\theta)$ is of TP2 given its definition. Now, assume it holds for all $t = 0, 1, 2, ...k-1$. Then, from Lemma B.1.3, we know that $\mathbb{P}^k(\theta) = \mathbb{P}^{k-1}(\theta) \cdot \mathbb{P}(\theta)$ is of TP2.

Proof for the second statement. By taking the TPM $\mathbb{P}(\theta)$ to the tth power, and combining like terms, then we have:

$$\begin{bmatrix} p_{11}^t & p_{12}\sum_{k=0}^{t-1}(p_{11}^k \cdot p_{22}^{t-1-k}) & 1 - p_{11}^t - p_{12}\sum_{k=0}^{t-1}(p_{11}^k \cdot p_{22}^{t-1-k}) \\ 0 & p_{22}^t & 1 - p_{22}^t \\ 0 & 0 & 1 \end{bmatrix}$$

By computing the sum of geometric series, we have the desired results. □

Proof of Corollary 3.3.1. Proof for the first statement. When $t = 0$, $\mathbb{P}^t(\theta)$ becomes an identity matrix, and of TP2. When $t = 1$, it is trivial to check that $\mathbb{P}(\theta)$ is of TP2 given its definition. Now, assume it holds for all $t = 0, 1, 2, ...k-1$. Then, from Lemma B.1.3, we know that $\mathbb{P}^k(\theta) = \mathbb{P}^{k-1}(\theta) \cdot \mathbb{P}(\theta)$ is of TP2.

Proof for the second statement. By taking the TPM $\mathbb{P}(\theta)$ to the tth power, and combining like terms, then we have:

$$\begin{bmatrix} p_{11}^t & p_{12}\sum_{k=0}^{t-1}(p_{11}^k \cdot p_{22}^{t-1-k}) & 1 - p_{11}^t - p_{12}\sum_{k=0}^{t-1}(p_{11}^k \cdot p_{22}^{t-1-k}) \\ 0 & p_{22}^t & 1 - p_{22}^t \\ 0 & 0 & 1 \end{bmatrix}$$

By computing the sum of geometric series, we have the desired results. □

Proof of Theorem 3.3.1. We start by providing an overview of the proof. To show $V(N)$ is quasi-concave, $V(N)$ is differentiable with respect to N, we only need to show $\forall N_1, N_2 \in (0, \infty)$ (from [19]),

$$V(N_1) \geq V(N_2) \Rightarrow \frac{\partial V}{\partial N}(N_2) \cdot (N_1 - N_2) \geq 0,$$

We start by analyzing the first order, and second order condition of $V(N)$, and complete the proof by showing $V(N)$ is unimodal, with a unique peak.

Now, we express the first order condition of $V(N)$:

$$\frac{\partial V}{\partial N} = \frac{\beta_1(q_{11}^N(q_{22}^N - 1)\log q_{11} - q_{22}^N(q_{11}^N - 1)\log q_{22}) - \beta_2 q_{11}^N \log q_{11}}{(q_{11}^N - 1)^2}, \tag{B.1}$$

where $\beta_1 = \frac{q_{12}}{(q_{11}-q_{22})(q_{22}-1)}\Big((q_{22}-1)(c-R) - r(s_2)\Big)$, $\beta_2 = c$. When $q_{11} > q_{22}$, we know $\beta_1 < 0$ from Assumption 3.3.1 (conversely, if $q_{11} \leq q_{22}$, $\beta_1 \geq 0$). Note that $((q_{11}^N - 1)^2) > 0$ (the denominator of $\frac{\partial V}{\partial N}$), $\forall N \in \mathbb{R}^+$. We then focus on figuring out the sign of its numerator (denoted as $f(N)$). For the limits of $f(N)$, we can derive $\lim_{N\to 0} f(N) = -\beta_2 q_{11}^N \log q_{11} > 0$, and $\lim_{N\to\infty} f(N) = 0$. For a general N that is finite, we take the derivative of $f(N)$:

$$\frac{\partial f}{\partial N} = \beta_1\left(q_{11}^N \log^2 q_{11}\left(q_{22}^N - 1\right) - \left(q_{11}^N - 1\right) q_{22}^N \log^2 q_{22}\right) - \beta_2 q_{11}^N \log^2 q_{11} \tag{B.2}$$

When $N \to 0$, we have

$$\lim_{N\to 0} \frac{\partial f}{\partial N} = -\beta_2 \log^2 q_{11}, \tag{B.3}$$

which is always negative. On the other hand, we have $\lim_{N\to\infty} \frac{\partial f}{\partial N} = 0$.

We claim that $f(N) = 0$ has a unique solution for $N \in \mathbb{R}^+$. To see this, We first investigate the sign of $\beta_1 + \beta_2$. From Assumption 3.3.3, we have:

$$p_{12}\left(R - \frac{r(s2)}{1 - \delta p_{22}}\right) > (p_{12} + p_{22} - p_{11})c \tag{B.4}$$

$$\iff q_{12}\left(R - \frac{r(s2)}{1 - q_{22}}\right) > (q_{12} + q_{22} - q_{11})c \tag{B.5}$$

$$\iff q_{12}\left((R-c) - \frac{r(s2)}{1 - q_{22}}\right) > (q_{22} - q_{11})c \tag{B.6}$$

The first equivalence follows by replacing $p's$ with $q's$. The second equivalence follows

by moving the cost term (c) to the LHS. Then, we have:

$$\beta_1 + \beta_2 = \frac{q_{12}}{q_{22} - q_{11}} \left((R - c) - \frac{r(s2)}{1 - q_{22}} \right) + c \begin{cases} > 0 & \text{if } q_{11} < q_{22} \\ \leq 0 & \text{otherwise.} \end{cases} \tag{B.7}$$

we rearrange $f(N) = 0$ in terms of N as follow:

$$\beta_1 \left(\log q_{22} - \log q_{11} \right) q_{11}^N q_{22}^N + \left(-\beta_1 \log q_{22} \right) q_{22}^N = -(\beta_1 + \beta_2) \log q_{11} q_{11}^N \tag{B.8}$$

We consider two cases.

Case I: $q_{11} < q_{22}$. For this case, the coefficient $\beta_1(\log q_{22} - \log q_{11}) > 0$ since $\beta_1 > 0$ and $q_{22} > q_{11}$. The other two coefficients $-\beta_1 \log q_{22}$ and $-(\beta_1 + \beta_2)$ are also positive. Then, we know both the left-hand side and right-hand side of Equation (B.8) are non-negative for $N \in \mathbb{R}^+$. Moreover, the exponent functions q_{11}^N, q_{22}^N and $q_{11}^N q_{22}^N$ are monotonically decreasing in N Since $q_{11} \neq q_{22}$, and the three coefficients ($\beta_1(\log q_{22} - \log q_{11})$, $-\beta_1 \log q_{22}$ and $-(\beta_1 + \beta_2) \log q_{11}$) are not equal. We further rearrange Eq. (B.8) as follow:

$$\beta_1 \left(\log q_{22} - \log q_{11} \right) q_{11}^N q_{22}^N + \left(-\beta_1 \log q_{22} \right) q_{22}^N = -(\beta_1 + \beta_2) \log q_{11} q_{11}^N \tag{B.9}$$

$$f_1(N) + f_2(N) = f_3(N) \tag{B.10}$$

Following the preceding analysis, we have $f_1(N)$ and $f_2(N)$ decreasing in N, $f_3(N)$ is increasing N. The equality can only hold for (at most) one such $N^* \in (0, \infty)$. Combining with the two limits of $f(N)$, $\lim_{N \to 0} \frac{\partial f}{\partial N} < 0$, and $\lim_{N \to \infty} \frac{\partial f}{\partial N} = 0$, we conclude that $f(N) = 0$, hold exactly only once $\mathbb{R}^+$. We then conclude that $V(N)$ is a unimodal function with a unique peak, for $q_{11} < q_{22}$.

Case II: $q_{11} \geq q_{22}$. The proof for this case is similar to Case I.

Now, we have for both cases $V(N)$ is a unimodal function with a unique peak. That is to say, $N_1 \geq N_2$ and $V(N_1) \geq V(N_2)$, we know $N_2 \leq N^*$, thus $\frac{\partial V}{\partial N}(N_2) \geq 0$. Further,

for any $N' \leq N^*$, we have

$$\frac{\partial V}{\partial N}(N') \geq 0$$

. We then have $\frac{\partial V}{\partial N}(N_2)(N_1 - N_2) \geq 0$. if $N_1 \geq N_2$ and $V(N_1) \geq V(N_2)$. On the other hand, suppose $N_1 < N_2$ and $V(N_1) \geq V(N_2)$, similarly as above, we may conclude that $\frac{\partial V}{\partial N}(N_2) \leq 0$, and thus $\frac{\partial V}{\partial N}(N_2)(N_1 - N_2) \geq 0$.

We have then proved the sufficient and necessary first-order condition for quasi-concavity to hold. □

Proof of Proposition 1. We consider two cases.

Case I: $q_{11} < q_{22}$. We first prove part (a) and (b). As θ increases, q_{11} increases and q_{12} decreases (and the sum $q_{11} + q_{12}$ is invariant). Let the change in q_{11} be Δ. Same as in the proof of Theorem 3.3.1, we define $f(N)$ as the derivative of $V(N)$. Setting $f(N) = 0$, we have

$$\beta_1(q_{11}^N(1 - q_{22}^N)\log q_{11} - q_{22}^N(1 - q_{11}^N)\log q_{22}) = -\beta_2 q_{11}^N \log q_{11}$$

Similar in the analysis of Equation B.8 in the proof of Theorem 3.3.1, we can show that both sides are non-negative. In addition, as θ increases, β_1 increases since:

$$q_{12}+q_{11} > q_{22} \Rightarrow q_{12}(q_{22}-(q_{11}+\Delta)) > (q_{12}-\Delta)(q_{22}-q_{11}) \Rightarrow \frac{q_{12}}{q_{22} - q_{11}} > \frac{q_{12} - \Delta}{q_{12} - (q_{11} + \Delta)},$$

The first inequality follows from the last statement of Assumption 3.3.1. The second inequality holds by some simple algebraic work. Furthermore, we have β_2 is invariant with respect to θ.

Now, we define $\kappa(q_{11})$ to be the ratio of the coefficient of β_1 over the coefficient of β_2 as in Equation (B.8):

$$\kappa(q_{11}) = \frac{q_{11}^N(1 - q_{22}^N)\log q_{11} - q_{22}^N(1 - q_{11}^N)\log q_{22}}{-q_{11}^N \log q_{11}}$$

We have $\kappa'(q_{11}) = \frac{N(q_{11}^N - 1)}{q_{11}} < 0$, $\forall q_{11} \in (0,1)$. Subsequently, we have $\kappa(q_{11})$ is strictly decreasing in q_{11}. Then, we conclude that as θ increases (i.e., q_{11} increases), N^* increases (i.e., we need a larger N to balance the increase in β_1).

For part (c), observing from Equation B.1, As R increases, $\beta_1 = \frac{q_{12}}{(q_{11}-q_{22})(q_{22}-1)}\Big((q_{22}-1)(c-R) - r(s_2)\Big) > 0$ increases. Setting $f(N) = 0$, we have

$$\beta_1(q_{11}^N(1-q_{22}^N)\log q_{11} - q_{22}^N(1-q_{11}^N)\log q_{22}) = -\beta_2 q_{11}^N \log q_{11}$$

Similarly, we define $\kappa(N)$ as the ratio between the multiplier of β_1 over the multiplier of β_2:

$$\kappa(N) = \frac{q_{11}^N(1-q_{22}^N)\log q_{11} - q_{22}^N(1-q_{11}^N)\log q_{22}}{-q_{11}^N \log q_{11}}$$

We have $\kappa'(N) = q_{11}^{-N-1}q_{22}^N\Big((q_{11}-q_{22})\,q_{11}^N \log q_{22} + q_{22}\,(\log q_{22} - \log q_{11})\Big) > 0$ since $q_{11}^{-N-1}q_{22}^N$, $(q_{11}-q_{22})\,q_{11}^N \log q_{22}$, and $q_{22}\,(\log q_{22} - \log q_{11})$ are all strictly positive. Then, we conclude that as R increases (i.e., $\frac{\beta_2}{\beta_1}$ decreases), N^* decreases.

Case II: $q_{11} \geq q_{22}$. The proof for the second case is similar to Case I

□

Proof of Lemma 3.4.1. We first construct two ancillary matrices $\mathcal{Q}_1$ and $\mathcal{Q}_2$ as follow:

$$\mathcal{Q}_1 = \begin{bmatrix} p_{11,\theta} & p_{11,\theta} & p_{12,\theta} & p_{12,\theta} & p_{13} & p_{13} \\ p_{11,\theta} & p_{11,\theta} & p_{12,\theta} & p_{12,\theta} & p_{13} & p_{13} \\ 0 & 0 & p_{22} & p_{22} & p_{23} & p_{23} \\ 0 & 0 & p_{22} & p_{22} & p_{23} & p_{23} \\ 0 & 0 & 0 & 0 & 0 & 1 \\ 0 & 0 & 0 & 0 & 0 & 1 \end{bmatrix}$$

$$\mathcal{Q}_2 = \begin{bmatrix} P(\overline{OI}|s_1) & P(OI|s_1) & P(\overline{OI}|s_1) & P(OI|s_1) & P(\overline{OI}|s_1) & P(OI|s_1) \\ P(\overline{OI}|s_1) & P(OI|s_1) & P(\overline{OI}|s_1) & P(OI|s_1) & P(\overline{OI}|s_1) & P(OI|s_1) \\ 0 & 0 & P(\overline{OI}|s_2) & P(OI|s_2) & P(\overline{OI}|s_2) & P(OI|s_2) \\ 0 & 0 & P(\overline{OI}|s_2) & P(OI|s_2) & P(\overline{OI}|s_2) & P(OI|s_2) \\ 0 & 0 & 0 & 0 & 0 & 1 \\ 0 & 0 & 0 & 0 & 0 & 1 \end{bmatrix}$$

It is trivial to check that both $\mathcal{Q}_1$ and $\mathcal{Q}_2$ are of TP2 (by definition). Then, we have $\mathcal{Q}_1(i',j')\mathcal{Q}_1(i,j) \geq \mathcal{Q}_1(i',j)\mathcal{Q}_1(i,j')$, and $\mathcal{Q}_2(i',j')\mathcal{Q}_2(i,j) \geq \mathcal{Q}_2(i',j)\mathcal{Q}_2(i,j')$ whenever $i \geq i'$, and $j \geq j'$ (and $i,i',j,j' \in |\mathcal{S}\times\mathcal{O}|$). Then, we have $\mathcal{Q}_1(i',j')\mathcal{Q}_1(i,j)\mathcal{Q}_2(i,j)\mathcal{Q}_2(i',j') \geq \mathcal{Q}_1(i',j)\mathcal{Q}_1(i,j')\mathcal{Q}_2(i',j)\mathcal{Q}_2(i,j')$, Then $\mathbb{Q} = \mathcal{Q}_1 \otimes \mathcal{Q}_2$, is also of TP2 (which can also be shown using the first statement of Lemma B.1.3). □

Definition B.1.2. *Monotone Likelihood Ratio (MLR) ordering. Let $\mathbb{b}$ and $\mathbb{b}'$ denote any two n-dimensional (and finite) probability vectors. Then $\mathbb{b}'$ dominates $\mathbb{b}$ with respect to the MLR order (i.e. $\mathbb{b}' \geq_r \mathbb{b}$) if $\mathbb{b}'(i)\mathbb{b}(j) \leq \mathbb{b}(i)\mathbb{b}'(j)$, for all $i < j \in \mathcal{S}$.*

Definition B.1.3. *First Order Stochastic Dominance. Let $\mathbb{b}$ and $\mathbb{b}'$ denote any two n-dimensional (and finite) probability vectors. Then, $\mathbb{b}'$ is said to first order stochastically dominate $\mathbb{b}$ (i.e. $\mathbb{b}' \geq_s \mathbb{b}$) if $\sum_{i=j}^{n} \mathbb{b}(i) \geq \sum_{i=j}^{n} \mathbb{b}'(i)$, for all $j \in \mathcal{S}$.*

It is well-known that MLR ordering of belief vectors implies first order stochastic dominance (a *partial* order) of these two belief vectors (i.e., $\mathbb{b}' \geq_r \mathbb{b} \rightarrow \mathbb{b}' \geq_s \mathbb{b}$) ([81]). Furthermore, we can show that MLR order is preserved under Bayes updates:

Lemma B.1.4. *MLR order preservation. Given two belief vector $\mathbb{b}'$ and $\mathbb{b}$, and observation o, denote*

$$P_o = diag(P(o|s_1), P(o|s_2), P(o|s_3)),$$

(i.e., P_o is a 3-dimensional diagonal matrix with the entries $P(o|s_1), P(o|s_2), P(o|s_3)$. Then $\mathbb{b}' \geq_r \mathbb{b}$ is equivalent to $\frac{P_o\mathbb{b}'}{\mathbb{1}'P_o\mathbb{b}'} \geq_r \frac{P_o\mathbb{b}}{\mathbb{1}'P_o\mathbb{b}}$.

Proof. Applying the definition of MLR ordering, we re-write the RHS as

$$P(o|i)P(o|j)\mathbb{b}'(i)\mathbb{b}(j) \leq P(o|i)P(o|j)\mathbb{b}(i)\mathbb{b}'(j), \forall i < j \in \mathcal{S}$$

which is equivalent to $\mathbb{b}' \geq_r \mathbb{b}$. Thus proved. □

Proof of Lemma 3.4.2. To prove the first statement, we first claim that $r(s, o)$ is decreasing in (s, o). To see this, note that $r(s, o) = \sum_{e\in\mathcal{E}} r_t(s, e, o)P_t(e|s)$. Then, given Assumption 3.3.1 and Assumption 3.4.1, we know that:

$$r(s_1, \overline{OI}) \geq r(s_1, OI) \geq r(s_2, \overline{OI}) \geq r(s_2, OI)$$

Without loss of generality, we assume $r(s_3, \overline{OI}) = r(s_3, OI) \leq r(s_2, OI)$. Then, we have the desired results.

We then prove the first point using induction. For $N = 1$, we have $pr_{(s,o)}(N) = r(s, o)$, which is decreasing in (s, o). Assume it holds up to $N - 1$. Then, we have

$$pr_{(s,o)}(N) = r(s, o) + \delta \sum_{(s',o')} Q\Big((s', o')|(s, o)\Big)pr_{(s',o')}(N - 1), \tag{B.11}$$

We know $pr_{(s,o)}(N - 1)$ is decreasing in (s, o), and $\mathbb{Q}$ is of TP2. That is to say, the j-th row of $\mathbb{Q}$ MLR dominates the i-th row, for every $j > i$. Since MLR dominance implies first order stochastic dominance (Theorem 4.1.3. from [81]), we have for any $i, j \in (\mathcal{S} \times \mathcal{O})$ such that $i \preceq j$ (i.e., the partial order defined in Equation 3.6), we have$\sum_k^{|\mathcal{S}\times\mathcal{O}|} Q(k|i) \leq \sum_k^{|\mathcal{S}\times\mathcal{O}|} Q(k|j)$, for any $k \in (\mathcal{S} \times \mathcal{O})$ (i.e., patient in a "bad" state are more likely to transit to "worse" states). Lastly, we have $\sum_{(s',o')} Q\Big((s', o')|(s, o)\Big) = 1$, we conclude that $\sum_{(s',o')} Q\Big((s', o')|(s, o)\Big)pr_{(s',o')}(N - 1)$ is decreasing in (s, o). This leads us to the conclusion that $pr_{(s,o)}(N)$ is decreasing in (s, o).

Now, for a given state (s,o), as θ increases, we know $p_{11,\theta}$ increases and $p_{12,\theta}$ decreases. Denote the TPM before the change in θ as Q_1, after the change as Q_2. We have $\sum_k^{|\mathcal{S}\times\mathcal{O}|} Q_1(k|i) \leq \sum_k^{|\mathcal{S}\times\mathcal{O}|} Q_2(k|i)$, for any $k \in (\mathcal{S}\times\mathcal{O})$. Then, similar to the proof of the first statement, we can use induction on N to show that $pr_{(s,o)}(N)$ is increasing in θ.

□

Proof of Proposition 2. We can prove both results using induction on the value iteration algorithm. For any given $(s,o) \in (\mathcal{S}\times\mathcal{O})$, consider the following recursive formulas:

$$\begin{aligned} V^0(s,o) &= 0; \\ v^{n+1}_{(s,o)}(N) &= pr_{(s,o)}(N-1) - \delta^N c + \delta^N \sum_{(s',o')} Q\Big((s',o')|(s,o)\Big) V^n(s',o'); \\ V^{n+1}(s,o) &= \max\{\max_{1\leq N\leq\infty} v^{n+1}_{(s,o)}(N),\ \ \mathbb{1}_{s\neq s_3}(R-c)\}; \end{aligned}$$

When $n=0$, for a given state(s,o), we have

$$\begin{aligned} v^1_{(s,o)}(N) &= pr_{(s,o)}(N-1) - \delta^N c \\ V^1(s,o) &= \max\{\max_{1\leq N\leq\infty} v^1_{(s,o)}(N),\ \ \mathbb{1}_{s\neq s_3}(R-c)\}; \end{aligned}$$

We have $v^1_{(s,o)}(N)$ is decreasing in (s,o) since $pr_{(s,o)}(N-1)$ is decreasing in (s,o). As a consequence, $V^1(s,o)$ is decreasing in (s,o). In addition, it also satisfies that $V^1(s,o)$ increasing in θ since $pr_{(s,o)}(N-1)$ is increasing in θ (from Lemma 3.4.2). Assume the the recursive formulas hold up to $n-1$. Then, for n, we have:

$$\begin{aligned} v^{n+1}_{(s,o)}(N) &= pr_{(s,o)}(N-1) - \delta^N c + \delta^N \sum_{(s',o')} Q\Big((s',o')|(s,o)\Big) V^n(s',o'); \\ V^{n+1}(s,o) &= \max\{\max_{1\leq N\leq\infty} v^{n+1}_{(s,o)}(N),\ \mathbb{1}_{s\neq s_3}(R-c)\}; \end{aligned}$$

Similar as in the proof of Lemma 3.4.2, $\mathbb{Q}$ is TP2, then we have $\sum_k^{|\mathcal{S}\times\mathcal{O}|} Q(k|i) \leq$

$\sum_{k}^{|\mathcal{S}\times\mathcal{O}|} Q(k|j)$, for any $k, i, j \in (\mathcal{S}\times\mathcal{O})$ and $i \preceq j$ (i.e., patient in a "bad" state are more likely to transit to "worse" states), and since $\mathbb{Q}$ is a TPM, we have $\sum_{(s',o')} Q\Big((s',o')|(s,o)\Big) = 1$. Given the induction assumption, we have $V^n(s,o)$ decreasing in (s,o), and together with Theorem B.1.1, we have $\sum_{(s',o')} Q\Big((s',o')|(s,o)\Big)V^n(s',o')$ is decreasing in (s,o). Given Lemma 3.4.2, we know $pr_{(s,o)}(N-1)$ is decreasing in (s,o). Now, for the expression of $v_{n+1}(o,N)$, all terms are either decreasing or invariant in (s,o). Then, we conclude that $v^{n+1}_{(s,o)}(N)$ (and subsequently, $V_{n+1}(s,o)$) is decreasing in (s,o).

The proof for the second point is similar as showing $pr_{(s,o)}(N)$ increasing in θ in Lemma 3.4.2. For a given state (s,o), as θ increases, we know $p_{11,\theta}$ increases and $p_{12,\theta}$ decreases. Denote the TPM before the increase in θ as Q_1, after the increase as Q_2. we have $\sum_{k}^{|\mathcal{S}\times\mathcal{O}|} Q_1(k|i) \geq \sum_{k}^{|\mathcal{S}\times\mathcal{O}|} Q_2(k|i)$, for any $k \in (\mathcal{S}\times\mathcal{O})$, which implies that $Q_1(\cdot|i) \geq_r Q_2(\cdot|i)$ (and thus $Q_1(\cdot|i) \geq_s Q_2(\cdot|i)$). Then, we can easily check that $\sum_{(s',o')} Q\Big((s',o')|(s,o)\Big)V^n(s',o')$ is increasing in θ from Theorem B.1.1. From Lemma 3.4.2, we know $pr_{(s,o)}(N-1)$ is increasing in θ. Then, all terms in the expression of $v^{n+1}_{(s,o)}(N)$ are either increasing or invariant in θ. Then, we conclude that $v^{n+1}_{(s,o)}(N)$ (and subsequently, $V_{n+1}(s,o)$) is increasing in θ.

□

In the next corollary, we show the optimal monitoring interval (denoted as I^*) follows a "control limit" fashion. Depending on the exact value of parameters, the threshold may be at different health state. Nevertheless, given our model assumptions, patients with state $(s_2, \overline{OI})$ or "worse", it is optimal to receive the terminal reward rather than stay in virologic failure.

Corollary B.1.1. *There exists* $K = (s_k, o_k)$ *such that* $I^* = \begin{cases} N^*(s,o) = argmax\, v_{(s,o)}(N) & for\ (s,o) \preceq K \\ 0 & for\ (s,o) \succeq K \end{cases}$

Further, $K \preceq (s_2, \overline{OI})$.

Proof of Corollary B.1.1. Subtract $R - c$ from $v_{(s,o)}(N)$, we have

$$pr_{(s,o)}(N-1) - \delta^N c + \delta^N \sum_{(s',o')} Q\Big((s',o')|(s,o)\Big)V(s',o') - R + c$$

From Lemma 3.4.2 and Proposition 2, we know that $v_{(s,o)}(N) - (R - C)$ is decreasing in (s, o), which implies the existence of such a threshold state K. To prove the second claim, we revisit the expression of $v_{(s_2,o)}(N)$

$$v_{(s_2,o)}(N) = pr_{(s_2,o)}(N-1) - \delta^N c + \delta^N \sum_{(s',o')} Q^N\Big((s',o')|(s,o)\Big)V(s',o'),$$

By definition of $\mathbb{Q}$ (Equation 3.7), we know that patients can only move towards "worse" health state $s \in \mathcal{S}$, or stay at the current health state. Together with Assumption 3.4.1, Proposition 2 and Lemma 3.4.2, we have

$$v_{(s_2,OI)}(N) \leq v_{(s_2,\overline{OI})}(N) \leq R - c$$

Then, we know

$$V(s_2, OI) \leq V(s_2, \overline{OI}) \leq R - c$$

Since we know $V(s, o)$ is decreasing in (s, o), we also know that

$$V(s_3, OI) \leq V(s_3, \overline{OI}) \leq R - c$$

This simply because the monthly reward $r(s_3, o, e)$ is assumed to be negative for any o and e, it is better to *quit* the decision process.

□

To further analysis the structure of optimal monitoring interval N^*, we first provide the following lemma for the behavior of difference in $v_{(s,o)}(N+1)$ and $v_{(s,o)}(N)$. We

define $D_{(s,o)}(N) \equiv v_{(s,o)}(N+1) - v_{(s,o)}(N)$. Using Equations 3.8 and 3.9, we have

$$v_{(s,o)}(N) = r(s,o) + \delta \sum_{(s',o')} Q\Big((s',o')|(s,o)\Big) v_{(s',o')}(N-1)$$

Then, we express $D_{(s,o)}(N)$ as

$$D_{(s,o)}(N) = \delta^N \sum_{(s',o')} Q^N\Big((s',o')|(s,o)\Big) b_{(s',o')} \tag{B.12}$$

where

$$b_{(s,o)} = r(s,o) - \delta c + \delta\Big[\sum_{(s',o')} Q\Big((s',o')|(s,o)\Big) V(s',o')\Big] - V(s,o) + c \tag{B.13}$$

Lemma B.1.5. *Let the primitives in Corollary B.1.1 hold. Then, $b_{(s,o)} \geq 0$ for $(s,o) \preceq K$, and $b_{(s,o)} \leq 0$, for $(s,o) \succeq K$.*

Proof of Lemma B.1.5. $b_{(s,o)}$ can be interpreted the difference between the "delayed" reward and the optimal reward. For $(s,o) \preceq K$, we have

$$V(s,o) = \begin{cases} v_{(s,o)}(N) & = r(s,o) - \delta c + \delta \sum_{(s',o')} Q\Big((s',o')|(s,o)\Big) V(s',o') \qquad \text{if } N = 1, \\ v_{(s,o)}(N) & = r(s,o) + \delta \sum_{(s',o')} Q\Big((s',o')|(s,o)\Big) v_{(s',o')}(N-1) \ \text{ if } N \geq 2 \\ & \leq r(s,o) + \delta \sum_{(s',o')} Q\Big((s',o')|(s,o)\Big) V(s',o') \end{cases} \tag{B.14}$$

Then, from Equation B.13 and B.14, we know that $b_{(s,o)}$ is positive. For $(s,o) \succeq (s_2, \overline{OI})$, we claim that $b_{(s,o)}$ is always negative given Corollary B.1.1. This completes the proof. □

Lemma B.1.6. *Let the primitives in Lemma B.1.5 hold. Then $D_{(s,o)}(N)$ changes its sign at most once in N. When changes occurs, it is from positive (to negative). Moreover, for states $(s,o) \preceq (s',o')$, if $D_{(s,o)}(N) \leq 0$, then $D_{(s',o')}(N) \leq 0$.*

Proof of Lemma B.1.6. First, note that from Lemma B.1.5, it implies that $b_{(s,o)}$ changes its sign at most once in (s, o), and it occurs from positive. Then, the remaining proof will be similar to the proof of Lemma 8.2.4 in [111], where the authors utilized the so-called variation diminishing property of TP2 function. In our context, it says if $b_{(s,o)}$ changes its sign at most once in (s, o), and it occurs from positive (which is given by Lemma B.1.5), then $\sum_{(s',o')} Q^N\Big((s', o')|(s, o)\Big) b_{(s',o')}$ changes its sign at most once in N for each (s, o), and in (s, o) for each N. This completes the proof for the first part.

To prove the second claim, first note that $\mathbb{Q}$ is a TP2 matrix, and only allows transition to "worse" health states, not vice versa. We have for $(s, o) \preceq (s', o')$, $Q(\cdot|(s, o)) \leq_r Q(\cdot|(s', o'))$, and thus $Q(\cdot|(s, o)) \leq_s Q(\cdot|(s', o'))$. Then, given the expression of $D_{(s,o)}(N)$ in Equation B.12, and the property of $b_{(s,o)}$ given in Lemma B.1.5, it is trivially true that if if $D_{(s,o)}(N) \leq 0$, then $D_{(s',o')}(N) \leq 0$. □

Lemma B.1.6 states that, for $(s, o) \preceq (s', o')$, argmax $v_{(s,o)}(N) \geq$ argmax $v_{(s',o')}(N)$, which is to say the optimal monitoring interval is larger for "better" patients. Moreover, Lemma B.1.6 implies that optimal N is unique.

Proof of Corollary 3.4.1. This follows since both $\mathbb{P}_\theta$ and $\mathbb{P}_o$ is TP2. □

Proof of Lemma 3.4.3. The belief state π_t is the only variable depends on adherence state A_t. Then, we could express the updated belief conditioning on θ. Then, the results follow from by applying the belief update formula Equation 3.13. instead of Equation 3.12. □

Proof of Theorem 3.4.2. The left-hand side of Equation 3.16 represents the difference in total health benefit between a healthier (with state distribution π_1) and a sicker (with state distribution π_2) patient upon taking action $Wait$. The right-hand side of Equation 3.16 represents the difference in health benefit between a healthier and sicker patients upon taking action *Perform VL test*. Intuitively, Equation 3.16 means that as patient gets sicker, the reduction in the benefit of watiing is greater than the reduction in the

benefit of performing a VL test. We prove part (a) and the proof for (b) is similar. Suppose the converse of the statement is True. Then we have:

$$V^w(\pi_1(1)) \leq V^v(\pi_1(1)) \text{ and } V^w(\pi_2(1)) > V^v(\pi_2(1))$$

By expanding these expressions using equation 3.15 and cancel the monthly rewards term in both $V^w(\pi)$ and $V^v(\pi)$, we get

$$\begin{aligned}
&\sum_s \mathbb{m}_1(s)\Big\{\delta \sum_{s'}\sum_o V^*(\pi_1'(1)|o,\theta)P(s'|s,\theta)P(o|s)\Big\} \\
\leq &\sum_s \mathbb{m}_1(s)\Big\{ -\delta c + \delta \sum_{s'}\sum_o \Big((\pi_1'(1)|o,\theta)V_1 + \big(1-(\pi_1'(1)|o,\theta)\big)\,R\Big)P(s'|s,\theta)P(o|s)\Big\}
\end{aligned}$$

and,

$$\begin{aligned}
&\sum_s \mathbb{m}_2(s)\Big\{\delta \sum_{s'}\sum_o V^*(\pi_2'(1)|o,\theta)P(s'|s,\theta)P(o|s)\Big\} \\
> &\sum_s \mathbb{m}_2(s)\Big\{ -\delta c + \delta \sum_{s'}\sum_o \Big((\pi_2'(1)|o,\theta)V_1 + \big(1-(\pi_2'(1)|o,\theta)\big)\,R\Big)P(s'|s,\theta)P(o|s)\Big\}
\end{aligned}$$

Then we multiply both slides by $\frac{1}{\delta}$ and rearrange terms, we get,

$$\begin{aligned}
&\sum_s\sum_{s'}\sum_o V^*(\pi_1'(1)|o,\theta)\pi_1(s)P(s'|s,\theta)P(o|s) \\
-&\sum_s\sum_{s'}\sum_o V^*(\pi_2'(1)|o,\theta)\pi_2(s)P(s'|s,\theta)P(o|s) \\
\leq &\sum_s\sum_{s'}\sum_o \Big((\pi_1'(1)|o,\theta)V_1 + \big(1-(\pi_1'(1)|o,\theta)\big)\,R\Big)\pi_1(s)P(s'|s,\theta)P(o|s) \\
-&\sum_s\sum_{s'}\sum_o \Big((\pi_2'(1)|o,\theta)V_1 + \big(1-(\pi_2'(1)|o,\theta)\big)\,R\Big)\pi_2(s)P(s'|s,\theta)P(o|s)
\end{aligned}$$

Since we have $\pi_1(1) \geq \pi_1(2)$ and from Proposition 4 we know $V^*(\pi(1))$ is monotonically

increasing in $\pi(1)$. We then again re-arrange the terms and get,

$$
\begin{aligned}
&\sum_{s}(\pi_1(s)-\pi_2(s))\Big[\sum_{s'}\sum_{o}V^*(\pi_2'(1)|o,\theta)P(s'|s,\theta)P(o|s)\Big]\\
\leq&\sum_{s}\sum_{s'}\sum_{o}V^*(\pi_1'(1)|o,\theta)\pi_1(s)P(s'|s,\theta)P(o|s)\\
-&\sum_{s}\sum_{s'}\sum_{o}V^*(\pi_2'(1)|o,\theta)\pi_2(s)P(s'|s,\theta)P(o|s)\\
\leq&\sum_{s}\sum_{s'}\sum_{o}\Big((\pi_1'(1)|o,\theta)V_1+\big(1-(\pi_1'(1)|o,\theta)\big)\,R\Big)\pi_1(s)P(s'|s,\theta)P(o|s)\\
-&\sum_{s}\sum_{s'}\sum_{o}\Big((\pi_2'(1)|o,\theta)V_1+\big(1-(\pi_2'(1)|o,\theta)\big)\,R\Big)\pi_2(s)P(s'|s,\theta)P(o|s)\\
\leq&\sum_{s}(\pi_1(s)-\pi_2(s))\Big[\sum_{s'}\sum_{o}\Big((\pi_1'(1)|o,\theta)V_1+\big(1-(\pi_1'(1)|o,\theta)\big)\,R\Big)P(s'|s,\theta)P(o|s)\Big]
\end{aligned}
$$

and we get

$$
\begin{aligned}
&\sum_{s}(\pi_1(s)-\pi_2(s))\Big[\sum_{s'}\sum_{o}V^*(\pi_2'(1)|o,\theta)P(s'|s,\theta)P(o|s)\Big]\\
\leq&\sum_{s}(\pi_1(s)-\pi_2(s))\Big[\sum_{s'}\sum_{o}\Big((\pi_1'(1)|o,\theta)V_1+\big(1-(\pi_1'(1)|o,\theta)\big)\,R\Big)P(s'|s,\theta)P(o|s)\Big]
\end{aligned}
$$

Which contradicts condition 3.16, and from which the result follows.

□

Proof of Corollary 3.4.2. Similar as in the proof of Lemma 3.4.2, as patient becomes more adherent, $p_{11,\theta}$ increases. For two individuals given the same starting belief $\pi_1 = \pi_2$, after one or more belief updates, we have $\pi_1 \leq_r \pi_2$. Given Theorem 3.4.2, the results thus trivially follows. □

Proof of Corollary 3.4.3. This statement follows by Theorem 3.4.2 and the fact that POMDP value function is monotonic (Proposition 4). □

Lemma B.1.7. $r(s_1) \geq r(s_2)$.

Proof. The statement of Lemma B.1.7 trivially follows by applying Assumption 3.4.1, and the definition of $r(s)$. □

Proposition 3. *$V^v(\pi(1))$ is increasing in $\pi(1)$.*

Proof. We first organize $V^v(\pi(1))$ as follow:

$$\begin{aligned}
V^v(\pi(1)) &= \sum_s \mathbb{m}(s)\Big\{r(s) - \delta c + \delta \sum_{s'}\sum_o \Big((\pi'(1)|o,\theta)V_1 + \big(1-(\pi'(1)|o,\theta)\big)\,R\Big)P(s'|s,\theta)P(o|s)\Big\} \\
&= \sum_s \mathbb{m}(s)r(s) + \delta \sum_s\sum_{s'}\sum_o \Big((\pi'(1)|o,\theta)V_1 + \big(1-(\pi'(1)|o,\theta)\big)\,R\Big)\pi(s)P(s'|s,\theta)P(o|s) - \delta c \\
&= f_1(\pi(1)) + \delta f_2(\pi(1)) - \delta c
\end{aligned}$$

We claim both $f_1(\pi(1))$ and $f_2(\pi(1))$ are increasing in $\pi(1)$ The first part $f_1(\pi(1))$ is the expected one-month reward gained (minus cost) given $Prob(s = s_1) = \pi(1)$. It is trivial to check that if $\pi_1(1) \geq \pi_2(1)$, the corresponding belief vector follows the MLR ordering: $\mathbb{m}_1 \leq_r \mathbb{m}_2$. Then, from Lemma B.1.7, and Theorem B.1.1, we know:

$$\sum_s \mathbb{m}_1(s)r(s) \geq \sum_s \mathbb{m}_2(s)r(s)$$

Then, we have for $\pi_1(1) \geq \pi_2(1)$, $f_1(\pi_1(1)) \geq f_1(\pi_2(1))$. The second part $f_2(\pi(1))$ is the expected future rewards. For a given θ, the updated belief vector is $\mathbb{m}^T\mathbb{P}_\theta\mathbb{P}_o$, From [81], if matrices $\mathbb{P}_\theta$ and $\mathbb{P}_o$ are of TP2, and $\pi_1 \leq_r \pi_2$, then $\mathbb{m}_1^T\mathbb{P}_\theta\mathbb{P}_o \leq_r \mathbb{m}_2^T\mathbb{P}_\theta\mathbb{P}_o$. From Lemma B.1.4, we have $\pi_1|o,\theta \leq_r \pi_2|o,\theta$, $\forall o \in \mathcal{O}$, and θ. Then, we have

$$(\pi_1'(1)|o,\theta)V_1 + \big(1-(\pi_1'(1)|o,\theta)\big)\,R \geq (\pi_2'(1)|o,\theta)V_1 + \big(1-(\pi_2'(1)|o,\theta)\big)\,R$$

for any o and θ. Combining with $\mathbb{m}_1^T\mathbb{P}_\theta\mathbb{P}_o \leq_r \mathbb{m}_2^T\mathbb{P}_\theta\mathbb{P}_o$, and Theorem B.1.1, we then have $f_2(\pi_1(1)) \geq f_2(\pi_2(1))$. Lastly, if both $f_1(\pi(1))$ and $f_2(\pi(1))$ is increasing in π, $f_1(\pi(1)) + f_2(\pi(1))$ is also increasing in $\pi(1)$. This completes the proof.

□

Proposition 4. *$V^*(\pi(1))$ is increasing in $\pi(1)$.*

Proof. Given Proposition 3, it remains to show that $V^w(\pi(1))$ is increasing in $\pi(1)$, and thus $V^*(\pi(1)) = \max\{V^w(\pi(1)), V^v(\pi(1))\}$ is increasing in $\pi(1)$, as the maximum of two increasing function is also increasing. We use mathematical induction on value iteration algorithm to prove the results. We first let $V_0 \geq R$, and initialize $V_0^w(\pi(1)) = V_0^v(\pi(1)) = V_0$, $\forall\ \pi$. For iteration $n = 1$, we have

$$V_1^w(\pi(1)) = \sum_s \mathbb{m}(s)\Big\{r(s) + \delta \sum_{s'} \sum_o V_0(\pi'(1)|o,\theta)P(s'|s,\theta)P(o|s)\Big\}$$

Where $V_0(\pi'(1)|o,\theta) = V_0$. Thus we have

$$\sum_{s'} \sum_o V_0(\pi'(1)|o,\theta)P(s'|s,\theta)P(o|s) = V_0 \tag{B.15}$$

Let $\pi_1(1) \geq \pi_2(1)$, Then, we have

$$V_1^w(\pi_1(1)) \geq V_1^w(\pi_2(1)), \forall\ \ \pi_1(1) \geq \pi_2(1) \tag{B.16}$$

Combined with the result of Proposition 3, we conclude that $V_1^*(\pi(1))$ is increasing in $\pi(1)$.

Now, assume that $V_{n-1}^*(\pi(1))$ is increasing in $\pi(1)$ by induction hypothesis. To facilitate our analysis, we assumed all the rewards are non-negative. Then, similar as

the proof in iteration $n = 1$, we have:

$$V_n^w(\pi_1(1)) = \sum_s \mathbb{m}_1(s)\Big\{r(s) + \delta \sum_{s'}\sum_o V_{n-1}^*(\pi_1'(1)|o,\theta)P(s'|s,\theta)P(o|s)\Big\} \tag{B.17}$$

$$\geq \sum_s \mathbb{m}_1(s)\Big\{r(s) + \delta \sum_{s'}\sum_o V_{n-1}^*(\pi_2'(1)|o,\theta)P(s'|s,\theta)P(o|s)\Big\} \tag{B.18}$$

$$\geq \sum_s \mathbb{m}_2(s)\Big\{r(s) + \delta \sum_{s'}\sum_o V_{n-1}^*(\pi_2'(1)|o,\theta)P(s'|s,\theta)P(o|s)\Big\} \tag{B.19}$$

$$= V_n^w(\pi_2(1)) \tag{B.20}$$

Similarly in the proof for Proposition 3, we have $\pi_1|o,\theta \leq_r \pi_2|o,\theta$ for any o and θ, given Lemma B.1.4. Then, by induction assumption, we have $V_{n-1}^*(\pi_1'(1)|o,\theta) \geq V_{n-1}^*(\pi_2'(1)|o,\theta)$. Thus the first inequality follows. The second inequality follows from Theorem B.1.1 and the fact that $\pi_1 \leq_r \pi_2$.

We now have $V_n^w(\pi(1))$ is increasing in $\pi(1)$, thus $V_n^*(\pi(1))$ is also increasing in $\pi(1)$. Since V_n converges uniformly to V, it follows that $V^*(\pi(1))$ is also increasing in $\pi(1)$. □

Next, we would like to show the monotonicity of $V^*(\pi(1))$ in θ: adherent patients should gain larger health benefit (i.e., higher quality-adjusted life years, lower healthcare-related costs) compared to non-adherent patients).

Theorem B.1.2. *$V^*(\pi(1))$ is increasing in θ, for any given $\pi(1)$.*

Proof. We use mathematical induction on value iteration algorithm to prove the result (similar as in the proof for Proposition 4). We set $V_0 = R$, and initialize $V_0^w(\pi(1)) =$

$V_0^v(\pi(1)) = V_0$, $\forall \pi(1)$. For iteration $n = 1$, we have

$$V_1^w(\pi(1)) = \sum_s \mathbb{m}(s)\Big\{r(s) + \delta \sum_{s'}\sum_o V_0^*(\pi'(1)|o,\theta)P(s'|s,\theta)P(o|s)\Big\}$$
$$V_1^v(\pi(1)) = \sum_s \mathbb{m}(s)\Big\{r(s) - \delta c + \delta \sum_{s'}\sum_o \Big((\pi'(1)|o,\theta)V^*(1) + \big(1 - (\pi'(1)|o,\theta)\big)\, R\Big)P(s'|s,\theta)P(o|s)\Big\}$$

Where $V_0^*(\pi'(1)|o,\theta) = V_0$. For any given state s, we have

$$\sum_{s'}\sum_o V_0^*(\pi'(1)|o,\theta)P(s'|s,\theta)P(o|s) = V_0 = R$$
$$\sum_{s'}\sum_o \Big((\pi'(1)|o,\theta)V_1 + \big(1 - (\pi'(1)|o,\theta)\big)\, R\Big)P(s'|s,\theta)P(o|s) = V_0 = R$$

Then, we have

$$\max\Big\{V_1^w(\pi(1)), V_1^v(\pi(1))\Big\}\Big|\theta_1 = V_1^*(\pi(1))\Big|\theta_1$$
$$\geq V_1^*(\pi(1))\Big|\theta_2 = \max\Big\{V_1^w(\pi(1)), V_1^v(\pi(1))\Big\}\Big|\theta_2,\ \forall\ \theta_1 \geq \theta_2$$

Now, assume that $V_{n-1}^*(\pi(1))|\theta$ is increasing in θ by induction hypothesis. We have for $\theta_1 \geq \theta_2$:

$$V_n^w(\pi(1))|\theta_1 = \sum_s \mathbb{m}(s)\Big\{r(s) + \delta \sum_{s'}\sum_o V_{n-1}^*(\pi'(1)|o,\theta_1)P(s'|s,\theta_1)P(o|s)\Big\} \quad \text{(B.21)}$$
$$\geq \sum_s \mathbb{m}(s)\Big\{r(s) + \delta \sum_{s'}\sum_o V_{n-1}^*(\pi'(1)|o,\theta_2)P(s'|s,\theta_1)P(o|s)\Big\} \quad \text{(B.22)}$$
$$\geq \sum_s \mathbb{m}(s)\Big\{r(s) + \delta \sum_{s'}\sum_o V_{n-1}^*(\pi'(1)|o,\theta_2)P(s'|s,\theta_2)P(o|s)\Big\} \quad \text{(B.23)}$$
$$= V_n^w(\pi(1))|\theta_2 \quad \text{(B.24)}$$

The first inequality follows by induction. Similar as in the proof of Lemma 3.4.2, we

can show that $\pi(1)|o,\theta_1 \geq \pi(1)|o,\theta_2$. Thus, the second inequality follows.

For a similar reason, we claim the following inequality is true:

$$
\begin{aligned}
V_n^v(\pi(1))|\theta_1 = \sum_s \mathbb{m}(s)\Big\{ & r(s) - \delta c + \\
& \delta \sum_{s'} \sum_o \Big((\pi'(1)|o,\theta_1) V^*(1) + \big(1 - (\pi'(1)|o,\theta_1)\big) R \Big) P(s'|s,\theta_1) P(o|s) \Big\} \\
& \geq \sum_s \mathbb{m}(s)\Big\{ r(s) - \delta c + \\
& \delta \sum_{s'} \sum_o \Big((\pi'(1)|o,\theta_2) V^*(1) + \big(1 - (\pi'(1)|o,\theta_2)\big) R \Big) P(s'|s,\theta_2) P(o|s) \Big\} \\
& = V_n^v(\pi(1))|\theta_2
\end{aligned}
$$

We now have both $V_n^v(\pi(1))$ and $V_n^w(\pi(1))$ is increasing in θ, thus $V_n^*(\pi(1))$ is also increasing in θ. Since V_n converges uniformly to V, it follows that $V^*(\pi(1))$ is also increasing in θ. □

B.2 Model Details

Disease Progression

Our previous work in [106] motivated this study, where we studied the cost-effectiveness of adaptive HIV VL monitoring in resource-limited settings. In that paper, we developed a microsimulation model that captures HIV disease progression (and transmission) in order to evaluate both the adaptive and fixed VL monitoring strategies. The model tracked patient demographics (such as age, gender, education level), CD4 cell counts (white blood cells), individual adherence status at each month to ART, and presence of virologic failure. Patient adherence status/measurement at the current month (which is a binary outcome, defined as whether having missed more than two doses in the previous month) was modeled using a mixed-effects logistic regression model fitted to a

longitudinal dataset. In the same dataset, virologic failure was defined as (i) 2 consecutive measurements of a VL >200 copies/mL, (ii) 1 VL measurement >1000 copies/mL, or (iii) not reaching virologic suppression within 6 months of either ART initiation or regimen change. Patient failure status (binary) at any month was estimated using a logit function of adherence status, patient demographics and ART attributes; or a fixed monthly probability of failure if the patient was on the first-line regimen, or second-line regimen respectively. In addition, the probability of spontaneous re-suppression after the first occurrence of virologic failure was also captured in the microsimulation model. Lastly, CD4 cell count changes were modeled using quantile regression where previous CD4 cell count, patient demographics and ART attributes.

Notably, the model 1) explicitly considered AIDS-defining opportunistic infections (OIs), where patients were monitored upon the development of OIs; 2) adjusted health outcomes by estimate the number of secondary HIV infections in the community, at each month as a function of the number of individuals in virologic failure.

Due to the level of complexity involved in the simulation model, we did not manage to develop a globally optimal solution to the problem. Our goal in this project is to take a step further, by constructing an analytically tractable and analyzable tractable optimization approach. To do so, we constructed a stylized simulation model based on the microsimulation model, capturing most of the important features mentioned above. First, we simplified the model where CD4 cell count is no longer tracked at each month (Section "Simplified Health State"). In Section "Bayesian reformulation of adherence heterogeneity", we provided an equivalent Bayesian representation of the frequentist adherence model. In Section 3.5, we present and discuss the optimal policies for a subgroup of patients (with pre-determined patient demographics) given the model, and we compared our optimal monitoring policies with the status quo (i.e., fixed policies).

Simplified Health State

Both VL, and CD4 cell count are arguably the two most important factor and index when considering HIV-infected patients health. However, a multi-dimensional state

space might lose the analytical tractability and required more complex analysis which is beyond the scope of this project. Subsequently, we decided to develop the model framework in Section 3.2 using one single covariate. We chose VL instead of CD4 cell count for a few reasons. First, various studies has found highly negative correlation between VL and CD4 cell count ([149], [95]). We acknowledge that incorporating CD4 cell count into the state space may give a better prediction on patient health outcome. However, we feel that either one of them would capture a sufficient amount of patients' risk and disease progression (due to the high negative correlation), while providing an analytically tractable (the base model) and a computationally tractable model (in Section 3.4.1, we extended the model to incorporate AIDS-defining Opportunistic Infections). Second, identifying the presence of virologic failure in a timely manner is important not only for the patient, but also for the society at large, since patients in virologic failure tend to have a much high rate of HIV transmission than those HIV-infected patients with undetectable VL.

Modelling ART adherence using Bayesian Hierarchical model

In [106], we modeled each patient's monthly (non)adherence status (adh_t) using mixed effect logistic regression as a function of his age at time t (age_t), gender (sex), education level (edu), and time between measurements (Δt), as well as his previous (non)adherence status (adh_{t-1}):

$$Prob(adh_t) = \frac{1}{1+\exp[-(\beta_0+\beta_1 age_t+\beta_2 sex+\beta_3 edu+\beta_4(adh_{t-1})+\beta_5\Delta t+\beta_6 adh_{t-1}\Delta t+p_i]}, \tag{B.25}$$

where p_i is the random intercept (i.e., heterogeneous pattern) of patient i. However, this patient-specific intercept term is intrinsically hard to incorporate into an analytically tractable decision-making framework. We then seek to find an alternative representation of the mixed effect logistic regression model. Instead of a frequentist approach, we construct a Bayesian hierarchical model to quantify the heterogeneity effect in HIV

patients' treatment adherence. Bayesian hierarchical modeling is a statistical model written in multiple levels (hierarchical form) that estimates the parameters of the posterior distribution using the Bayesian method [62]. Since our response adh_t is binary, we consider a Beta-Binomial hierarchical model (denote by M_{b1}) and compare to a null model (M_{b0}) assuming no heterogeneity effect.

In model M_{b1}, we assume each patient $i \in \{1, 2, ..., m\}$ has his/her own probability $\theta_i \in [0, 1]$ of being nonadherent (i.e., $\theta_i \neq \theta_j$). On the contrary, in the null model M_{b0}, we assume $\theta_1 = \theta_2 = ...\theta_m$, for any patient i. Denote n_i is the total counts of clinical visits for patient i, and y_i is the frequency of nonadherence for patient i. For model M_{b1}, we sample $\theta_i's$ (independent and identically distributed) from $Beta(a, b)$ distribution and let D stands for the entire sub-dataset, then we have:

$$\begin{aligned} y_i &\sim Binomial(n_i, \theta_i) \\ p(\theta_i|y_i, a, b) &= Beta(a + y_i, b + n - y_i) \\ P(y_i|a, b) &= \binom{n_i}{y_i} \frac{B(a + y_i, b + n_i - y_i)}{B(a, b)} \\ P(D|a, b) &= \prod_{i=1}^{m} P(y_i|a, b) \end{aligned} \tag{B.26}$$

We use the empirical bayes approach to choose a, b. We denote $\mu = \frac{a}{a+b}$ and $S = a + b$, and apply the " iterated method of moments" estimator:

$$\begin{aligned} \text{(sample mean) } \hat{\mu} &= \frac{1}{m} \sum_{i=1}^{m} \frac{y_i}{n_i} \\ \text{(sample variance) } s^2 &= \frac{1}{m} \sum_{i=1}^{m} \frac{\hat{u}(1 - \hat{u})}{n_i} (1 + \frac{n_i - 1}{\widehat{S} + 1}) \end{aligned} \tag{B.27}$$

For model M_{b0}, we assume the probability of being (non)adherent at time t is *not* patient-specific ($\theta_1 = ... = \theta_m = \theta$), let $\theta \sim Beta(1, 1)$. Then, under model M_{b0}, we have

$$y \sim Binomial(n, \theta),$$

where

$$n = \sum_{i=1}^{m} n_i, \;\; y = \sum_{i=1}^{m} y_i$$

Then, we have the marginal for M_{b0} as

$$P(D|M_{b0}) = \left[\prod_{i=1}^{m} \binom{n_i}{y_i}\right] Beta(1+y, 1+n-y) \tag{B.28}$$

The Bayes Factor for M_1 over M_0 is defined as

$$\frac{P(D|M_{b1})}{P(D|M_{b0})} = \frac{P(D|a,b)}{P(D|M_{b0})} \tag{B.29}$$

To examine the statistical significance of this model, we first create synthetic adherence measurement dataset using Equation B.25 by sampling 10,000 data points for different age, gender and educational level. For example, We first restrict the categorical covariate *age* to be within 20 - 30, *sex* as male, and high educational level. We also aggregated age to make sure we have sufficient data points to fit the model. Plugging the data into Equation B.27, we estimate $\hat{a} = 0.141$, $\hat{b} = 0.304$. Then, we compute the Bayes Factor for M_1 over M_0 given in Equation B.29 is $\frac{8.309734e-21}{8.216354e-27}$ ($> 10^6$), which means the strength of evidence that hierarchical model is superior is decisively strong ([76]). Sub-datasets with different covariate combination also provide evidence with heuristically decisive Bayes factors (i.e., $>= 10^4$, see [76]). We provide the summary statistics in Bayes factors for all sub-datasets in Appendix Table B.2.

We then conclude that the mixed effect logistic regression model, a frequentist formulation of adherence heterogeneity, can be alternative represented using a Bayesian hierarchical model.

We denote the mean adherence level as $\bar{\theta}$. In Figure B.1, we plot the mean adherence level with increasing age. We generally observe $\bar{\theta}$ increasing as patients get older. Excluding the outliers (one standard deviation from the mean), we see the maximum difference in $\bar{\theta}$ is within 0.25. The maximum difference becomes smaller by further

differentiating patients by gender (Appendix Figure B.2 and B.3).

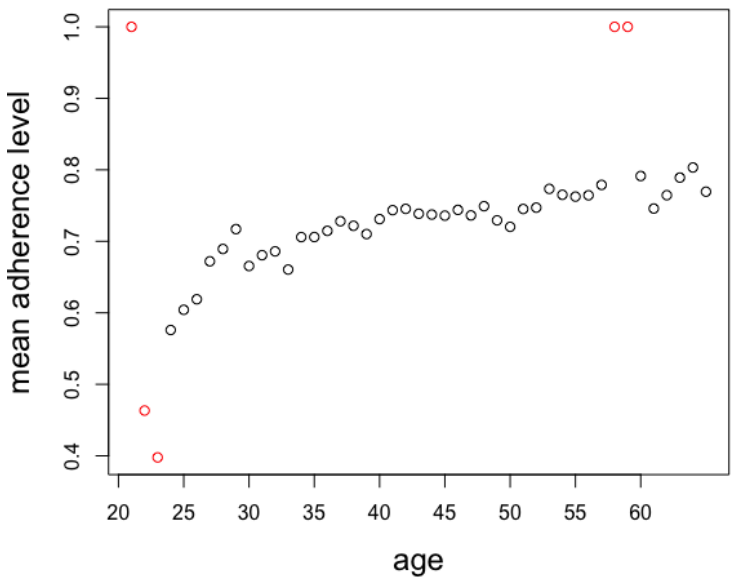

Figure B.1: $\bar{\theta}$ with increasing age

By constructing a Beta-binomial Bayesian hierarchical model and compared with the alternative model where we assume no heterogeneity effect, we conclude that the adherence pattern is different among patients. While some patients are more likely to be adherent at each month (i.e., not missing more than 2 pills), other patients might be always less adherent. From Figures B.1, B.2 and B.3, we generally observe an increasing trend in mean adherence level $\bar{\theta}$ with age. Moreover, we found the maximum difference in $\bar{\theta}$ is small.

Although a dynamic, time-dependent adherence type (θ_t) is more realistic, we feel it might add an additional level of complexity to our problem. Thus, differentiating patients by gender, and use the gender-specific mean adherence level might be a better choice.

We further divided the synthetic dataset into sub-dataset by gender (male, female).

We adjusted the starting mean adherence level for age 20 to match the figures has been reported in the literature [157], [169]. In both Figure B.2 and Figure B.3, the maximum change in terms of mean adherence level in 40 years did not exceed 15%.

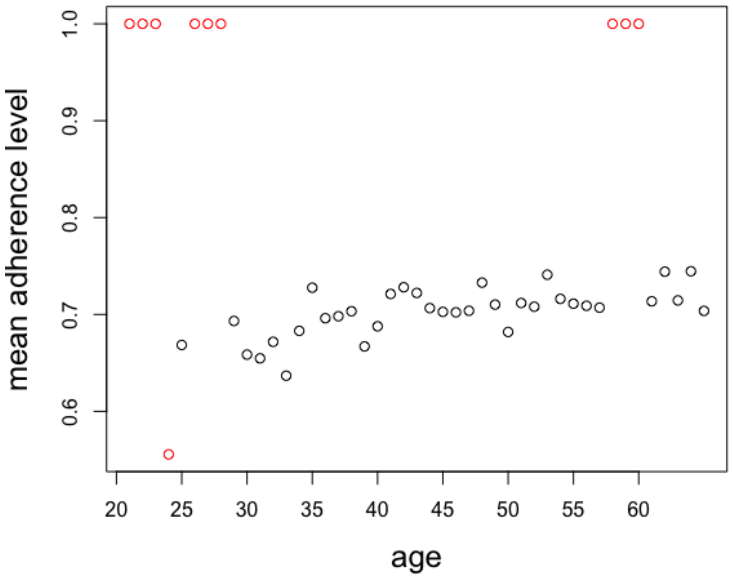

Figure B.2: $\bar{\theta}$ with increasing age in male patient

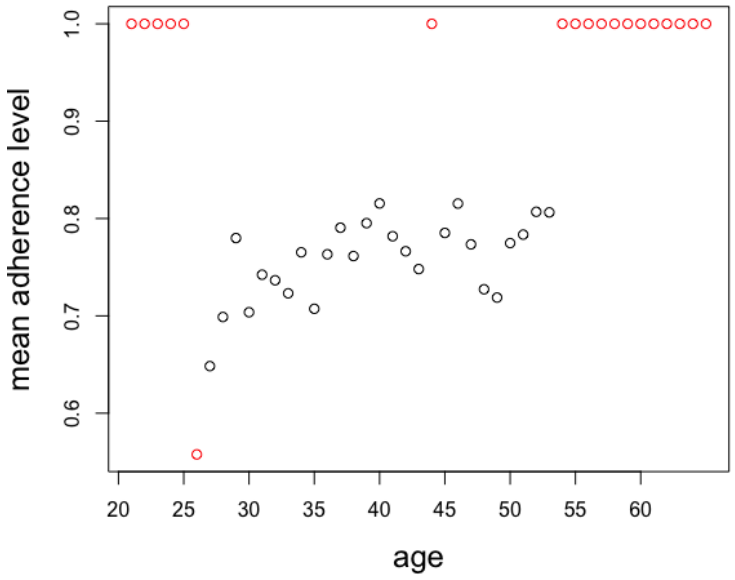

Figure B.3: $\bar{\theta}$ with increasing age in female patient

B.3 Figures and Tables

Variable	Description	Value	Source
Opportunistic infection rates			
	virally suppressed	0.0228	[106]
	in failure	0.2	
p_{v10}, **per sex-act transmission rate**			
	male to female	$4.3 * 10^{-5}$	
	female to male	$2.2 * 10^{-5}$	[122]
	male to male	$4.3 * 10^{-4}$	
	monthly sec acts	9	[106]
health utilities			
	yearly utility, virally suppressed	0.865	[106]
	yearly utility in failure s_2	0.526	
costs			

Continued on next page

Table B.1 – continued from previous page

Variable	Description	Value	Source
c	VL test cost	\$100 USD	[75]
	yearly cost if virally suppressed	\$160 USD	
	yearly cost, first-line ART	\$120 USD	[106]
	yearly cost, second-line ART	\$345 USD	
r	yearly discount factor	0.03	[106]

Table B.1: **Parameters and data sources.**

Beta-Binomial	
Min.	1.08e+04
1st Quantile	1.97e+06
Median	2.63e+11
Mean	5.58e+20
3rd Quantile	9.33e+12
Max	4.46e+21

Table B.2: Summary of hierarchical modeling Bayes factors (hierarchical models over null models)

Figure B.4: Remaining Rewards Comparison: Male Patients

(a) Remaining Rewards Adjusting Secondary Infection

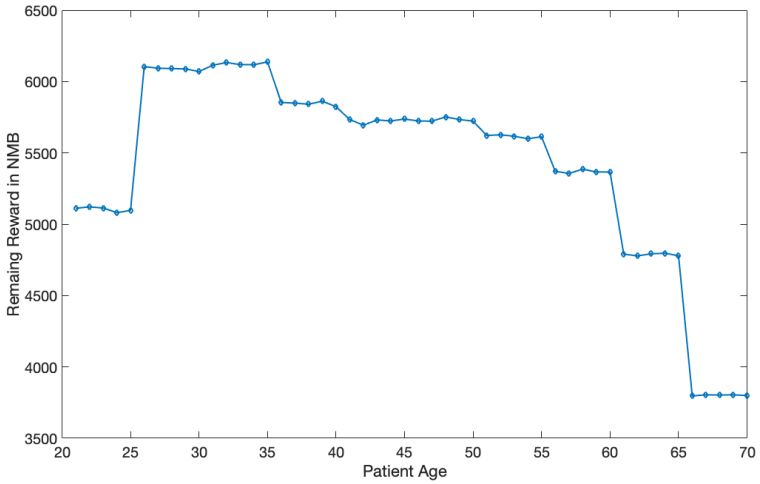

(b) Remaining Rewards not Adjusting Secondary Infection

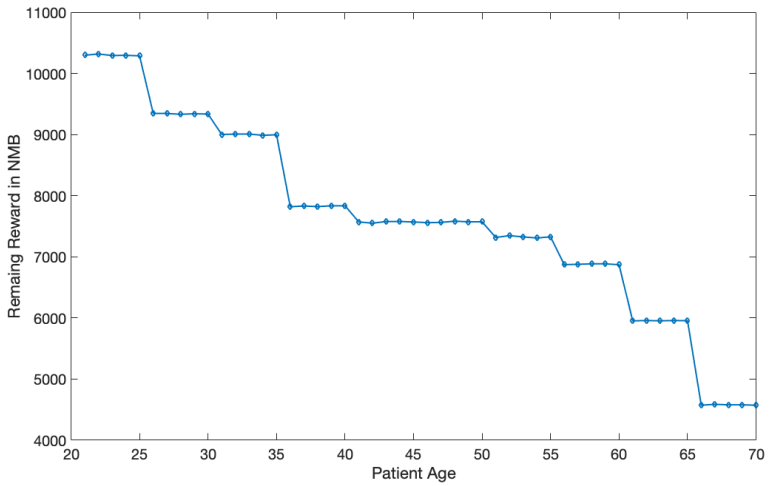

Appendix C

Chapter 3 Supplement Material

C.1 Tables and Figures

Variable	Description	Value	Source
β	Per-contact transmission rate in the age-stratified SEIR model	2.95%	[100]
	Viral infection rate in the SIR model)	0.3540	
Monetized utility term associated with infection, by age category			
$b_{3,1}$	Youth	\$1740.189	Supplement C.2
$b_{3,2}$	Adult	\$46640.377	
$b_{3,3}$	Elderly	\$39638.333	
b_3	An average person	\$24844.44	
b_1	Monetized utility term	\$88.41	Supplement C.2
b_2	Monetized utility term	\$99.02	
Parameters of social distancing implementation			
ϕ	Shape parameter	1	[128]
$q_{\max}$	Daily cost of strict social distancing per person	\$123.25	Supplement C.2
$k_{\max}$	Maximum possible contact reduction	50%	[168]

Continued on next page

Table C.1 – continued from previous page

Variable	Description	Value	Source
d_1	Daily cost of lockdown per person	\$389.929	Supplement C.2
	Health care cost per clinical confirmed COVID-19 case	\$3045	[14]
Proportion of infections that are clinically confirmed			
	Youth	36.2%	Supplement C.2
	Adult	81.9%	
	Elderly	100%	
	An average person	66.7%	
Economic cost per non-fatal COVID-19 case			
	Youth	\$3029.325	Supplement C.2
	Adult	\$9987.139	
	Elderly	\$2494.109	
Economic cost per fatal COVID-19 case			
	Youth	\$4487932.6	Supplement C.2
	Adult	\$2549369.7	
	Elderly	\$487733.8	
Contact pattern			
C_{11}, C_{12}, C_{13}	Youth to (Youth, Adult, Elderly)	8.74, 4.48, 0.74	Supplement C.2
C_{21}, C_{22}, C_{23}	Adult to (Youth, Adult, Elderly)	2.77, 9.46, 0.86	
C_{31}, C_{32}, C_{33}	Elderly to (Youth, Adult, Elderly)	0.99, 2.55, 1.52	
$\overline{C}$	Average daily contacts	12	
a^{-1}	Average days in incubation	5.2	[100]
r^{-1}	Average days in infectious state	7.8	
COVID-19 prevalence (cumulative) as of Dec 13, 2020 in Minnesota			
	Confirmed infections	378823	[98]
	Recovered cases	341530	
	COVID-19 deaths	4444	
	Minnesota population	5.69 million	[100]
Age distribution			
	Youth	25.49%	
	Adult	50.93%	
	Elderly	23.58%	

Continued on next page

Table C.1 – continued from previous page

Variable	Description	Value	Source
COVID-19 daily mortality rate, by age category			
μ_1	Youth	0.003%	Supplement C.2
μ_2	Adult	0.3%	
μ_3	Elderly	2.40%	
μ	An average person	0.75%	

Table C.1: **Parameters and data sources.**

C.2 Model Parameterization

In this section, we detail our estimation of parameters on disease dynamics, disease burden and socioeconomic loss of policy implementation.

C.2.1 Disease Dynamics Parameters

We obtain disease dynamic parameters, including infection rate β, recovery rate r, and initial disease states $S(1), I(1), R(1)$ using public epidemiological data in Minnesota [98] and a validated Minnesota COVID-19 micro-simulation model [100]. We obtain the per-contact transmission rate of 0.0295 (for the homogeneous model, $\beta = 0.0295 \cdot \overline{C}$, where $\overline{C} = 12$ is the average daily contacts in Table C.1), recovery rate $r = 0.1282$ and the average incubation period $a^{-1} = 5.2$ days from [100]. We extrapolate the initial disease prevalence $I(1)$ using the difference between total confirmed COVID-19 cases and total recovered cases $R(1)$ from [98]. In the heterogeneous model Eq.(4.24), no immediate data is available to parametrize $E(1)$. We assume $E(1) = I(1)$. We have tested that our model outcome is not sensitive to the value of $E(1)$ when $E(1) \leq 2 \times I(1)$.

We aggregate the contact information from [100] to estimate the contact matrix as follows (subscript 1, 2 and 3 corresponds to the Youth, Adult and Elderly group): $C_{11} = 8.74$, $C_{12} = 4.48$, $C_{13} = 0.74$, $C_{21} = 2.77$, $C_{22} = 9.46$, $C_{23} = 0.86$, $C_{31} = 0.99$, $C_{32} = 2.55$, $C_{33} = 1.52$, and the age-proportional average daily counts $\overline{C} = 12$.

We obtain the mortality rate by taking the multiplication of the symptomatic mortality rate of (0.01%, 0.55%, 5.61%) and the symptomatic infection ratio of (30.3%, 67.5%, 42.8%) for the Youth, Adult and Elderly group, respectively [171]. We calculate the population average symptomatic infection ratio as 52.2% and population average mortality rate as 0.75% based on Minnesota age distribution. We obtain clinical confirmation percentage over symptomatic cases as (9.5%, 81.9%, 100%) for different age groups [171] and calculate a population average clinical confirmation rate as 67.7%.

C.2.2 Disease Burden

We quantify the overall health impact of COVID-19 and personal utility parameters related to infection using the disability-adjusted life-year (DALY), and Net Monetary Benefit (NMB) framework [159, 57]. The overall disease burden associated with COVID-19 infection includes both fatal and non-fatal cases in Eq.(C.1), which we break down in the following paragraphs.

$$\begin{aligned}\text{Disease Burden} =&(\text{treatment cost} + \text{cost per non-fatal case}) \times \text{symptomatic rate} \\ &\times \text{clinical confirmation rate} + \text{cost per fatal case} \times \text{mortality rate}.\end{aligned} \tag{C.1}$$

Net Monetary Benefit Following the classical approach in healthcare economics, we combine different outcome measures into a single NMB objective based on willingness-to-pay (WTP) and DALYs. DALYs reflect the years of life lost (YLL) due to premature mortality associated with a given health condition, and the years lost due to disability (YLD) resulting from the condition. DALYs can be converted to a cost scale by multiplying an appropriate WTP. WTP is typically estimated to be 1 - 3 times of GDP per capita [158] and the GDP per-capita in the U.S. in 2019 is $65118 [165]).

Fatal cases The YLL due to a single COVID-19 death is calculated by taking the difference between life expectancy and the average age of each age group in Minnesota.

Given Minnesota age composition [100], we calculate the mean age to be 9.58, 39.35, and 71.01 years old for the Youth, Adult, and Elderly group, respectively; and the population mean age as 39.22 years old. Then, based on a population average life expectancy of 78.5 years [161], we calculate YLL as 68.92, 39.15, and 7.49 for the Youth, Adult, and Elderly group; and the population average as 39.27 YLL. The cost per fatal case of COVID-19 is then calculated as the corresponding WTP $\times$ YLL.

Non-fatal cases The duration of disability and lost workday is assumed to be 60 days [101]. Following the same estimation procedure as in [171], we calculate the temporary productivity loss as the multiplication of WTP per day, average number of lost workdays, and the age-specific productivity weights (0.15 for Youth, 0.8 for Adult, 0.1 for Elderly and 0.469 for the population average).

$$\text{Productivity loss} = \text{WTP/day} \times \text{workdays lost} \times \text{productivity weight.}$$

To calculate YLD due to COVID-19 infection, we follow the standard approach in the COVID-19 medical literature [e.g., 110]. A disability weight of 0.133 is adopted to account for lower respiratory tract infection. The cost per non-fatal case of COVID-19 is calculated as follows.

$$\text{Cost per non-fatal case} = \text{WTP} \times \text{YLD} + \text{temporary productivity loss.}$$

This monetary disease burden only applies to clinically confirmed cases (moderate to severe), as undetected mild cases are assumed to result in a negligible number of YLD. The cost of supportive treatment of a clinically confirmed (moderate to severe) and symptomatic case of COVID-19 is estimated to be \$3045 - \$14366 [14].

Combining preceding calculation, we calculate the overall disease burden associated with COVID-19 infection using Eq.(C.1). We estimate the overall health cost as $b_3 =$ 72381.16 for the homogeneous model, and $b_{3,1} =$ \$1740.189 , $b_{3,2} =$ \$46640.377 , $b_{3,3} =$ \$39638.333 for the Youth, Adult, and Elderly group, respectively.

C.2.3 Socioeconomic Loss

In this section, we estimate the socioeconomic cost of implementing social distancing and lockdown and associated personal utility parameters.

Cost of policy implementation We estimate the socioeconomic loss due to social distancing and lockdown. In the U.S., different control measures have been implemented simultaneously, which makes it difficult to decompose the cost of lockdown and social distancing. China, on the other hand, implemented city-wise lockdown in the epicenter Wuhan, and strict social distancing in other regions during COVID-19 outbreak. Therefore, we assume a similar GDP decline percentage between the U.S. and China due to control measures, and hence estimate their costs in the U.S..

China implemented city-wide lockdown in Wuhan, and mandated social distancing in other regions from Jan 23, 2020 till the end of March or April. GDP loss in China was 12.8% in 2020 Q1 compared to 2019 Q1 [171]. We assume this loss is mainly due to the mandated strict social distancing. Meanwhile, Wuhan saw a 40.5% GDP decline in 2020 Q1 [171], which we assume is a result of lockdown. The duration of lockdown in Wuhan and social distancing in other regions in 2020 Q1 was 69 days [171]. Therefore, we estimate a $40.5\%/69 = 0.5869\%$ daily GDP loss for lockdown institution, and $12.8\%/69 = 0.1855\%$ daily GDP loss for mandated strict social distancing. We assume that this daily 0.1855% GDP loss is caused by a strict social distancing with a maximum possible contact reduction $\kappa_{\max} = 0.5$ [168].

We assume that implementing lockdown and social distancing would cause the same GDP decline percentage in the U.S. as in China. We observe that the GDP loss in the U.S. was 31.4% [147] in Q2 2020, where different states implemented social distancing and lockdown periodically. Thus, our estimation of GDP loss percentage is aligned with the underlying value in U.S.. Given Minnesota 2019 Q1 GDP of 378047.3 million [147], we estimate the social distancing cost as $q_{\max} = 123.25$ per person per day for a strict social distancing with $\kappa_{\max} = 0.5$. Similarly, we estimate the daily cost of lockdown

\$2218.7 Million and the lockdown cost as $d_1 = \$389.929$ per person per day.

Utility parameters We estimate parameters b_1 and b_2 in the utility functions. We use the annual average income in Minnesota in 2019 [42] to estimate the total economic gain of going out and having normal social activities and estimate $b_1 + b_2 = \$187.43$ per day per person. We estimate that b_2 contributes to 52.83% of this daily economic gain, since lockdown results in a daily decline of 0.5869% in the quarterized GDP and thus a total decline of $0.5869\% \times 90 = 52.83\%$ in a quarter. Therefore, we estimate $b_2 = 52.83\% \times 187.43 = \$99.02$ and $b_1 = 187.43 - 99.02 = \$88.41$.

C.3 Theorems and Proofs

C.3.1 Proof of Proposition 4.4.1

Proof. Proof: We first prove the "only if" part. We omit t in α^*_{aw}, and I for simplicity. We write $\widehat{b}_2 \equiv b_2 - b_3\beta I$. In the quadratic function $u^{\text{aw}}(\alpha) = \alpha(b_1 + \widehat{b}_2\alpha)$, if $\widehat{b}_2 \geq 0$ or equivalently $I \leq \dfrac{b_2}{b_3\beta}$, $u^{\text{aw}}(\alpha)$ is increasing in $\alpha \in [0,1]$ and thus $\alpha^*_{\text{aw}} = 1 > \alpha^*_B$. Otherwise if $\widehat{b}_2 < 0$ or equivalently $I > \dfrac{b_2}{b_3\beta}$, we have

$$\frac{du^{\text{aw}}(\alpha)}{d\alpha} = b_1 + 2\widehat{b}_2\alpha.$$

We denote $\alpha_U \equiv -\dfrac{b_1}{2\widehat{b}_2}$ where $\dfrac{du^{\text{aw}}(\alpha)}{d\alpha} = 0$. If $\widehat{b}_2 < 0$ and $\alpha_U \geq 1$, or equivalently, $\dfrac{b_2}{b_3\beta} < I \leq \dfrac{b_2 + 0.5b_1}{b_3\beta}$, $u^{\text{aw}}(\alpha)$ is increasing in $\alpha \in [0,1]$ and thus $\alpha^*_{\text{aw}} = 1 > \alpha^*_B$. If $\widehat{b}_2 < 0$ and $\alpha_U < 1$, or equivalently, $I > \dfrac{b_2 + 0.5b_1}{b_3\beta}$, $u^{\text{aw}}(\alpha)$ attains its maximum at $\alpha^*_{\text{aw}} = \alpha_U$.

We define function $h(\alpha)$ as

$$h(\alpha) \equiv \log\left(\frac{\alpha}{1-\alpha}\right) - b_1 - \widehat{b}_2\alpha.$$

One may easily verify that Eq.(4.5) satisfies $h(\alpha_B^*) = 0$. If $\widehat{b}_2 < 0$, we have $h'(\alpha) = \frac{1}{\alpha(1-\alpha)} - \widehat{b}_2 > 0$ for $\alpha \in (0,1)$. Therefore, if $\widehat{b}_2 < 0$ and $\alpha_U < 1$, $\alpha_{\text{aw}}^* = \alpha_U < \alpha_B^*$ if and only if $h(\alpha_U) < 0$. We note that

$$\begin{aligned} & h(\alpha_U) = \log\left(\frac{\alpha_U}{1-\alpha_U}\right) - b_1 - \widehat{b}_2\alpha_U = \log\left(\frac{-b_1}{b_1 + 2\widehat{b}_2}\right) - \frac{b_1}{2} < 0 \\ \iff & 0.5b_1 + \frac{0.5b_1}{\exp(0.5b_1)} < -\widehat{b}_2 \\ \iff & I > \frac{1}{b_3\beta}\left[0.5b_1 + \frac{0.5b_1}{\exp(0.5b_1)} + b_2\right]. \end{aligned}$$

Combining all conditions, if $\alpha_{\text{aw}}^* < \alpha_B^*$, then we have

$$I > \frac{1}{b_3\beta}\left[0.5b_1 + \frac{0.5b_1}{\exp(0.5b_1)} + b_2\right].$$

We omit the "if" part of the proof, which directly follows from the previous proof. □

□

C.3.2 Proof of Theorem 4.4.1

Proof. Proof: To prove Theorem 4.4.1, we only need to show that for any $t = 1, \cdots, T-1$, given $I(t)$ and $A(t)$, there exists a unique equilibrium activity level $\alpha_A^*(t)$. If it holds, there are only finite possible values of $\boldsymbol{A}$. We can obtain that there must exist one optimal solution $\boldsymbol{A}^*$ of the lockdown model. Thus, given any $\boldsymbol{A}$ and initial states $S(0)$, $I(0)$ and $R(0)$, we can recursively compute $\alpha(t)$ based on (4.8), and then compute $S(t+1)$, $I(t+1)$ and $R(t+1)$ from the dynamics (4.1). By doing this we could obtain $\alpha_A^*(t)$ for all $t = \{1, \cdots, T\}$.

Consider any $t \in \{1, \cdots, T\}$. We write $\alpha(t)$, $I(t)$ and $A(t)$ as α, I and A for simplicity. Define $\widehat{b}_2 \equiv b_2(1-A) - b_3\beta I$. Then Eq.(4.8) can be rewritten as

$$h(\alpha) \equiv \log\left(\frac{\alpha}{1-\alpha}\right) - b_1 - \widehat{b}_2\alpha = 0. \tag{C.2}$$

Obviously, h is continuous on $(0,1)$. We also have

$$\lim_{t\downarrow 0} h(t) = -\infty - b_1 = -\infty \quad \text{and} \quad \lim_{t\uparrow 1} h(t) = +\infty - b_1 - \widehat{b}_2 = +\infty.$$

It then follows from the intermediate value theorem that there must exist $\alpha_A^* \in [\varepsilon, 1-\varepsilon]$ for some sufficiently small positive scalar ε such that $h(\alpha_A^*) = 0$. Next, we prove the uniqueness of the solution for Eq.(4.8). We consider two cases.

Case I: $\widehat{b}_2 < 4$. We then have $h'(\alpha) = \dfrac{1}{\alpha(1-\alpha)} - \widehat{b}_2 > 0$, i.e., $h(\alpha)$ is strictly increasing on $(0,1)$. Hence, there exists at most one α_A^* such that $h(\alpha_A^*) = 0$.

Case II: $\widehat{b}_2 \geq 4$. The critical point of h satisfying $h'(\alpha) = 0$ is $\overline{\alpha}_+/\overline{\alpha}_- = \frac{1}{2}\left(\pm\sqrt{1-4\widehat{b}_2^{-1}}+1\right) \in (0,1)$. We may observe the following two facts: 1) h is strictly decreasing on $[\overline{\alpha}_-, \overline{\alpha}_+]$ and strictly increasing on $(0, \overline{\alpha}_-] \cup [\overline{\alpha}_+, 1)$; 2) $h(\bar{\alpha}_-) < 0$, and $\lim_{t\downarrow 0} h(t) = -\infty$. Putting them together one may obtain that $h(\alpha) < 0$ for all $\alpha \in (0, \overline{\alpha}_+]$, which further implies that there exists at most one α_A^* such that $h(\alpha_A^*) = 0$.

Since t is arbitrarily chosen from $\{1, \cdots, T\}$, the proof of this theorem is thus completed. □

□

C.3.3 Proof of Proposition 4.4.2

Proof. Proof:

Following the notation in the proof of Theorem 4.4.1, we consider any $t \in \{1, \cdots, T\}$ and write $\widehat{b}_2 \equiv b_2(1-A) - b_3\beta I$ without explicitly spelling out t. To establish the stated results in the proposition, it suffices to show that α_A^* is increasing in both $\widehat{b}_2$ and b_1. It is known from the proof of Theorem 4.4.1 that $h'(\alpha_A^*) = \dfrac{1}{\alpha_A^*(1-\alpha_A^*)} - \widehat{b}_2 > 0$. Therefore, we know from the implicit function theorem that α_A^* satisfying Eq.(4.8) can be taken

as a single-valued function of b_1 and $\widehat{b}_2$ such that

$$(\alpha_A^*)'(b_1, \widehat{b}_2) = \left[\frac{1}{\alpha_A^*(1-\alpha_A^*)} - \widehat{b}_2 \right]^{-1} \begin{pmatrix} 1 \\ \alpha_A^*(b_1, \widehat{b}_2) \end{pmatrix} > 0.$$

The above inequality shows that α_A^* is an increasing function in both b_1 and $\widehat{b}_2$. The stated results of this proposition thus hold. □

□

C.3.4 Lemma C.3.1

Lemma C.3.1. *Given any nonnegative initial disease state $(S(1), I(1), R(1))$ satisfying $S(1) + R(1) + I(1) = 1$ and a societal activity level time sequence $\boldsymbol{\alpha}$, the following two properties hold:*

(a) The disease state $(S(t), I(t), R(t))$ at any time $t \in \{1, 2, .., T\}$ are non-negative and bounded.

(b) The trajectory of disease states is uniquely determined by $\boldsymbol{\alpha}$.

Proof. Proof: It follows from the disease dynamics in (4.1) that for any $t \in \{1, \cdots, T-1\}$,

$$S(t+1) + R(t+1) + I(t+1) = S(t) + R(t) + I(t) = \cdots = S(1) + R(1) + I(1) = 1.$$

Therefore, to prove part (a), it suffices to show that $(S(t), I(t), R(t))$ are nonnegative for all t. Notice that Eq.(4.1) can be reformulated as

$$\begin{cases} S(t+1) = [1 - \beta\alpha(t)I(t)]S(t) \\ I(t+1) = (1-r)I(t) + \beta\alpha(t)S(t)I(t) \\ R(t+1) = R(t) + rI(t). \end{cases}$$

Recall that in the above equations, $\alpha(t) \in (0, 1)$, $\beta < 1$ and $r < 1$. By induction, one could easily obtain the nonnegativity of all $(S(t), I(t), R(t))$. Part (b) on the uniqueness

of $\{S(t), I(t), R(t)\}$ given $\boldsymbol{\alpha}$ can be seen easily from the above disease dynamics. □ □

C.3.5 Proof of Proposition 4.4.3

To prove this proposition, we first show the following lemma by treating lockdown decision A as a continuous variable $A \in [0, 1]$.

Lemma C.3.2. *For $0 \leq I_1 < I_2 \leq 1$, the following two properties hold:*
(a) if $I_1 < I_2 \leq I_L \leq 1$ and $b_3\beta I_L + \dfrac{2 - 3\alpha^*_{A=1}(I_L)}{\alpha^*_{A=1}(I_L)(1 - \alpha^*_{A=1}(I_L))^2} \leq 0$, then $\dfrac{\partial \alpha^*_A(I_2)}{\partial A} < \dfrac{\partial \alpha^*_A(I_1)}{\partial A} < 0$ at any $A \in [0, 1]$;
(b) if $0 \leq I_H \leq I_1 < I_2$ and $b_3\beta I_H - b_2 + \dfrac{2 - 3\alpha^*_{A=0}(I_H)}{\alpha^*_{A=0}(I_H)(1 - \alpha^*_{A=0}(I_H))^2} \geq 0$, then $\dfrac{\partial \alpha^*_A(I_1)}{\partial A} < \dfrac{\partial \alpha^*_A(I_2)}{\partial A} < 0$ at any $A \in [0, 1]$.

Proof. Proof of Lemma C.3.2 Based on Eq.(4.8), the equilibrium activity levels $\alpha^*_A(I) \in (0, 1)$ at given lockdown decisions A are solutions to the following equation:

$$b_1 + b_2(1 - A)\alpha^*_A(I) = \log(\alpha^*_A(I)) - \log(1 - \alpha^*_A(I)) + b_3\beta I\alpha^*_A(I).$$

From Proposition 4.4.2, we have $\alpha^*_{A=0}(I) > \alpha^*_{A=1}(I)$ and $\dfrac{\partial \alpha^*_A(I)}{\partial A} < 0$. It follows from the implicit function theorem that

$$\frac{\partial \alpha^*_A(I)}{\partial A} = -\frac{b_2\alpha^*_A(I)}{b_3\beta I + b_2 A - b_2 + (\alpha^*_A(I))^{-1} + (1 - \alpha^*_A(I))^{-1}} < 0.$$

Denoting $g(\alpha) \equiv -\dfrac{b_2\alpha}{b_3\beta I + b_2(A - 1) + \alpha^{-1} + (1 - \alpha)^{-1}}$, we may derive that

$$g'(\alpha) = -b_2\left[\frac{b_3\beta I + b_2(A - 1) + (2 - 3\alpha)\alpha^{-1}(1 - \alpha)^{-2}}{(b_3\beta I + b_2(A - 1) + \alpha^{-1} + (1 - \alpha)^{-1})^2}\right].$$

We have $\alpha^*_A(I)$ is decreasing in I from Proposition 4.4.2 and the function $\dfrac{2 - 3x}{x(1 - x)^2}$ is decreasing for $x \in (0, 1)$.

For statement (a), if $b_3\beta I_L + \dfrac{2-3\alpha^*_{A=1}(I_L)}{\alpha^*_{A=1}(I_L)(1-\alpha^*_{A=1}(I_L))^2} \le 0$, we have for any $A \in [0,1]$ and $I \in [I_1, I_2]$,

$$\begin{aligned} b_3\beta I + b_2(A-1) + \frac{2-3\alpha^*_A(I)}{\alpha^*_A(I)(1-\alpha^*_A(I))^2} &\le b_3\beta I_2 + b_2(A-1) + \frac{2-3\alpha^*_A(I_2)}{\alpha^*_A(I_2)(1-\alpha^*_A(I_2))^2} \\ &\le b_3\beta I_L + \frac{2-3\alpha^*_{A=1}(I_L)}{\alpha^*_{A=1}(I_L)(1-\alpha^*_{A=1}(I_L))^2} \le 0. \end{aligned}$$

Therefore, $g'(\alpha) \ge 0$ for $\alpha \in [\alpha^*_A(I_2), \alpha^*_A(I_1)]$ at any $A \in [0,1]$, where the equality could only hold at $A = 1$ and $I_2 = I_L$. Thus, $g(\alpha^*_A(I_2)) = \dfrac{\partial \alpha^*_A(I_2)}{\partial A} < \dfrac{\partial \alpha^*_A(I_1)}{\partial A} = g(\alpha^*_A(I_1))$ at any $A \in [0,1]$.

Similarly for statement (b), if $b_3\beta I_H - b_2 + \dfrac{2-3\alpha^*_{A=0}(I_H)}{\alpha^*_{A=0}(I_H)(1-\alpha^*_{A=0}(I_H))^2} \ge 0$, we have for any $A \in [0,1]$ and $I \in [I_1, I_2]$,

$$\begin{aligned} b_3\beta I + b_2(A-1) + \frac{2-3\alpha^*_A(I)}{\alpha^*_A(I)(1-\alpha^*_A(I))^2} &\ge b_3\beta I_1 + b_2(A-1) + \frac{2-3\alpha^*_A(I_1)}{\alpha^*_A(I_1)(1-\alpha^*_A(I_1))^2} \\ &\ge b_3\beta I_H - b_2 + \frac{2-3\alpha^*_{A=0}(I_H)}{\alpha^*_{A=0}(I_1)(1-\alpha^*_{A=0}(I_H))^2} \ge 0. \end{aligned}$$

Therefore, $g'(\alpha) \le 0$ for $\alpha \in [\alpha^*_A(I_2), \alpha^*_A(I_1)]$ at any $A \in [0,1]$, where the equality could only hold at $A = 0$ and $I_1 = I_H$. Thus, $\dfrac{\partial \alpha^*_A(I_1)}{\partial A} < \dfrac{\partial \alpha^*_A(I_2)}{\partial A}$ at any $A \in [0,1]$. □

□

Next, we show that $\overline{I} > \underline{I}$. One can verify that $\underline{I}$ and $\overline{I}$ are the only real roots to the following equations, respectively:

$$\begin{aligned} b_3\beta + \frac{2-3\alpha^*_{A=1}(\underline{I})}{\alpha^*_{A=1}(\underline{I})(1-\alpha^*_{A=1}(\underline{I}))^2} &= 0, \\ -b_2 + \frac{2-3\alpha^*_{A=0}(\overline{I})}{\alpha^*_{A=0}(\overline{I})(1-\alpha^*_{A=0}(\overline{I}))^2} &= 0. \end{aligned}$$

We note that γ and δ in the expression of $\underline{I}$ and $\overline{I}$ are the only real root to equation

$b_3\beta + \dfrac{2-3\gamma}{\gamma(1-\gamma)^2} = 0$ and $-b_2 + \dfrac{2-3\delta}{\delta(1-\delta)^2} = 0$, and are defined as follows:

$$\gamma = \frac{1}{3}\left(\frac{\sqrt[3]{3\sqrt{3}\sqrt{-b_3^5\beta^5 - 9b_3^4\beta^4 - 27b_3^3\beta^3} - \beta^3 b_3^3}}{\beta b_3} + \frac{\beta b_3 + 9}{\sqrt[3]{3\sqrt{3}\sqrt{-b_3^5\beta^5 - 9b_3^4\beta^4 - 27b_3^3\beta^3} - \beta^3 b_3^3}} + 2 \right)$$

$$\delta = \frac{1}{3}\left(\frac{\sqrt[3]{3\sqrt{3}\sqrt{b_2^5 - 9b_2^4 + 27b_2^3} - b_2^3}}{b_2} + \frac{9 - b_2}{\sqrt[3]{\sqrt[3]{3\sqrt{3}\sqrt{b_2^5 - 9b_2^4 + 27b_2^3} - b_2^3}}} + 2 \right).$$

Since $\dfrac{2-3x}{x(1-x)^2}$ is decreasing for $x \in (0,1)$, we have $\alpha^*_{A=0}(\overline{I}) < \alpha^*_{A=1}(\underline{I})$. Since $\alpha^*_{A=1}(\underline{I}) < \alpha^*_{A=0}(\underline{I})$ and thus $\alpha^*_{A=0}(\overline{I}) < \alpha^*_{A=0}(\underline{I})$, we have $\overline{I} > \underline{I}$ by Proposition 4.4.2. Now we proceed to prove Proposition 4.4.3.

Proof. Proof of Proposition 4.4.3 We only prove the first statement. The proof of the second statement can be derived in a similar fashion. As we define that $\underline{I}$ satisfies that $b_3\beta + \dfrac{2-3\alpha^*_{A=1}(\underline{I})}{\alpha^*_{A=1}(\underline{I})(1-\alpha^*_{A=1}(\underline{I}))^2} = 0$, therefore $b_3\beta\underline{I} + \dfrac{2-3\alpha^*_{A=1}(\underline{I})}{\alpha^*_{A=1}(\underline{I})(1-\alpha^*_{A=1}(\underline{I}))^2} \leq 0$. From Lemma C.3.2, we know that $\dfrac{\partial \alpha^*_A(I_2)}{\partial A} < \dfrac{\partial \alpha_A(I_1)}{\partial A} < 0$ at any $A \in [0,1]$ for $I_1 < I_2 \leq \underline{I}$. Therefore, we have

$$\frac{\partial \alpha^*_A(I_2)}{\partial A} < \frac{\partial \alpha^*_A(I_1)}{\partial A} < 0,$$

which yields that

$$\int_{A=0}^{A=1} \frac{\partial \alpha^*_A(I_2)}{\partial A} dA < \int_{A=0}^{A=1} \frac{\partial \alpha^*_A(I_1)}{\partial A} dA.$$

Hence,

$$\alpha^*_{A=1}(I_2) - \alpha^*_{A=0}(I_2) < \alpha^*_{A=1}(I_1) - \alpha^*_{A=0}(I_1) < 0.$$

Rearranging the terms in the above inequality, we can obtain the first statement of this proposition. The second statement can be proved similarly and we omit the details here. □

□

C.3.6 Proof of Lemma 4.4.1

To proceed, we write $u_i(\text{go out}, \alpha_{-i}(t))$ as the expected utility gain for the individual i that chooses to *go out* when all others hold the same activity level $\alpha_{-i}(t)$, i.e.,

$$u_i(\text{go out}, \alpha_{-i}(t)) = b_1 + b_2\alpha_{-i}(t) - b_3\alpha_{-i}(t)\beta I(t). \tag{C.3}$$

By definition, the feasible region of $\alpha_i(t)$ is as follows:

$$\alpha_i(t) \in [0, 1 - \kappa(t)]. \tag{C.4}$$

Denote

$$F_i(\alpha_{-i}(t)) \equiv \frac{\exp(b_1 + \widehat{b}_2\alpha_{-i}(t))}{1 + \exp(b_1 + \widehat{b}_2\alpha_{-i}(t))}, \tag{C.5}$$

where the right side comes from the logit model Eq.(4.5) except that the utility term is replaced by $u_i(\text{go out}, \alpha_{-i}(t))$. We note that $F_i(\alpha_{-i}(t))$ could be outside the feasible region of $\alpha_i(t)$ given in Eq.(C.4). It can be easily verified that the function $F_i(\cdot)$ in Eq. (C.5) is increasing in $\widehat{b}_2$. Moreover, $F_i(\cdot)$ is increasing in α_{-i} if $\widehat{b}_2 \geq 0$, and decreasing in α_{-i} if $\widehat{b}_2 < 0$.

Proof. Proof of Lemma 4.4.1

We have $F_i(\alpha_B^*(t)) = \alpha_B^*(t)$ by definition of $\alpha_B^*(t)$, and $\alpha_B^*(t) > 1 - \kappa(t)$ from the lemma condition. To proceed, we consider a variation of Eq.(C.2) as follow:

$$h(\alpha_{-i}(t)) = \log\left(\frac{\alpha_{-i}(t)}{1 - \alpha_{-i}(t)}\right) - b_1 - \widehat{b}_2\alpha_{-i}(t). \tag{C.6}$$

From the proof of Theorem 4.4.1, we have $h(\alpha_{-i}(t)) < 0$ for any $\alpha_{-i}(t) \in [0, \alpha_B^*(t))$.

With some simple algebraic work, we have:

$$\alpha_{-i}(t) < F_i(\alpha_{-i}(t)), \quad \text{for any } \ \alpha_{-i}(t) \in [0, \alpha_B^*(t)).$$

Thus, we have individual i's best response to $\alpha_{-i}(t) = 1-\kappa(t)$ is larger than $1-\kappa(t)$ (i.e., $F_i(1-\kappa(t)) > 1-\kappa(t)$). That is, $F_i(1-\kappa(t))$ is outside the feasible region of $\alpha_i(t)$, defined in Eq.(C.4). Thus, under the social distancing constraint such that $\alpha_B^*(t) > 1-\kappa(t)$, the best response to $\alpha_{-i}(t) = 1-\kappa(t)$ is $1-\kappa(t)$. The proof is thus completed. □

□

C.3.7 Proof of Theorem 4.4.2

Proof. Proof: We consider two cases.

Case I: $\alpha_B^*(t) \leq 1-\kappa(t)$. Since $\alpha_B^*(t) \in [0, 1-\kappa(t)]$, we know from Theorem 4.4.1 that $\alpha_B^*(t)$ is unique (by setting $A = 0$).

Case II: $\alpha_B^*(t) > 1-\kappa(t)$. From Lemma 4.4.1, we know $\alpha_\kappa(t) = 1-\kappa(t)$ is a symmetric equilibrium solution. Suppose there exists another symmetric equilibrium solution $\alpha_\kappa^{'}(t)$ such that $0 < \alpha_\kappa^{'}(t) < 1-\kappa(t)$. Set $\alpha_{-i}(t) = \alpha_\kappa^{'}(t)$. Following the proof of Lemma 4.4.1, we have $F_i(\alpha_\kappa^{'}(t)) > \alpha_\kappa^{'}(t)$. Thus, the best response of individual i is $\min(F(\alpha_\kappa^{'}(t)), 1-\kappa(t)) > \alpha_\kappa^{'}(t)$. This contradicts the definition of a symmetric equilibrium. Thus, $\alpha_\kappa(t) = 1-\kappa(t)$ is the unique symmetric equilibrium (under Case II condition). The proof is thus completed. □

□

C.3.8 Proof of Proposition 4.4.4

Proof. Proof of Proposition 4.4.4 Given a disease prevalence I, a social distancing policy $\kappa \leq \kappa_{\max}$ can affect the disease dynamics on a day if $\kappa > 1-\alpha_B^*(I)$ and cannot if $\kappa \leq 1-\alpha_B^*(I)$. Moreover, if $\kappa \leq 1-\alpha_B^*(I)$, social distancing policy does not change the epidemiological outcome but may incur social distancing cost $q(\kappa)$. Given $q(\kappa)$ is

an increasing function in κ, it is better to have $\kappa = 0$ instead of $0 < \kappa \leq 1 - \alpha_B^*(I)$. Therefore, the optimal social distancing policy is either 1) $\kappa^* > 1-\alpha_B^*(I)$ and $\kappa^* \leq \kappa_{\max}$, or 2) $\kappa^* = 0$. □ □

C.3.9 Proofs of Proposition 4.4.5 and Corollary 4.4.1

Proof. Proof of Proposition 4.4.5: We first prove the first statement. From Eq.(4.12), we have $\alpha^*(\kappa, I) = \min(1 - \kappa, \alpha_B^*(I))$. Based on Proposition 4.4.2 (by setting $A = 0$), we can derive that $\alpha_B^*(I)$ is decreasing in I and thus $\alpha_B^*(I_1) > \alpha_B^*(I_2)$. Therefore,

$$\alpha_B^*(I_1)-\alpha^*(\kappa, I_1) = \max(\alpha_B^*(I_1)-1+\kappa, 0) \geq \max(\alpha_B^*(I_2)-1+\kappa, 0) = \alpha_B^*(I_2)-\alpha^*(\kappa, I_2).$$

We now prove the second statement. Since $\alpha_B^*(I_1) > \alpha_B^*(I_2)$ and $\alpha_B^*(I_1) - \alpha^*(\kappa_1, I_1) = \alpha_B^*(I_2) - \alpha^*(\kappa_2, I_2) \geq 0$, we have $\alpha^*(\kappa_1, I_1) > \alpha^*(\kappa_2, I_2)$. If $\alpha_B^*(I_1) - \alpha^*(\kappa_1, I_1) = \alpha_B^*(I_2) - \alpha^*(\kappa_2, I_2) > 0$, from Theorem 4.4.2 and Proposition 4.4.4, we have $\kappa_2 - \kappa_1 = [1 - \alpha^*(\kappa_2, I_2)] - [1 - \alpha^*(\kappa_1, I_1)] > 0$. If $\alpha_B^*(I_1) - \alpha^*(\kappa_1, I_1) = \alpha_B^*(I_2) - \alpha^*(\kappa_2, I_2) = 0$, from Theorem 4.4.2, we have $\kappa_2 = \kappa_1$. Given that $\kappa_2 \geq \kappa_1$ and $q(\kappa)$ is increasing in κ, the result is thus proved. □ □

Proof. Proof of Corollary 4.4.1 By plugging $\overline{I}_\kappa$ into Eq.(4.3) and Eq.(4.5), one can verify that $\alpha_B^*(\overline{I}_\kappa) = 1 - \kappa_{\max}$. Thus, the result follows from Proposition 4.4.4. □ □

References

[1] G Abongomera, A Cook, V Musiime, C Chabala, M Lamorde, J Abach, M Thomason, V Mulenga, A Kekitiinwa, R Colebunders, et al. Improved adherence to antiretroviral therapy observed among hiv-infected children whose caregivers had positive beliefs in medicine in sub-saharan africa. *AIDS and Behavior*, 21(2):441–449, 2017.

[2] Anas Abou-Ismail. Compartmental models of the covid-19 pandemic for physicians and physician-scientists. *SN comprehensive clinical medicine*, pages 1–7, Jun 2020.

[3] Daron Acemoglu, Victor Chernozhukov, Ivan Werning, and Michael D Whinston. Optimal targeted lockdowns in a multi-group sir model. Working Paper 27102, National Bureau of Economic Research, May 2020.

[4] Nishat Hussain Ahmed and Shobha Broor. Comparison of NS1 antigen detection ELISA, real time RT-PCR and virus isolation for rapid diagnosis of dengue infection in acute phase. *Journal of vector borne diseases*, 51(3):194, 2014.

[5] Diane Alexander and Ezra Karger. Do Stay-at-Home Orders Cause People to Stay at Home? Effects of Stay-at-Home Orders on Consumer Behavior. Available at SSRN: https://ssrn.com/abstract=3583625, 2020.

[6] Laura Alfaro, Ester Faia, Nora Lamersdorf, and Farzad Saidi. Social interactions

in pandemics: Fear, altruism, and reciprocity. Working Paper 27134, National Bureau of Economic Research, May 2020.

[7] Linda J.S. Allen. Some discrete-time SI, SIR, and SIS epidemic models. *Mathematical Biosciences*, 124(1):83 – 105, 1994.

[8] Fernando E Alvarez, David Argente, and Francesco Lippi. A simple planning problem for covid-19 lockdown. Working Paper 26981, National Bureau of Economic Research, April 2020.

[9] Katie B Anderson, Supamit Chunsuttiwat, Ananda Nisalak, Mammen P Mammen, Daniel H Libraty, Alan L Rothman, Sharone Green, David W Vaughn, Francis A Ennis, and Timothy P Endy. Burden of symptomatic dengue infection in children at primary school in Thailand: a prospective study. *The Lancet*, 369(9571):1452–1459, 2007.

[10] Roy M Anderson, Hans Heesterbeek, Don Klinkenberg, and T Déirdre Hollingsworth. How will country-based mitigation measures influence the course of the COVID-19 epidemic? *The Lancet*, 395(10228):931–934, 2020.

[11] Turgay Ayer, Oguzhan Alagoz, and Natasha K Stout. Or forum—a pomdp approach to personalize mammography screening decisions. *Operations Research*, 60(5):1019–1034, 2012.

[12] Turgay Ayer, Oguzhan Alagoz, Natasha K Stout, and Elizabeth S Burnside. Heterogeneity in women's adherence and its role in optimal breast cancer screening policies. *Management Science*, 62(5):1339–1362, 2015.

[13] Turgay Ayer, Oguzhan Alagoz, Natasha K Stout, and Elizabeth S Burnside. Heterogeneity in women's adherence and its role in optimal breast cancer screening policies. *Management Science*, 62(5):1339–1362, 2016.

[14] Sarah M Bartsch, Marie C Ferguson, James A McKinnell, Kelly J O'Shea, Patrick T Wedlock, Sheryl S Siegmund, and Bruce Y Lee. The Potential Health Care Costs And Resource Use Associated With COVID-19 In The United States: A simulation estimate of the direct medical costs and health care resource use associated with COVID-19 infections in the United States. *Health Affairs*, pages 10–1377, 2020.

[15] Moshe Ben-Akiva and Steven R Lerman. *Discrete choice analysis: theory and application to travel demand*. Transportation Studies, 2018.

[16] Ajay R Bharti, Jarlath E Nally, Jessica N Ricaldi, Michael A Matthias, Monica M Diaz, Michael A Lovett, Paul N Levett, Robert H Gilman, Michael R Willig, and Eduardo Gotuzzo. Leptospirosis: a zoonotic disease of global importance. *The Lancet infectious diseases*, 3(12):757–771, 2003.

[17] David E Bloom, Michael Kuhn, and Klaus Prettner. Modern infectious diseases: Macroeconomic impacts and policy responses. Working Paper 27757, National Bureau of Economic Research, August 2020.

[18] BLS. U.S. Bureau Of Labor Statistics (BLS): Employment Situation Summary, April 2020. Last accessed Jan 29, 2021.

[19] Stephen Boyd and Lieven Vandenberghe. *Convex optimization*. Cambridge university press, 2004.

[20] Ronald Scott Braithwaite, Kimberly A Nucifora, Christopher Toohey, Jason Kessler, Lauren M Uhler, Sherry M Mentor, Daniel Keebler, and Timothy Hallett. How do different eligibility guidelines for antiretroviral therapy affect the cost–effectiveness of routine viral load testing in sub-saharan africa? *AIDS (London, England)*, 28(0 1):S73, 2014.

[21] Luiz Brotherhood, Philipp Kircher, Cezar Santos, and Michèle Tertilt. An economic model of the Covid-19 pandemic with young and old agents: Behavior, testing and policies. Working Papers w202014, Banco de Portugal, Economics and Research Department, 2020.

[22] Kate M. Bubar, Kyle Reinholt, Stephen M. Kissler, Marc Lipsitch, Sarah Cobey, Yonatan H. Grad, and Daniel B. Larremore. Model-informed covid-19 vaccine prioritization strategies by age and serostatus. *Science*, 2021.

[23] Luis R Carrasco, Linda K Lee, Vernon J Lee, Eng Eong Ooi, Donald S Shepard, Tun L Thein, Victor Gan, Alex R Cook, David Lye, and Lee Ching Ng. Economic impact of dengue illness and the cost-effectiveness of future vaccination programs in Singapore. *PLoS neglected tropical diseases*, 5(12):e1426, 2011.

[24] CDC. Centers for Disease Control and Prevention (CDC): Frequently Asked Questions, Dec 2020. Last accessed Dec 30, 2020.

[25] CDC. Centers for Disease Control and Prevention (CDC): EXPLORE HUMAN MOBILITY AND COVID-19 TRANSMISSION IN YOUR LOCAL AREA, Feb 2021. Last accessed Feb 21, 2021.

[26] CDC. Centers for Disease Control and Prevention (CDC): Guidance for Businesses and Employers Responding to Coronavirus Disease 2019, Jan 2021. Last accessed Jan 29, 2021.

[27] CDC. Centers for Disease Control and Prevention (CDC): New Variants of the Virus that Causes COVID-19, January 2021. Last accessed Feb 2, 2021.

[28] CDC. Centers for Disease Control and Prevention (CDC): When Vaccine is Limited, Who Should Get Vaccinated First?, January 2021. Last accessed Jan 29, 2021.

[29] Centers for Disease Control and Prevention. Antibiotic Resistance: A Global Threat, 2019.

[30] Pui Y Chan, Michael A Joseph, Don C Des Jarlais, and Uusk. Perceived effectiveness of antiretroviral therapy, self-rated health and treatment adherence among hiv-positive people who inject drugs in estonia. *International journal of STD & AIDS*, 29(1):13–22, 2018.

[31] Arthur Charpentier, Romuald Elie, Mathieu Lauriere, and Viet Chi Tran. Covid-19 pandemic control: balancing detection policy and lockdown intervention under icu sustainability*. *Math. Model. Nat. Phenom.*, 15:57, 2020.

[32] Naveed Chehrazi, Lauren E Cipriano, and Eva A Enns. Dynamics of drug resistance: Optimal control of an infectious disease. *Operations Research*, 67(3):619–650, 2019.

[33] Ningyuan Chen, Ming Hu, and Chaoyu Zhang. Capacitated SIR Model with an Application to COVID-19, 2020. Available at SSRN: http://dx.doi.org/10.2139/ssrn.3692751.

[34] Zhiyuan Chen and Guangwen Kong. Hospital Admission and Social Distancing Intervention in COVID-19 Pandemic: An Operations Management Perspective, 2020. Available at SSRN: https://ssrn.com/abstract=3704897.

[35] L Christou. The global burden of bacterial and viral zoonotic infections. *Clinical Microbiology and Infection*, 17(3):326–330, 2011.

[36] CNN. A group of young adults held a coronavirus party in Kentucky to defy orders to socially distance. Now one of them has coronavirus, March 2020. Last accessed Jan 29, 2021.

[37] CNN. US is still 'knee-deep' in the first wave of the coronavirus pandemic, Fauci says, July 2020. Last accessed Jan 29, 2021.

[38] Federico Costa, José E Hagan, Juan Calcagno, Michael Kane, Paul Torgerson, Martha S Martinez-Silveira, Claudia Stein, Bernadette Abela-Ridder, and Albert I Ko. Global morbidity and mortality of leptospirosis: a systematic review. *PLoS neglected tropical diseases*, 9(9):e0003898, 2015.

[39] Christopher J Cronin and William N Evans. Private Precaution and Public Restrictions: What Drives Social Distancing and Industry Foot Traffic in the COVID-19 Era? Working Paper 27531, National Bureau of Economic Research, July 2020.

[40] J Crump, Paul N Newton, Sarah J Baird, and Yoel Lubell. Febrile illness in adolescents and adults. 2017.

[41] John A Crump, Sandy Gove, and Christopher M Parry. Management of adolescents and adults with febrile illness in resource limited areas. *BMJ-British Medical Journal*, 343(8):d4847, 2011.

[42] Cubit Planning Inc. INCOME BY ZIP CODE, Jan 2021. Last accessed Jan 5, 2021.

[43] Shiliang Cui, Zhongbin Wang, and Luyi Yang. Design of COVID-19 Testing Queues, 2020. Available at SSRN:http://dx.doi.org/10.2139/ssrn.3722022.

[44] Krishna Dasaratha. Virus dynamics with behavioral responses, 2020.

[45] Michael Day. Covid-19: four fifths of cases are asymptomatic, china figures indicate, 2020.

[46] Joseph L Dieleman, Tara Templin, Nafis Sadat, Patrick Reidy, Abigail Chapin, Kyle Foreman, Annie Haakenstad, Tim Evans, Christopher JL Murray, and Christoph Kurowski. National spending on health by source for 184 countries between 2013 and 2040. *The Lancet*, 387(10037):2521–2535, 2016.

[47] Kimon Drakopoulos and Ramandeep S Randhawa. Why perfect tests may not be worth waiting for: Information as a commodity, 2020. Available at SSRN: http://dx.doi.org/10.2139/ssrn.3565245.

[48] Chenhao Du, William L Cooper, and Zizhuo Wang. Optimal pricing for a multinomial logit choice model with network effects. *Operations Research*, 64(2):441–455, 2016.

[49] Julien Dupouey, Benoît Faucher, Sophie Edouard, Hervé Richet, Angeli Kodjo, Michel Drancourt, and Bernard Davoust. Human leptospirosis: an emerging risk in Europe? *Comparative immunology, microbiology and infectious diseases*, 37(2):77–83, 2014.

[50] Kara N Durski, Michel Jancloes, Tej Chowdhary, and Eric Bertherat. A global, multi-disciplinary, multi-sectorial initiative to combat leptospirosis: Global Leptospirosis Environmental Action Network (GLEAN). *International journal of environmental research and public health*, 11(6):6000–6008, 2014.

[51] Martin S Eichenbaum, Sergio Rebelo, and Mathias Trabandt. The macroeconomics of epidemics. Working Paper 26882, National Bureau of Economic Research, March 2020.

[52] Romuald Elie, Emma Hubert, and Gabriel Turinici. Contact rate epidemic control of COVID-19: an equilibrium view. *Math. Model. Nat. Phenom.*, 15:35, 2020.

[53] John J Engemann, Yehuda Carmeli, Sara E Cosgrove, Vance G Fowler, Melissa Z Bronstein, Sharon L Trivette, Jane P Briggs, Daniel J Sexton, and Keith S Kaye. Adverse clinical and economic outcomes attributable to methicillin resistance among patients with Staphylococcus aureus surgical site infection. *Clinical infectious diseases*, 36(5):592–598, 2003.

[54] Faramroze G Engineer, Pınar Keskinocak, and Larry K Pickering. OR

practice—catch-up scheduling for childhood vaccination. *Operations Research*, 57(6):1307–1319, 2009.

[55] Maryam Farboodi, Gregor Jarosch, and Robert Shimer. Internal and external effects of social distancing in a pandemic. Working Paper 27059, National Bureau of Economic Research, April 2020.

[56] Elisabeth Fenwick, Bernie J O'Brien, and Andrew Briggs. Cost-effectiveness acceptability curves–facts, fallacies and frequently asked questions. *Health economics*, 13(5):405–415, 2004.

[57] Alan M Garber and Charles E Phelps. Economic foundations of cost-effectiveness analysis. *Journal of Health Economics*, 16(1):1–31, 1997.

[58] Pietro Garibaldi, Espen R. Moen, and Christopher Pissarides. Static and dynamic inefficiencies in an optimizing model of epidemics, 2020. Available at SSRN: https://ssrn.com/abstract=3730442.

[59] Claude Giry, Bénédicte Roquebert, Ghislaine Li-Pat-Yuen, Philippe Gasque, and Marie-Christine Jaffar-Bandjee. Simultaneous detection of chikungunya virus, dengue virus and human pathogenic Leptospira genomes using a multiplex TaqMan® assay. *BMC microbiology*, 17(1):105, 2017.

[60] Austan Goolsbee and Chad Syverson. Fear, lockdown, and diversion: Comparing drivers of pandemic economic decline 2020. *Journal of Public Economics*, 193:104311, 2021.

[61] Marga G A Goris, Mariska M G Leeflang, Martin Loden, Jiri F P Wagenaar, Paul R Klatser, Rudy A Hartskeerl, and Kimberly R Boer. Prospective evaluation of three rapid diagnostic tests for diagnosis of human leptospirosis. *PLoS neglected tropical diseases*, 7(7):e2290, 2013.

[62] Rajiv Grover and Marco Vriens. *The handbook of marketing research: uses, misuses, and future advances*. Sage, 2006.

[63] Maria G Guzman, Scott B Halstead, Harvey Artsob, Philippe Buchy, Jeremy Farrar, Duane J Gubler, Elizabeth Hunsperger, Axel Kroeger, Harold S Margolis, and Eric Martínez. Dengue: a continuing global threat. *Nature Reviews Microbiology*, 8(12supp):S7, 2010.

[64] Maria G Guzman and Eva Harris. Dengue. *The Lancet*, 385(9966):453–465, 2015.

[65] Jessica E Haberer, Angella Musiimenta, Esther C Atukunda, Nicholas Musinguzi, Monique A Wyatt, Norma C Ware, and David R Bangsberg. Short message service (sms) reminders and real-time adherence monitoring improve antiretroviral therapy adherence in rural uganda. *AIDS (London, England)*, 30(8):1295, 2016.

[66] Jessica E Haberer, Lora Sabin, K Rivet Amico, Catherine Orrell, Omar Galárraga, Alexander C Tsai, Rachel C Vreeman, Ira Wilson, Nadia A Sam-Agudu, Terrence F Blaschke, et al. Improving antiretroviral therapy adherence in resource-limited settings at scale: a discussion of interventions and recommendations. *Journal of the International AIDS Society*, 20(1):21371, 2017.

[67] Nils Haug, Lukas Geyrhofer, Alessandro Londei, Elma Dervic, Amelie Desvars-Larrive, Vittorio Loreto, Beate Pinior, Stefan Thurner, and Peter Klimek. Ranking the effectiveness of worldwide COVID-19 government interventions. *Nature Human Behaviour*, 4(12):1303–1312, Dec 2020.

[68] Siriwan Hoontrakul, Chuanpit Suttinont, Kitti Losuwanaluk, and Yupin Suputtamongkol. Performance of SD Bioline Tsutsugamushi assays for the diagnosis of scrub typhus in Thailand. *J Med Assoc Thai*, 95(2):S18–S22, 2012.

[69] Peter J Hotez, Maria Elena Bottazzi, Ulrich Strych, Li-Yen Chang, Yvonne A L Lim, Maureen M Goodenow, and Sazaly AbuBakar. Neglected tropical diseases

among the Association of Southeast Asian Nations (ASEAN): overview and update. *PLoS neglected tropical diseases*, 9(4):e0003575, 2015.

[70] Solomon Hsiang, Daniel Allen, Sébastien Annan-Phan, Kendon Bell, Ian Bolliger, Trinetta Chong, Hannah Druckenmiller, Luna Yue Huang, Andrew Hultgren, Emma Krasovich, and et al. The effect of large-scale anti-contagion policies on the covid-19 pandemic. *Nature*, June 2020.

[71] David W Hutton and Margaret L Brandeau. Too much of a good thing? when to stop catch-up vaccination. *Medical Decision Making*, 33(7):920–936, 2013.

[72] IMF. COVID's Impact in Real Time: Finding Balance Amid the Crisis, October 2020. Last accessed Jan 29, 2021.

[73] IMF. World Economic Outlook Report: A Long and Difficult Ascent, October 2020. Last accessed Jan 29, 2021.

[74] Evin Uzun Jacobson, Nilay TanÄ±k Argon, and Serhan Ziya. Priority assignment in emergency response. *Operations Research*, 60(4):813–832, 2012.

[75] Vivek Jain, Wei Chang, Dathan M Byonanebye, Asiphas Owaraganise, Ellon Twinomuhwezi, Gideon Amanyire, Douglas Black, Elliot Marseille, Moses R Kamya, Diane V Havlir, et al. Estimated costs for delivery of hiv antiretroviral therapy to individuals with cd4+ t-cell counts¿ 350 cells/ul in rural uganda. *PloS one*, 10(12):e0143433, 2015.

[76] Harold Jeffreys. *The theory of probability*. OUP Oxford, 1998.

[77] Greg Kaplan, Benjamin Moll, and Giovanni L Violante. The great lockdown and the big stimulus: Tracing the pandemic possibility frontier for the u.s. Working Paper 27794, National Bureau of Economic Research, September 2020.

[78] Alan R Katz, Vernon E Ansdell, Paul V Effler, Charles R Middleton, and David M Sasaki. Assessment of the clinical presentation and treatment of 353 cases of

laboratory-confirmed leptospirosis in Hawaii, 1974 to 1998. *Clinical Infectious Diseases*, 33(11):1834–1841, 2001.

[79] William Ogilvy Kermack and Anderson G McKendrick. A contribution to the mathematical theory of epidemics. *Proceedings of the Royal Society of London*, 115(772):700–721, 1927.

[80] Sung-Hee Kim, Sarah M Gerver, Sarah Fidler, and Helen Ward. Adherence to antiretroviral therapy in adolescents living with hiv: systematic review and meta-analysis. *AIDS (London, England)*, 28(13):1945, 2014.

[81] Vikram Krishnamurthy. Structural results for partially observed markov decision processes. *arXiv preprint arXiv:1512.03873*, 2015.

[82] Kamolwish Laoprasopwattana, Wanwipa Chaimongkol, Pornpimol Pruekprasert, and Alan Geater. Acute respiratory failure and active bleeding are the important fatality predictive factors for severe dengue viral infection. *PloS one*, 9(12):e114499, 2014.

[83] Bruce Y Lee, Diana L Connor, Sarah B Kitchen, Kristina M Bacon, Mirat Shah, Shawn T Brown, Rachel R Bailey, Yongjua Laosiritaworn, Donald S Burke, and Derek A T Cummings. Economic value of dengue vaccine in Thailand. *The American journal of tropical medicine and hygiene*, 84(5):764–772, 2011.

[84] Kathy Leung, Joseph T Wu, Di Liu, and Gabriel M Leung. First-wave COVID-19 transmissibility and severity in China outside Hubei after control measures, and second-wave scenario planning: a modelling impact assessment. *The Lancet*, 2020.

[85] Charles Loewner. On totally positive matrices. *Mathematische Zeitschrift*, 63(1):338–340, 1955.

[86] Elisa F Long, Eike Nohdurft, and Stefan Spinler. Spatial resource allocation

for emerging epidemics: A comparison of greedy, myopic, and dynamic policies. *Manufacturing & Service Operations Management*, 20(2):181–198, 2018.

[87] Yoel Lubell, Thomas Althaus, Stuart D Blacksell, Daniel H Paris, Mayfong Mayxay, Wirichada Pan-Ngum, Lisa J White, Nicholas P J Day, and Paul N Newton. Modelling the impact and cost-effectiveness of biomarker tests as compared with pathogen-specific diagnostics in the management of undifferentiated fever in remote tropical settings. *PloS one*, 11(3):e0152420, 2016.

[88] Dih-Ling Luh, Cheng-Chieh Liu, Yun-Ru Luo, and Szu-Chieh Chen. Economic cost and burden of dengue during epidemics and non-epidemic years in Taiwan. *Journal of infection and public health*, 2017.

[89] Viravarn Luvira, Udomsak Silachamroon, Watcharapong Piyaphanee, Saranath Lawpoolsri, Wirongrong Chierakul, Pornsawan Leaungwutiwong, Charin Thawornkuno, and Yupaporn Wattanagoon. Etiologies of acute undifferentiated febrile illness in bangkok, thailand. *The American Journal of Tropical Medicine and Hygiene*, 100(3):622–629, 2019.

[90] Savi Maharaj and Adam Kleczkowski. Controlling epidemic spread by social distancing: do it well or not at all. *BMC public health*, 12:679–679, Aug 2012.

[91] Brett Marroquin, Vera Vine, and Reed Morgan. Mental health during the covid-19 pandemic: Effects of stay-at-home policies, social distancing behavior, and social resources. *Psychiatry Research*, 293:113419, 2020.

[92] Leslie R Martin, Summer L Williams, Kelly B Haskard, and M Robin DiMatteo. The challenge of patient adherence. *Therapeutics and clinical risk management*, 1(3):189, 2005.

[93] Paola Martin, Diwakar Gupta, and Karthik V Natarajan. Vaccine procurement contracts for developing countries. *Production and Operations Management*, 29(11):2601–2620, 2020.

[94] David McAdams. Economic epidemiology in the wake of COVID-19. *Covid Economics*, 48:1–45, September 2020.

[95] John W Mellors, Alvaro Munoz, Janis V Giorgi, Joseph B Margolick, Charles J Tassoni, Phalguni Gupta, Lawrence A Kingsley, John A Todd, Alfred J Saah, Roger Detels, et al. Plasma viral load and cd4+ lymphocytes as prognostic markers of hiv-1 infection. *Annals of internal medicine*, 126(12):946–954, 1997.

[96] W H O Metrics. disability-adjusted life year (DALY), 2012.

[97] MN Dept. of Health. COVID-19 vaccine, Nov 2020. Last accessed Dec 29, 2020.

[98] MN Dept. of Health. MN COVID-19 Situation Update, Dec 2020. Last accessed Dec 30, 2020.

[99] MN Dept. of Health. MN stay safe plan 2020, Dec 2020. Last accessed Dec 29, 2020.

[100] MN Dept. of Health. UMN/MDH Minnesota COVID-19 Modeling Collaboration. `https://github.com/MN-COVID19-Model`, May 2020. Last accessed Dec 29, 2020.

[101] Sanjay K Mohanty, Manisha Dubey, Udaya S Mishra, and Umakanta Sahoo. Impact of covid-19 attributable deaths on longevity, premature mortality and daly: Estimates of usa, italy, sweden and germany, 2020.

[102] Mélodie Monod, Alexandra Blenkinsop, Xiaoyue Xi, Daniel Hebert, Sivan Bershan, Simon Tietze, Marc Baguelin, Valerie C. Bradley, Yu Chen, Helen Coupland, Sarah Filippi, Jonathan Ish-Horowicz, Martin McManus, Thomas Mellan, Axel Gandy, Michael Hutchinson, H. Juliette T Unwin, Sabine L. van Elsland,

Michaela A. C. Vollmer, Sebastian Weber, Harrison Zhu, Anne Bezancon, Neil M. Ferguson, Swapnil Mishra, Seth Flaxman, Samir Bhatt, and Oliver Ratmann. Age groups that sustain resurging COVID-19 epidemics in the United States. *Science*, 2021.

[103] Jean B Nachega, Edward J Mills, and Mauro Schechter. Antiretroviral therapy adherence and retention in care in middle-income and low-income countries: current status of knowledge and research priorities. *Current Opinion in HIV and AIDS*, 5(1):70–77, 2010.

[104] NBC Chicago. What You Can and Cannot Do During a Stay-at-Home or Shelter-in-Place Order, Mar 2020. Last accessed Jan 29, 2021.

[105] NBER. National bureau of economic research (nber): Determination of the february 2020 peak in us economic activity, June 2020.

[106] Diana Negoescu, Zhenhuan Zhang, Heiner Bucher, and Eran Bendavid. Differentiated hiv rna viral load monitoring in resource limited settings: An economic analysis. *Clinical infectious diseases*, 64(12):1724–1730, 03 2017.

[107] Diana M Negoescu, Kostas Bimpikis, Margaret L Brandeau, and Dan A Iancu. Dynamic learning of patient response types: An application to treating chronic diseases. *Management science*, 64(8):3469–3488, 2018.

[108] New York Times. Government Orders Alone Didn't Close the Economy. They Probably Can't Reopen It., May 2020. Last accessed Jan 29, 2021.

[109] New York Times. Lockdown Delays Cost at Least 36,000 Lives, Data Show, May 2020. Last accessed Jan 29, 2021.

[110] Mario Cesare Nurchis, Domenico Pascucci, Martina Sapienza, Leonardo Villani, Floriana D'Ambrosio, Francesco Castrini, Maria Lucia Specchia, Patrizia Laurenti, and Gianfranco Damiani. Impact of the Burden of COVID-19 in Italy:

Results of Disability-Adjusted Life Years (DALYs) and Productivity Loss. *International Journal of Environmental Research and Public Health*, 17(12):4233, 2020.

[111] Masamitsu Ohnishi, Hajime Kawai, and Hisashi Mine. An optimal inspection and replacement policy under incomplete state information. *European Journal of Operational Research*, 27(1):117–128, 1986.

[112] LeighAnne Olsen, Robert S Saunders, Pierre L Yong, et al. *The healthcare imperative: Lowering costs and improving outcomes: Workshop series summary.* National Academies Press, 2010.

[113] World Health Organization. Dengue and severe dengue. 2014.

[114] World Health Organization. Global health observatory (GHO) data, 2015.

[115] Aaron Z Palmer, Zelda B Zabinsky, and Shan Liu. Optimal control of COVID-19 infection rate with social costs. *arXiv preprint*, 2020.

[116] Nirmita Panchal, Rabah Kamal, Kendal Orgera, Cynthia Cox, Rachel Garfield, Liz Hamel, Cailey Munana, and Priya Chidambaram. The Implications of COVID-19 for Mental Health and Substance Use, August 2020. Last accessed Jan 29, 2021.

[117] Sen Pei, Sasikiran Kandula, and Jeffrey Shaman. Differential Effects of Intervention Timing on COVID-19 Spread in the United States. *medRxiv*, 2020.

[118] Andrew Phillips, Amir Shroufi, Lara Vojnov, Jennifer Cohn, Teri Roberts, Tom Ellman, Kimberly Bonner, Christine Rousseau, Geoff Garnett, Valentina Cambiano, et al. Sustainable hiv treatment in africa through viral load-informed differentiated care. *Nature*, 528(7580):S68, 2015.

[119] Fernando P Polack, Stephen J Thomas, Nicholas Kitchin, Judith Absalon, Alejandra Gurtman, Stephen Lockhart, John L Perez, Gonzalo Pérez Marc, Edson D

Moreira, Cristiano Zerbini, et al. Safety and efficacy of the BNT162b2 mRNA Covid-19 vaccine. *New England Journal of Medicine*, 2020.

[120] Namrata Prasad, David R Murdoch, Hugh Reyburn, and John A Crump. Etiology of severe febrile illness in low-and middle-income countries: a systematic review. *PLoS One*, 10(6):e0127962, 2015.

[121] Kiesha Prem, Yang Liu, Timothy W Russell, Adam J Kucharski, Rosalind M Eggo, Nicholas Davies, Stefan Flasche, Samuel Clifford, Carl AB Pearson, James D Munday, et al. The effect of control strategies to reduce social mixing on outcomes of the COVID-19 epidemic in Wuhan, China: a modelling study. *The Lancet Public Health*, 2020.

[122] Thomas C Quinn, Maria J Wawer, Nelson Sewankambo, David Serwadda, Chuanjun Li, Fred Wabwire-Mangen, Mary O Meehan, Thomas Lutalo, and Ronald H Gray. Viral load and heterosexual transmission of human immunodeficiency virus type 1. *New England journal of medicine*, 342(13):921–929, 2000.

[123] Heather Reese, A Danielle Iuliano, Neha N Patel, Shikha Garg, Lindsay Kim, Benjamin J Silk, Aron J Hall, Alicia Fry, and Carrie Reed. Estimated incidence of COVID-19 illness and hospitalization - United States, February-September, 2020. *Clinical Infectious Diseases*, 11 2020.

[124] Robert C Reiner, Ryan M Barber, James K Collins, Peng Zheng, Christopher Adolph, James Albright, Catherine M Antony, Aleksandr Y Aravkin, Steven D Bachmeier, Bree Bang-Jensen, et al. Modeling COVID-19 scenarios for the United States. *Nature Medicine*, pages 94–105, 2021.

[125] Irina N Riediger, Robyn A Stoddard, Guilherme S Ribeiro, Sueli M Nakatani, Suzana D R Moreira, Irene Skraba, Alexander W Biondo, Mitermayer G Reis, Alex R Hoffmaster, Joseph M Vinetz, Albert I Ko, and Elsio A Wunder. Rapid,

actionable diagnosis of urban epidemic leptospirosis using a pathogenic Leptospira lipL32-based real-time PCR assay. *PLoS Neglected Tropical Diseases*, 11(9):e0005940, sep 2017.

[126] Matthew L Robinson and Yukari C Manabe. Reducing Uncertainty for Acute Febrile Illness in Resource-Limited Settings: The Current Diagnostic Landscape. *The American journal of tropical medicine and hygiene*, 96(6):1285–1295, 2017.

[127] Alexander K Rowe, Don de Savigny, Claudio F Lanata, and Cesar G Victora. How can we achieve and maintain high-quality performance of health workers in low-resource settings? *The Lancet*, 366(9490):1026–1035, 2005.

[128] Robert Rowthorn and Jan Maciejowski. A cost–benefit analysis of the COVID-19 disease. *Oxford Review of Economic Policy*, 36(Supplement_1):S38–S55, 2020.

[129] AJ Scheen and D Giet. Non compliance to medical therapy; causes, consequences, solutions. *Revue medicale de Liege*, 65(5-6):239–245, 2010.

[130] Scientific American. Doing the Touchy Math on Who Should Get a COVID Vaccine First, November 2020. Last accessed Jan 29, 2021.

[131] Laura J Shallcross and Dame Sally C Davies. Antibiotic overuse: a key driver of antimicrobial resistance. *The British Journal of General Practice*, 64(629):604–605, dec 2014.

[132] Steven M Shechter, Matthew D Bailey, Andrew J Schaefer, and Mark S Roberts. The optimal time to initiate hiv therapy under ordered health states. *Operations Research*, 56(1):20–33, 2008.

[133] Donald S Shepard, Eduardo A Undurraga, and Yara A Halasa. Economic and disease burden of dengue in Southeast Asia. *PLoS neglected tropical diseases*, 7(2):e2055, 2013.

[134] Poojan Shrestha, Ben S Cooper, Joanna Coast, Raymond Oppong, Nga Do Thi Thuy, Tuangrat Phodha, Olivier Celhay, Philippe J Guerin, Heiman Wertheim, and Yoel Lubell. Enumerating the economic cost of antimicrobial resistance per antibiotic consumed to inform the evaluation of interventions affecting their use. *Antimicrobial Resistance & Infection Control*, 7(1):98, 2018.

[135] Matthew Sperrin and Brian McMillan. Prediction models for COVID-19 outcomes. *BMJ*, 371, 2020.

[136] Sze-chuan Suen, Margaret L Brandeau, and Jeremy D Goldhaber-Fiebert. Optimal timing of drug sensitivity testing for patients on first-line tuberculosis treatment. *Health care management science*, pages 1–15, 2018.

[137] Sze-chuan Suen, Diana Negoescu, and Joel Goh. Design of Incentive Programs for Optimal Medication Adherence, 2018. Available at SSRN: http://dx.doi.org/10.2139/ssrn.3308510.

[138] Yupin Suputtamongkol, Kanigar Niwattayakul, Chuanpit Suttinont, Kitti Losuwanaluk, Roongroeng Limpaiboon, Wirongrong Chierakul, Vanaporn Wuthiekanun, Surapee Triengrim, Mongkol Chenchittikul, and Nicholas J White. An open, randomized, controlled trial of penicillin, doxycycline, and cefotaxime for patients with severe leptospirosis. *Clinical Infectious Diseases*, 39(10):1417–1424, 2004.

[139] Yupin Suputtamongkol, Wirichada Pongtavornpinyo, Yoel Lubell, Chuanpit Suttinont, Siriwan Hoontrakul, Kriangsak Phimda, Kitti Losuwanaluk, Duangjai Suwancharoen, Saowaluk Silpasakorn, and Wirongrong Chierakul. Strategies for diagnosis and treatment of suspected leptospirosis: a cost-benefit analysis. *PLoS neglected tropical diseases*, 4(2):e610, 2010.

[140] C Suttinont, K Losuwanaluk, K Niwatayakul, S Hoontrakul, W Intaranongpai, S Silpasakorn, D Suwancharoen, P Panlar, W Saisongkorh, and J M Rolain.

Causes of acute, undifferentiated, febrile illness in rural Thailand: results of a prospective observational study. *Annals of Tropical Medicine & Parasitology*, 100(4):363–370, 2006.

[141] Wiwit Tantibhedhyangkul, Ekkarat Wongsawat, Saowaluk Silpasakorn, Duangdao Waywa, Nuttawut Saenyasiri, Jintapa Suesuay, Wilawan Thipmontree, and Yupin Suputtamongkol. Use of multiplex real-time PCR to diagnose scrub typhus. *Journal of clinical microbiology*, 55(5):1377–1387, 2017.

[142] Andrew J Taylor, Daniel H Paris, and Paul N Newton. A systematic review of mortality from untreated scrub typhus (Orientia tsutsugamushi). *PLoS neglected tropical diseases*, 9(8):e0003971, 2015.

[143] Vipa Thanachartwet, Nittha Oer-Areemitr, Supat Chamnanchanunt, Duangjai Sahassananda, Akanitt Jittmittraphap, Plengsakoon Suwannakudt, Varunee Desakorn, and Anan Wattanathum. Identification of clinical factors associated with severe dengue among Thai adults: a prospective study. *BMC infectious diseases*, 15(1):420, 2015.

[144] Paul R Torgerson, José E Hagan, Federico Costa, Juan Calcagno, Michael Kane, Martha S Martinez-Silveira, Marga G A Goris, Claudia Stein, Albert I Ko, and Bernadette Abela-Ridder. Global Burden of Leptospirosis: Estimated in Terms of Disability Adjusted Life Years. *PLoS Neglected Tropical Diseases*, 9(10):e0004122, oct 2015.

[145] UNAIDS. Hiv and aid estimates, Dec 2020. Last accessed 16th Jan 2021.

[146] UNESCO. The united nations educational, scientific and cultural organization (unesco): Covid-19 impact on education, 2020. Last accessed Jan 29, 2021.

[147] U.S. Department of Commerce. Gross Domestic Product, Third Quarter 2020 (Advance Estimate), Oct 2020. Last accessed Nov 28, 2020.

[148] USA Today. Coronavirus in the US: How all 50 states are responding – and why eight still refuse to issue stay-at-home orders, Mar 2020. Last accessed Jan 29, 2021.

[149] Alain Venet, Wei Lu, Kheira Beldjord, and Jean-Marie Andrieu. Correlation between cd4 cell counts and cellular and plasma viral load in hiv-1-seropositive individuals. *AIDS (London, England)*, 5(3):283–288, 1991.

[150] C Lee Ventola. The Antibiotic Resistance Crisis: Part 1: Causes and Threats. *Pharmacy and Therapeutics*, 40(4):277–283, apr 2015.

[151] Jesse J Waggoner, Janaki Abeynayake, Ilana Balassiano, Martina Lefterova, Malaya K Sahoo, Yuanyuan Liu, Juliana Magalhães Vital-Brazil, Lionel Gresh, Angel Balmaseda, and Eva Harris. Multiplex nucleic acid amplification test for diagnosis of dengue fever, malaria, and leptospirosis. *Journal of clinical microbiology*, 52(6):2011–2018, 2014.

[152] Ruxian Wang and Zizhuo Wang. Consumer choice models with endogenous network effects. *Management Science*, 63(11):3944–3960, 2017.

[153] Xutong Wang, Remy Pasco, Zhanwei Du, Michaela Petty, Spencer Fox, Alison Galvani, Michael Pignone, S. Claiborne Johnston, and Lauren Ancel Meyers. Impact of Social Distancing Measures on Coronavirus Disease Healthcare Demand, Central Texas, USA. *Emerging Infectious Disease*, 26(10):2361, 2020.

[154] Tri Wangrangsimakul, Thomas Althaus, Mavuto Mukaka, Pacharee Kantipong, Vanaporn Wuthiekanun, Wirongrong Chierakul, Stuart D Blacksell, Nicholas P Day, Achara Laongnualpanich, and Daniel H Paris. Causes of acute undifferentiated fever and the utility of biomarkers in Chiangrai, northern Thailand. *PLoS neglected tropical diseases*, 12(5):e0006477, 2018.

[155] Washington Post. Coronavirus updates: Seven-day average case total in the U.S. sets record for 27th straight day, July 2020. Last accessed Jan 29, 2021.

[156] George Watt, M A Linda Tuazon, Edna Santiago, LaurenaP Padre, Carmen Calubaquib, CatherineP Ranoa, and LarryW Laughlin. Placebo-controlled trial of intravenous penicillin for severe and late leptospirosis. *The Lancet*, 331(8583):433–435, 1988.

[157] Hillard Weinstock, Stuart Berman, and Willard Cates Jr. Sexually transmitted diseases among american youth: incidence and prevalence estimates, 2000. *Perspectives on sexual and reproductive health*, 36(1):6–10, 2004.

[158] WHO. World health organization (WHO):macroeconomics and health : investing in health for economic development, Dec 2001. Last accessed Mar 6, 2020.

[159] WHO. World health organization (WHO): Disability-adjusted life-year (DALY): Quantifying the Burden of Disease from mortality and morbidity, Feb 2012. Last accessed March 6 2020.

[160] WHO. World health organization (WHO): Coronavirus disease (COVID-19) outbreak, May 2020. Last accessed May 28 2020.

[161] WHO. World health organization (WHO): Life expectancy and healthy life expectancy data by country, Nov 2020. Last accessed Nov 27, 2020.

[162] WHO. World Heath Organization (WHO): WHO SAGE Roadmap For Prioritizing Uses Of COVID-19 Vaccines In The Context Of Limited Supply, November 2020. Last accessed Jan 29, 2021.

[163] Annelies Wilder-Smith, Calvin J Chiew, and Vernon J Lee. Can we contain the COVID-19 outbreak with the same measures as for SARS? *The Lancet Infectious Diseases*, 20(5):e102 – e107, 2020.

[164] David P Wilson, Matthew G Law, Andrew E Grulich, David A Cooper, and John M Kaldor. Relation between hiv viral load and infectiousness: a model-based analysis. *The Lancet*, 372(9635):314–320, 2008.

[165] World Bank. GDP per capita (current US dollar) - United States, Nov 2020. Last accessed Nov 27, 2020.

[166] World Health Organization. Viral load testing, Dec 2020. Last accessed 11th Jan 2021.

[167] Worldbank. GDP per capita (2016), 2019.

[168] Joseph T Wu, Kathy Leung, and Gabriel M Leung. Nowcasting and forecasting the potential domestic and international spread of the 2019-nCoV outbreak originating in Wuhan, China: a modelling study. *The Lancet*, 395(10225):689–697, 2020.

[169] Luyi Xu, Kerim Munir, Cheeraya Kanabkaew, and Sophie Le Coeur. Factors influencing antiretroviral treatment suboptimal adherence among perinatally hiv-infected adolescents in thailand. *PloS one*, 12(2):e0172392, 2017.

[170] Dan Yamin and Arieh Gavious. Incentives' effect in influenza vaccination policy. *Management Science*, 59(12):2667–2686, 2013.

[171] Anthony Zhenhuan Zhang and Eva Enns. Optimal timing and effectiveness of COVID-19 outbreak responses in China: a modelling study, 2020. Available at SSRN: http://dx.doi.org/10.2139/ssrn.3558339.